Mode Coupling Theory of Active Brownian Hard Disks

Inaugural-Dissertation

zur Erlangung des Doktorgrades
der Mathematisch-Naturwissenschaftlichen Fakultät
der Heinrich-Heine-Universität Düsseldorf

vorgelegt von

Alexander Liluashvili

aus Tbilisi, Georgien

supervised by
Prof. Dr. Thomas Voigtmann

Köln, Oktober 2017.

aus dem Institut für Theoretische Physik II, der weichen Materie
der Heinrich-Heine-Universität Düsseldorf

Gedruckt mit der Genehmigung der
Mathematisch-Naturwissenschaftlichen Fakultät der
Heinrich-Heine-Universität Düsseldorf

Berichterstatter:

1. Prof. Dr. Thomas Voigtmann

2. Prof. Dr. Hartmut Löwen

Tag der mündlichen Prüfung: 12.12.2017

Eidesstattliche Versicherung

Ich, Herr Alexander Liluashvili, versichere an Eides statt, dass die vorliegende Dissertation von mir selbstständig und ohne unzulässige fremde Hilfe unter Beachtung der "Grundsätze zur Sicherung guter wissenschaftlicher Praxis an der Heinrich-Heine-Universität Düsseldorf" erstellt worden ist.

Köln, 12.10.2017.

Unterschrift

Publications

The following publications that are based on this thesis have been submitted. They cover the results of chapters 2-5.

Mode-Coupling Theory for Active Brownian Particles, arXiv:1707.07373.
Alexander Liluashvili, Jonathan Onody, Thomas Voigtmann.
(under review for Phys. Rev. E).

Active Brownian Particle Dynamics at High Densities.
Alexander Liluashvili, Thomas Voigtmann.
(to appear in: Proceedings of the NIC Symposium 2018, edited by Kurt Binder et al., NIC Series vol. 49, Jülich, Germany).

Abstract

The collective dynamics of the active Brownian hard disks in two dimensions under very high densities is studied. To do so the Mode Coupling Theory (MCT) of the glass transition is used.

The system is characterized by the dynamical density-density correlator matrix $\mathbf{\Phi}(t)$. The starting point of the theoretical calculations is the Smoluchowski equation determining the time evolution of the observables uniquely.

Following the steps of Mori and Zwanzig the equation of motion for the density correlator is derived. The so-called integro differential equation is closed by the MCT approximation of the memory kernel. The final equations are solved numerically over many orders of magnitude in time.

By evaluating the results, glassy behavior of the system is analyzed and the critical parameters (activity v_0^c, rotational diffusion D_r^c and the packing fraction ϕ^c), which separate the glassy and fluid, phase are determined.

Integration Through Transients (ITT) formalism is used to determine non-equilibrium averages (e.g. average swim speed) as a function of equilibrium averages only. The transient correlators appearing in the ITT formalism are approximated by MCT methods.

The numerical values are compared with simulation data.

Zusammenfassung

In dieser Arbeit untersuchen wir die kollektive Dynamik von aktiven Brownschen harten Kugeln in zwei Raumdimensionen bei sehr großen Dichten. Um dies zu erreichen wird die Modenkopplungstheorie (MCT) für den Glasübergang verwendet.

Das System ist durch die dynamische Dichte-Dichte-Korrelator Matrix $\mathbf{\Phi}(t)$ charakterisiert. Den Ausgangspunkt für die theoretischen Rechnungen stellt die Smoluchowski Gleichung dar, welche die Zeitentwicklung von allen Observablen eindeutig bestimmt.

Durch die Anwendung des Mori-Zwanzig Formalismus leiten wir die Bewegungsgleichung für den Dichte-Dichte Korrelator her. Die so genannte Integro Differentialgleichung wird durch die MCT-Nährung des Memory-Kerns geschlossen und unter Verwendung von numerischen Methoden, über mehrere Größenordnungen in der Zeit gelöst.

Durch das Auswerten der numerischen Ergebnisse untersuchen wir das glasartige Verhalten des Systems und bestimmen die kritischen Parameter (Aktivität v_0^c, Rotationsdiffusion D_r^c und die Packungsdichte ϕ^c), welche den glasartigen vom flüssigen Zustand trennen.

Wir verwenden die Integration durch die Transienten (ITT) Formalismus um die Nichtgleichgewichts Erwartungswerte (z.B. mittlere Schwimmgeschwindigkeit) nur als Funktion von Gleichgewichts Erwartungswerten zu bestimmen. Die transiente Korrelationsfunktionen, welche im ITT Formalismus auftreten, werden durch die MCT Methoden genähert.

Zuletzt werden die numerischen Ergebnisse mit Simulationsdaten verglichen.

Acknowledgments

First of all I want to thank my supervisor Prof. Thomas Voigtmann, not only for introducing me in the field of Mode Coupling Theory also for giving me enough freedom and support to try out things myself (make my own mistakes).

I want to thank my officemate and friend Heliana Cárdenas (I did not forget the accent) for many many physics non related (and some related) discussions and to make the time pass by very quickly, not to forget the improve of my English language skills.

I am very grateful for the precise corrections of my calculation by Jonathan Ónody, without his effort I would never find the mistakes in my work.

I want to thank Thomas Voigtmann, Jonathan Ónody and Julian Reichert for the proofreading.

I also want to thank my mentor Hartmut Löwen in university of Düsseldorf.

The work was funded by DFG in the special priority program SPP 1726.

Finally I also want to thank the supercomputer center in Jülich for allowing us to use their powerful cluster "JURECA" accelerating the data production significantly.

Contents

Chapter 1

Introduction

Active or self-propelled particles like microswimmers in dense environments are important model systems to study various problems in biology or medicine like wound healing [1] or collective dynamics of bacteria [2,3]. The collective dynamics of bacteria or cells show slow dynamics, arising from crowding effects at very high densities and is closely related to glassy systems [4, 5].
E.coli bacteria, spermatozoa or Chlamydomonas represent biological microswimmers, with $0.5 - 10\,\mu$m size and achieve swim velocities of $1 - 100\,\mu$m/sec by using the beating of the flagellum as self-propulsion mechanism. From mathematical point of view already a single flagellum has a very complex geometry [6] and is too complicated for a study of the collective dynamics.
Colloidal systems of self-propelled particles are more common model systems to study effects related to activity. In this work our main focus will be the model of "Active Brownian Disks " (ABD) [7, 8] in a liquid solvent to simplify the complex structure of biological microswimmers, but still sustain important aspects of their complex motion. ABD are orientable colloidal particles in two dimensions, which undergo translational and rotational Brownian motion, superimposed with motility (activity force or self-propulsion force). Due to the activity which consumes energy from the environment to maintain the driving force, the systems of ABD are intrinsically out of equilibrium violating fluctuation-dissipation theorem relations and offer insight into non-equilibrium phenomena.
On the other hand ABD suspension can be easily modeled experimentally by using so called "Janus Particles" [9–11]. Janus particles represent a class of particles with their surface having two or more physical properties. A Janus particle described in [10] is a SiO_2 sphere capped by graphite on one hemisphere. These so called "carbon-coated " particles are suspended in a water-lutidine mixture and are self-propelled by diffusiophoresis. As an energy source a laser beam is used. The laser light gets absorbed by the carbon capped part of the particle which locally heats up the solvent above the critical temperature and due to the demixing

a phoretic force is propelling the particles. The self-propulsion strength can be varied by changing the laser intensity. The dynamics of ABD suspensions can also be captured by relatively simple computer simulation methods [12–14] (e.g. Monte Carlo simulations or molecular dynamics simulation).
At high densities ABD suspensions (with size polydispersity) with strong short range repulsion (hard disks) are known to form a "glassy" system as suggested by different computer simulation methods [15–17] and also known from passive colloidal suspensions [18, 19]. The dynamics of the ABD system we consider in this work is characterized by four parameters: D_t the translational diffusion, D_r rotational diffusion, v_0 the self-propulsion velocity and density ρ.
Systems of active Brownian particles at low densities were studied broadly in recent years (e.g. [20–22]). For large time scales $D_r t \gg 1$ such systems can be analyzed by introducing activity induced effective-diffusion constant (effective-diffusion limit) $D_{\text{eff}} = D_t(1+v_0^2/2D_rD_t)$, mapping the original problem to a Brownian motion with an effective-diffusion constant. That kind of mapping requires all length scales to be larger than the persistence length $l_p = v_0/D_r$.
The dynamics of ABD systems at high densities are less well understood. To analyze the glassy behavior of ABD systems the theories of glass transition for passive systems have been adapted to activity. One of such theories is the Mode-Coupling Theory of glass transition (MCT) developed for 3D and 2D passive systems [23–25]. The MCT theory was extended to high-density ABD system by Farage and Brader [26] in the effective-diffusion limit assuming all length scales to be larger than the persistence length l_p. In the effective-diffusion limit the activity enters the theory only through the Péclet number $\text{Pe} := v_0^2/D_rD_t$ and increasing the activity shifts the glass transition point to higher densities which agrees qualitatively with computer simulation methods [13]. The glass transition point separates the glassy and fluid phase and mathematically it is a bifurcation point. The glassy phase (solid like) is characterized by a drastic decrease of particle mobility and by "caging effects" where every particle is enclosed by neighbor particles over a very long time period.
A model of Active Ornstein-Uhlenbeck Particles (AOUP) represents another model of active particles introduced and studied in [27]. The velocity vector of the particles is modeled by the Ornstein- Uhlenbeck process.
In this work we want develop a theory to study high-density ABD systems without using the effective-diffusion limit, corresponding to have two independent parameters v_0 and D_r and not only an effective parameter Pe. The goal is to analyze the glassy behavior of the system and the influence of the activity to the glass transition point at different persistence lengths. The question how the activity changes the glass transition is not a trivial question and is not fully understood yet. One might presume that the glassy dynamics at high densities is stable enough

to sustain strong non-equilibrium driving forces. Which turned out to be wrong for systems under steady shear, where the glass transition is destroyed for arbitrarily small shear rates [28, 29]. To understand the interplay between the glass transition and the non-equilibrium driving will be main goal in this work. Recent experiments provide information about dynamical structure factor, which contains information about glassy behavior of the system without tracking all the particles. The theory we develop to investigate such ABD suspensions is an extension of MCT developed for passive systems (for very detailed introduction into the field of MCT we refer to the book from Wolfgang Götze [23]). The MCT is a powerful method which makes it possible to derive an non-perturbatively approximated equation of motion for the density correlation function at high densities. It is proven that MCT approximations describe the glassy dynamics especially the "caging effect" qualitatively correctly [30].
The so-called "Integration Through Transients" (ITT) formalism provides an elegant way to deal with non-equilibrium averages (e.g. non-equilibrium swim speed or non-equilibrium structure factor). The ITT formalism was applied on dense suspensions by Cates and Fuchs [28] successfully, linking the transport coefficients to the transient correlator of microscopic quantities. The transient correlation functions which are needed by using the ITT formalism can be determined by Mode Coupling approximation, which is an additional strength of MCT.

Chapter 2

Mathematical Model

2.1 Motivation

2.1.1 Single Brownian Particle

The starting point for the theoretical calculations is the Langevin equation which is a force balance equation containing a stochastic term which makes it to a stochastic differential equation (for deep introduction into the stochastic processes see [31]). As a motivation we consider a single particle in two dimensions in a solvent getting random kicks from the solvent molecules, so the dynamics of the particle is described by the following equation which is the simplest form of the Langevin equation,

$$\underbrace{m\frac{d^2\vec{x}(t)}{dt^2}}_{\text{Inertia}} = \underbrace{-\gamma\frac{d}{dt}\vec{x}(t)}_{\text{Friction}} + \overbrace{\sqrt{\Gamma}\vec{\xi}(t)}^{\text{Random noise}}, \tag{2.1}$$

where the stochastic term $\vec{\xi}$ is a Gaussian white noise with zero mean and zero correlation for different times.

$$\begin{aligned} &\left\langle \xi^i(t) \right\rangle = 0, \quad i \in \{x, y\}, \\ &\left\langle \xi^i(t)\xi^j(t') \right\rangle = \delta_{i,j}\delta(t-t'). \end{aligned} \tag{2.2}$$

The friction term γ describes the strength of dissipation and Γ describes the strength of fluctuations. If the system is close to thermal equilibrium the friction term is given by the Stokes-Einstein formula [32] $\gamma = k_B T/D_t = 3\pi\eta\sigma$, where D_t is the translational diffusion, η is the shear viscosity of the solvent and σ is the particle diameter. If we do not consider the short time dynamics we can drop the inertia term in the equation (2.1) which leads to the overdamped Langevin

equation.

$$d\vec{x}(t) = \frac{\sqrt{\Gamma}}{\gamma}\vec{\xi}(t)dt = \frac{\sqrt{\Gamma}}{\gamma}\overbrace{d\vec{W}(t)}^{\text{Wiener Process}} \quad \Rightarrow \quad \vec{x}(t) \overset{\vec{x}_0=0}{=} \frac{\sqrt{\Gamma}}{\gamma}\int_0^t d\vec{W}(t'). \tag{2.3}$$

Using the properties of the white noise we can calculate the mean-squared displacement $\langle \vec{x}(t)^2 \rangle$, which is a very important quantity by dealing with stochastic processes, since it is the first nonvanishing moment containing information about the distance traveled by the particle.

$$\begin{aligned} &\langle \vec{x}(t) \rangle = 0, \\ &\left\langle \vec{x}(t)^2 \right\rangle = \frac{1}{\gamma^2}\int_0^t \int_0^t dt'dt'' \left\langle \vec{\xi}(t') \cdot \vec{\xi}(t'') \right\rangle = \frac{2\Gamma}{\gamma^2}t. \end{aligned} \tag{2.4}$$

In Einsteins theory of Brownian dynamics [32] the mean-squared displacement is related to the transport coefficient D_t.

$$4D_t t = \left\langle \vec{x}(t)^2 \right\rangle \overset{!}{=} \frac{2\Gamma}{\gamma^2}t \quad \Rightarrow \quad \frac{\sqrt{\Gamma}}{\gamma} = \sqrt{2D_t}. \tag{2.5}$$

The equation 2.5 is a well known "Fluctuation-Dissipation Theorem" (FDT) [33] connecting the strength of dissipation due to the friction and the strength of fluctuation due to the random kicks. The FDT is only valid in or close to thermal equilibrium.
We rewrite the Langevin equation (2.1) in a more common form

$$d\vec{x}(t) = \sqrt{2D_t}\vec{\xi}(t)dt, \tag{2.6}$$

where the assumption was made, that the friction force of the solvent to be much bigger than the inertia term, which is generally an appropriate assumption for colloidal particles, but not for granular particles.

2.1.2 Single Active Brownian Particle

We extend now the theory by adding more degrees of freedom. We consider a single spherical particle described by the position coordinates $\vec{x}(t)$ and the orientation $\varphi(t)$. The particle does not only undergo a Brownian motion it also has a self-propulsion force in the direction of its orientation. This model is still analytically solvable but already much more complicated than the previous model. We have to deal with two random processes (two Wiener Processes $\vec{W}^{\vec{x}}(t)$ and $W^{\varphi}(t)$). The

model can be described by a coupled stochastic differential equation.

$$\begin{aligned} d\vec{x}(t) &= \overbrace{v_0\vec{o}(\varphi)dt}^{\text{activity}} + \overbrace{\sqrt{2D_t}d\vec{W}^{\vec{x}}(t)}^{\text{random jumps}}, \\ d\varphi(t) &= \underbrace{\sqrt{2D_r}dW^{\varphi}(t)}_{\text{random orientation}}. \end{aligned} \tag{2.7}$$

The position variable $\vec{x}(t)$ is coupled to the angle by the "activity term" with the orientation vector $\vec{o}(\varphi) = (\cos(\varphi), \sin(\varphi))^{\top}$. It should be noticed that there are two diffusion constants in this model. D_t is responsible for the strength of translational motion and D_r for the rotations. Now we want to determine the mean displacement and the mean-squared displacement for the model and investigate how the activity influences the system. Integrating the equations (2.7) leads to:

$$\begin{aligned} \varphi(t) &\overset{\varphi_0=0}{=} \sqrt{2D_r}\int_0^t dW^{\varphi}(\tau), \\ \vec{x}(t) &= v_0\int_0^t \begin{pmatrix} \cos\left(\sqrt{2D_r}W^{\varphi}(\tau)\right) \\ \sin\left(\sqrt{2D_r}W^{\varphi}(\tau)\right) \end{pmatrix} d\tau + \sqrt{2D_t}\vec{W}^{\vec{x}}(t). \end{aligned} \tag{2.8}$$

Terms like $\cos(W^{\varphi}(t))$ and $\sin(W^{\varphi}(t))$ need to be evaluated, to do so it can be used, that the Wiener process has Gaussian density function $f_W(x) = \mathcal{N}[0,t](x) = \frac{1}{\sqrt{2\pi t}}\mathrm{e}^{-x^2/(2t)}$ and the corresponding characteristic function $\varphi_W(k) = \left\langle \mathrm{e}^{ikW}\right\rangle_W = \mathrm{e}^{-k^2t/2}$.

$$\begin{aligned} &\left\langle \cos\left(\alpha W^{\varphi}(t)\right)\right\rangle = \Re\left\langle \mathrm{e}^{i\alpha W^{\varphi}(t)}\right\rangle = \Re\Big(\varphi_W(\alpha)\Big) = \mathrm{e}^{-\alpha^2 t/2}, \\ \Rightarrow\ &\left\langle \cos\left(\sqrt{2D_r}W^{\varphi}(t)\right)\right\rangle = \mathrm{e}^{-D_r t}, \\ \Rightarrow\ &\left\langle \sin\left(\sqrt{2D_r}W^{\varphi}(t)\right)\right\rangle = 0. \end{aligned} \tag{2.9}$$

Using the zero mean value of the Wiener process, the mean displacement will be determined.

$$\langle \vec{x}(t)\rangle = \frac{v_0}{D_r}\left(1 - \mathrm{e}^{-D_r t}\right)\vec{e_x}. \tag{2.10}$$

One should notice that there is a nonvanishing drift only in x direction because of the initial choice of the angle $\varphi_0 = 0$, making the initial velocity aligned parallel to the x-axis. The calculation for the mean-squared displacement is analogous but lengthy since evaluation of the two-point functions $\langle \cos(W(t))\cos(W(t'))\rangle$ and $\langle \sin(W(t))\sin(W(t'))\rangle$ are needed.

$$\left\langle \vec{x}(t)^2\right\rangle = 4D_t t + \frac{2v_0^2}{D_r}t + \frac{2v_0^2}{Dr^2}\Big(\mathrm{e}^{-D_r t} - 1\Big). \tag{2.11}$$

The mean-squared displacement behaves differently for different time regimes:

$$\begin{aligned} t \to 0: \quad & \left\langle \vec{x}(t)^2 \right\rangle = 4D_t t + v_0^2 t^2 + \mathcal{O}\left(t^3\right), \\ t \to \infty: \quad & \left\langle \vec{x}(t)^2 \right\rangle = 4D_t t + \frac{2v_0^2}{D_r} t = 4D_{\text{eff}} t. \end{aligned} \tag{2.12}$$

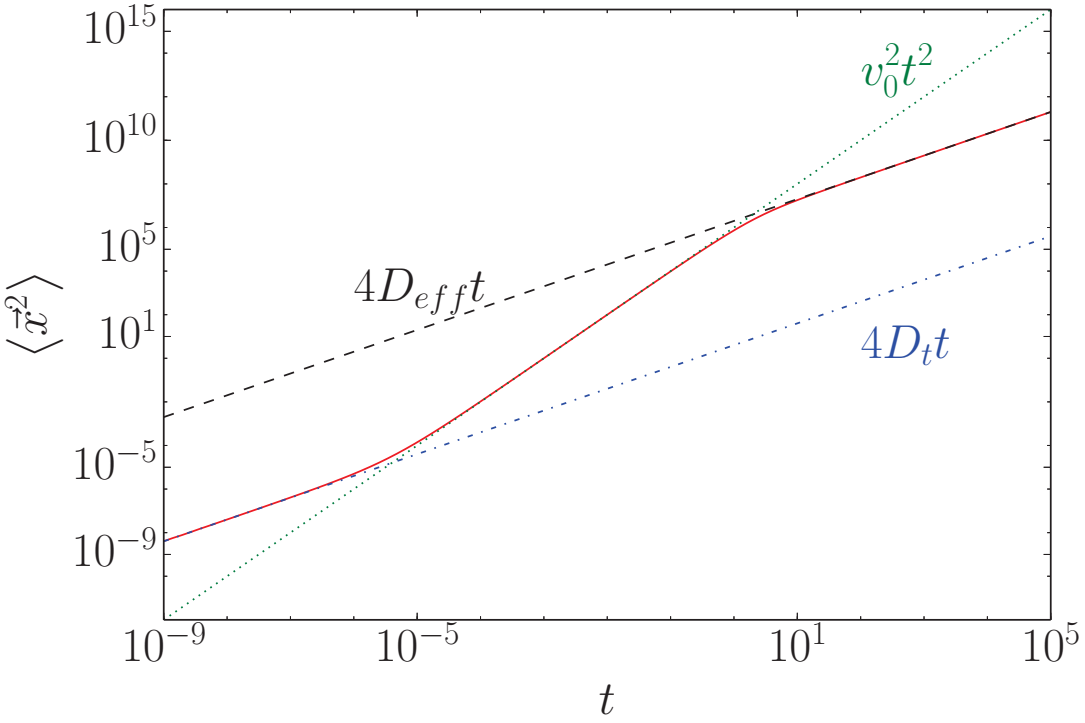

Figure 2.1: Mean-squared displacement of an active Brownian hard disk in a solvent (solid line) and the corresponding different time regimes.

In the Figure 2.1 three different regimes are illustrated. For very short times a purely diffusive regime with the diffusion constant of D_t can be observed, at intermediate times the diffusive regime is superimposed to the ballistic regime, and for very large times we again have a purely diffusive regime with an effective diffusion constant $D_{\text{eff}} = D_t + \frac{v_0^2}{2D_r}$. Already such a simplistic model including only a single particle and no particle-particle interactions is cumbersome to calculate analytically. Solving a model with N active particles in a solvent in 2 dimensions corresponds to solving $3N$ coupled stochastic differential equations, since a general particle-particle interaction potential depends on spacial coordinates and orientations of all particles e.g. $U = U(\{\vec{x}_1, \varphi_1, \cdots, \vec{x}_N, \varphi_N\})$. Solving such a system analytically is hopeless and needs to be treated differently.

One possible approach to solve the system of coupled stochastic differential equations is by using computer simulation methods [12–14] (Molecular dynamics simulation, Monte-Carlo simulation). Those simulation methods take as an input the interaction forces of the particles, and generate as an output the time dependent coordinates of all particles. Although those methods are straightforward to understand, they give little theoretical insight about the system and its properties.
Our focus will be on a different method which transforms the set of coupled SDEs to a Fokker-Planck type of equation for the probability density function and uses the Mode Coupling Theory (MCT) of glass transition to investigate the behavior of the system at very high densities. The Mode coupling theory was already applied to passive systems successfully.
From the theory of stochastic processes [31] we use the expansion formula. For a general stochastic differential equation,

$$d\vec{X}(t) = \vec{A}\left(\vec{X},t\right)dt + \boldsymbol{B}\left(\vec{X},t\right)d\vec{W}^{\vec{X}}(t), \tag{2.13}$$

with the coefficient vector $\vec{A}$ and coefficient matrix $\boldsymbol{B}$ the corresponding Fokker-Planck equation is

$$\partial_t \mathcal{P}\left(\vec{X},t\right) = -\sum_i \partial_{X_i}\left[A_i \mathcal{P}\left(\vec{X},t\right)\right] + \frac{1}{2}\sum_{ijk}\partial_{X_i}\boldsymbol{B}_{ik}\partial_{X_j}\boldsymbol{B}_{jk}\mathcal{P}\left(\vec{X},t\right). \tag{2.14}$$

The equation (2.14) is a transformation of a set of coupled SDEs to a deterministic partial differential equation for the probability density function. The transformation will be demonstrated for the the Langevin equation (2.7),

$$\begin{pmatrix} x \\ y \\ \varphi \end{pmatrix} = \underbrace{v_0 \begin{pmatrix} \cos(\varphi) \\ \sin(\varphi) \\ 0 \end{pmatrix}}_{\vec{A}\left(\vec{X},t\right)} dt + \underbrace{\begin{pmatrix} \sqrt{2D_t} & 0 & 0 \\ 0 & \sqrt{2D_t} & 0 \\ 0 & 0 & \sqrt{2D_t} \end{pmatrix}}_{\boldsymbol{B}\left(\vec{X},t\right)} \begin{pmatrix} dW^x \\ dW^y \\ dW^\varphi \end{pmatrix}. \tag{2.15}$$

The corresponding Fokker-Plank equation for the PDF can be determined by applying equation (2.14).

$$\partial_t \mathcal{P} = -v_0\Big(\cos(\varphi)\,\partial_x + \sin(\varphi)\,\partial_y\Big)\mathcal{P} + \Big(D_t\partial_x^2 + D_t\partial_y^2 + D_r\partial_\varphi^2\Big)\mathcal{P}. \tag{2.16}$$

Solving (2.16) for the probability density $\mathcal{P}$ makes it also possible to determine the mean-squared displacement, which should coincide with (2.11).

2.2 Active Brownian Hard Disks

2.2.1 Langevin Equation

Now we extend the model of a single active Brownian particle to interacting active Brownian hard disks (ABD). The Langevin equation describing this model contains in addition to (2.7) an interaction term characterized by particle-particle interaction potential.

$$\begin{aligned} d\vec{x}_i(t) &= \overbrace{D_t\beta\vec{F}_i dt}^{\text{interaction}} + \overbrace{v_0\vec{o}_i(\varphi)dt}^{\text{activity}} + \overbrace{\sqrt{2D_t}d\vec{W}_i^{\vec{x}}(t)}^{\text{random jumps}}, \\ d\varphi_i(t) &= \underbrace{\sqrt{2D_r}dW_i^{\varphi}(t)}_{\text{random orientation}}. \end{aligned} \tag{2.17}$$

The subindex i denotes the i-th particle $i \in \{1, \cdots, N\}$ and the interaction force $\vec{F}_i$ is a gradient of an interaction potential $\vec{F}_i = -\vec{\nabla}U(\{\vec{x}_1, \varphi_1, \cdots, \vec{x}_N, \varphi_N\})$. In

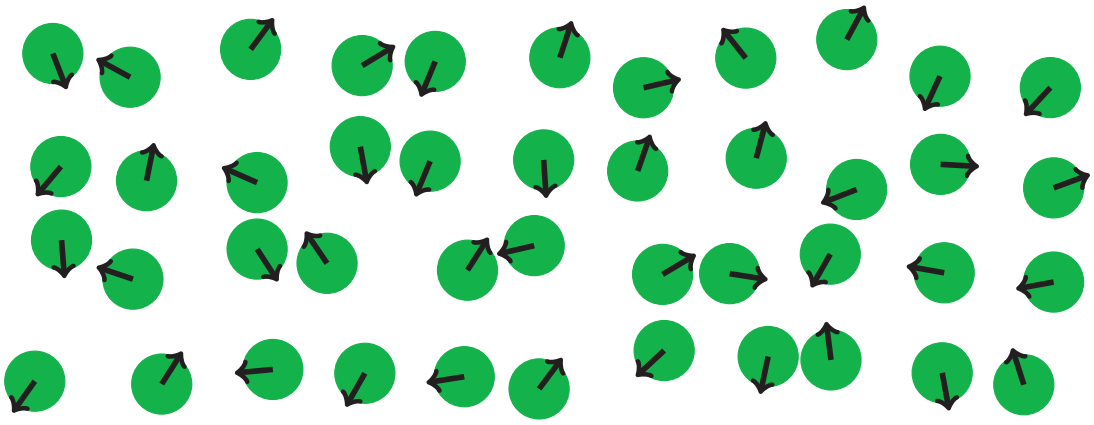

Figure 2.2: Schematic representation of Active Brownian hard disks.

Figure 2.2 the schematic representation of active Brownian disks is illustrated. The small arrows denote the direction of the orientation of the particles which is also the direction of the self-propulsion force. The angle $\varphi_i(t)$ describes the angle between the x-axis and the orientation vector. In this work we consider the particle-particle interaction potential U to be a hard sphere interaction.

$$U\left(\{\vec{x}_i\}\right) \equiv U\left(\vec{x}_1, \cdots, \vec{x}_N\right) = \begin{cases} \infty & \text{if} \quad |\vec{x}_i - \vec{x}_j|_{\substack{\forall i,j \\ i \neq j}} < \sigma \\ 0 & \text{if} \quad |\vec{x}_i - \vec{x}_j|_{\substack{\forall i,j \\ i \neq j}} \geq \sigma \end{cases}, \tag{2.18}$$

with the particle diameter σ. The interaction potential depends only at the position vectors of the particles, and the interactions are completely decoupled from the orientations.

2.2.2 Smoluchowski Equation

Using the results from previous section we transform the Langevin equation for the ABD to the corresponding Fokker-Planck or Smoluchowski equation.

$$\begin{aligned}&\partial_t \mathcal{P}\left(\{\vec{x}_i\},\{\varphi_i\},t\right) = \Omega \mathcal{P}\left(\{\vec{x}_i\},\{\varphi_i\},t\right),\\ &\Omega = \sum_i D_t \vec{\partial}_i \cdot \left(\vec{\partial}_i - \beta \vec{F}_i\right) - v_0 \vec{\partial}_i \cdot \vec{o}_i + D_r \partial^2_{\varphi_i},\end{aligned} \tag{2.19}$$

with the differential operator Ω, which is often called Smoluchowski operator in the literature. The shorthand notation convention for the gradient vector will be used frequently $\vec{\partial}_i \equiv (\partial_{x_i}, \partial_{y_i})^\top$. The Smoluchowski operator is a sum of the equilibrium contribution describing passive Brownian hard disks and a non-equilibrium part being proportional to the activity:

$$\begin{aligned}&\Omega = \Omega_{\mathrm{eq}} + \delta\Omega,\\ &\Omega_{\mathrm{eq}} = \sum_i D_t \vec{\partial}_i \cdot \left(\vec{\partial}_i - \beta \vec{F}_i\right) + D_r \partial^2_{\varphi_i},\\ &\delta\Omega = -\sum_i v_0 \vec{\partial}_i \cdot \vec{o}_i.\end{aligned} \tag{2.20}$$

The activity brings the system out of equilibrium since energy is absorbed from the environment to produce the driving force. The non-equilibrium part cannot be assumed to be small in comparison to the equilibrium part which makes a perturbation expansion not feasible. The Smoluchowski equation (2.19) describes the time evolution of the probability density $\mathcal{P}$ in the N particle configuration space. We introduce the configuration space $\Gamma(\{x_i\},\{\varphi_i\})$ which is important for defining the scalar product $\langle\cdot|\cdot\rangle$ and the average $\langle\cdot\rangle$. The configuration space is a function of all position coordinates of the N particles and their orientations with the configuration space differential

$$d\mathbf{\Gamma} \equiv d\vec{x}_1 \cdots d\vec{x}_N d\varphi_1 \cdots d\varphi_N. \tag{2.21}$$

For two configuration space observables A and B we define the scalar products and the averages

$$\begin{aligned}&\langle A|B\rangle = \int d\mathbf{\Gamma} \mathcal{P}_{\mathrm{eq}} A^*(\Gamma) B(\Gamma), \quad \langle A\rangle = \int d\mathbf{\Gamma} \mathcal{P}_{\mathrm{eq}} A(\Gamma), && \text{Equilibrium weighted}\\ &\langle A|B\rangle_{\mathrm{non}} = \int d\mathbf{\Gamma} \mathcal{P} A^*(\Gamma) B(\Gamma), \quad \langle A\rangle_{\mathrm{non}} = \int d\mathbf{\Gamma} \mathcal{P} A(\Gamma), && \text{full weighted}\\ &[[A|B]] = \int d\mathbf{\Gamma} A^*(\Gamma) B(\Gamma), \qquad [[A]] = \int d\mathbf{\Gamma} A(\Gamma), && \text{unweighted.}\end{aligned} \tag{2.22}$$

In this work the angular bracket always denotes the equilibrium average if not stated differently (e.g. subscript non).
The formal solution of the Smoluchowski equation (2.19) for the probability density can be written in a simplified form (without using the path integral formalism) if we take into account that the Smoluchowski operator is time independent.

$$\mathcal{P}\left(\Gamma, t\right) = \mathrm{e}^{\Omega t}\mathcal{P}\left(\Gamma, t=0\right). \tag{2.23}$$

We assume the system to be in equilibrium at $t = 0$ so the initial value of the probability density can be identified as an equilibrium probability function known from the thermodynamics.

$$\begin{aligned} &\mathcal{P}\left(\Gamma, t=0\right) \stackrel{!}{=} \mathcal{P}_{\mathrm{eq}} = \frac{1}{Z}\mathrm{e}^{-\beta U(\{\vec{x}_i\})}, \\ &Z = \int d\mathbf{\Gamma}\mathrm{e}^{-\beta U(\{\vec{x}_i\})} \quad \text{beeing the partition sum.} \end{aligned} \tag{2.24}$$

One should notice following properties of the equilibrium probability density:

$$\begin{aligned} &\vec{\partial}_i\mathcal{P}_{\mathrm{eq}} = -\beta\vec{\partial}_i U(\{\vec{x}_i\})\mathcal{P}_{\mathrm{eq}} = \beta\vec{F}_i\mathcal{P}_{\mathrm{eq}}, \\ &\Omega_{\mathrm{eq}}\mathcal{P}_{\mathrm{eq}} = 0, \quad \Rightarrow \quad \Omega\mathcal{P}_{\mathrm{eq}} = \delta\Omega\mathcal{P}_{\mathrm{eq}}. \end{aligned} \tag{2.25}$$

For a general time dependent observable A we can write the time evolution by using the adjoint Smoluchowski operator:

$$\begin{aligned} &\langle A\rangle_{\mathrm{non}}\left(t\right) = \int d\mathbf{\Gamma}\mathcal{P}(\Gamma, t)A(\Gamma) = \int d\mathbf{\Gamma}\mathrm{e}^{\Omega t}\mathcal{P}_{\mathrm{eq}}A(\Gamma) = \int d\mathbf{\Gamma}\mathcal{P}_{\mathrm{eq}}\mathrm{e}^{\Omega^\dagger t}A(\Gamma) = \langle A(t)\rangle \\ &A(\Gamma, t) = \mathrm{e}^{\Omega^\dagger t}A(\Gamma, t=0), \end{aligned} \tag{2.26}$$

with the adjoint Smoluchowski operator $\Omega^\dagger$ with respect to the unweighted scalar product.

$$[[A\Omega B]] = [[B\Omega^\dagger A]]. \tag{2.27}$$

By applying integration by parts twice and dropping the surface terms the adjoint Smoluchowski operator for the ABD can be calculated.

$$\boxed{\Omega^\dagger = \sum_i D_t\left(\vec{\partial}_i + \beta\vec{F}_i\right)\cdot\vec{\partial}_i + v_0\vec{o}_i\cdot\vec{\partial}_i + D_r\partial^2_{\varphi_i}.} \tag{2.28}$$

2.2.3 Integration Through Transients

By dealing with non-equilibrium averages e.g. non-equilibrium velocity or non-equilibrium structure factor, one needs to solve the full Smoluchowski equation

for the probability distribution function $\mathcal{P}(\Gamma, t)$. The Integration Through Transients (ITT) provides an elegant method to express non-equilibrium averages by equilibrium averages over a time integral of correlation functions. For the time integral all the transients of the correlation function are needed. The correlation function of the active force which drives the system out of equilibrium can be determined by the projection formalism of Mori and Zwanzig [34, 35] which will be introduced in great detail in the next chapter. We use the formal solution of the Smoluchowski equation for $\mathcal{P}$ and use $\mathrm{e}^{\Omega t} = 1 + \int_0^t dt' \mathrm{e}^{\Omega t'} \Omega$. For a general time dependent observable $A(\Gamma, t)$ we derive the ITT formalism.

$$\begin{aligned}
\langle A \rangle_{\text{non}}(t) &= \int d\mathbf{\Gamma} \mathcal{P}(\Gamma, t) A(\Gamma) = \int d\mathbf{\Gamma} A(\Gamma) \mathrm{e}^{\Omega t} \mathcal{P}_{\text{eq}}(\Gamma) \\
&= \int d\mathbf{\Gamma} A(\Gamma) \left(1 + \int_0^t dt' \mathrm{e}^{\Omega t'} \Omega\right) \mathcal{P}_{\text{eq}}(\Gamma) \\
&\overset{2.25}{=} \langle A \rangle + \int d\Gamma A(\Gamma) \int_0^t dt' \mathrm{e}^{\Omega t'} \delta\Omega \mathcal{P}_{\text{eq}} \\
&\overset{2.20}{=} \langle A \rangle - v_0 \beta \sum_i \int d\mathbf{\Gamma} A(\Gamma) \int_0^t dt' \mathrm{e}^{\Omega t'} \vec{o}_i \cdot \vec{F}_i \mathcal{P}_{\text{eq}} \\
&\overset{2.27}{=} \langle A \rangle - v_0 \beta \sum_i \int_0^t dt' \left\langle \vec{o}_i \cdot \vec{F}_i \mathrm{e}^{\Omega^\dagger t'} A(\Gamma) \right\rangle .
\end{aligned} \tag{2.29}$$

This is the generalized Green Kubo relation, where the non-equilibrium average of a phase space observable A is expressed by the equilibrium averages only, at the cost of having to evaluate the time integral of the correlation function. Up to this point it is not clear at all how to evaluate the correlation function including the adjoint Smoluchowski operator. The necessary tools to evaluate correlation functions of this kind nonperturbatively will be derived in the next chapter.

2.3 Dimensional Analysis

We take a close look at the Smoluchowski operator describing the dynamics of all configuration space observables. It depends on 4 undetermined parameters:

- Translation diffusion $D_t \leftrightarrow$ Translational strength of thermal kicks.
- Rotational diffusion $D_r \leftrightarrow$ Rotational strength of thermal kicks.
- Self-propulsion velocity $v_0 \leftrightarrow$ Strength of non-equilibrium driving force.
- Particle diameter $\sigma \leftrightarrow$ Entering the hard disk potential 2.18.

Now we want to link the abstract parameters to real physical values mentioned in the introductory part and express all quantities as a function of D_t and σ. We assume the Brownian disks to be of the size $0.5\,\mu$m and have a swim velocity of $1-100\,\mu$m/sec. In equilibrium the diffusion constant satisfies the Stokes-Einstein relation

$$D_t = \frac{k_B T}{3\pi\eta\sigma} \sim 1\,\mu\mathrm{m}^2/\mathrm{sec}. \tag{2.30}$$

In the following table the connection between the physical units and the model units used in following chapters are illustrated.

Quantity	Physical Units	Model Units
D_t	$1\,\mu\mathrm{m}^2/\mathrm{sec}$	$1\,[D_t]$
σ	$0.5\,\mu\mathrm{m}$	$1\,[\sigma]$
v_0	$1-100\,\mu\mathrm{m}/\mathrm{sec}$	$0.5-50\,[D_t/\sigma]$
D_r	sec^{-1}	$1/4\,[D_t/\sigma^2]$
t	sec	$4\,[\sigma^2/D_t]$

Table 2.1: Link between physical units and the model units for relevant quantities.

One should notice that the rotational diffusion is a free to choose parameter in our model (and is not calculated by the Stokes-Einstein formula). That fact is motivated by the existence of microswimmers with long persistence length $l_p = v_0/D_r$ modeled by choosing $D_r \ll D_t/\sigma^2$ [36].

2.4 Summary

In this chapter we introduced the main model in this work the active Brownian hard disks in two dimensions. The model is characterized by being intrinsically out of equilibrium since the particles not only undergo Brownian motion (rotational and translational) they are also self-propelled. Constant input of energy is needed to maintain the active force.
The Smoluchowski equation of motion was derived from the Langevin equation, by transforming the stochastic differential equation for the coordinates vector to a deterministic equation of the probability density.
Finally we introduced the Integration Through Transients formalism being an elegant method for evaluating non-equilibrium averages by calculating time integrals over the whole past of the force correlation function. By calculating the force correlation function the problem arises by not knowing how to evaluate the time evolution term $\mathrm{e}^{\Omega^\dagger t}$. Performing series expansion does not lead to the desired result since the term $\Omega^\dagger t$ is by no means a small quantity. In the next chapter we

introduce a method which makes it feasible to calculate correlations of this kind by using the projection formalism of Mori and Zwanzig and using the Mode Coupling approximation.

Chapter 3

Main Theory

This chapter will be the key chapter in this work where we will introduce the main theoretical framework the whole thesis is based on. We extend the Mode Coupling Theory of the glass transition derived for passive Brownian Particles by Gazuz and Fuchs [37], to active Brownian particles. The main goal will be to get deeper theoretical understanding of the glassy dynamics in active systems, especially how the glass-transition point depends on activity v_0 and the rotational diffusion D_r which is still an open question.
The central quantity by dealing with glassy systems is the dynamical structure factor (or time dependent density-density correlator) which provides information about glassy physics without the need to track the trajectories of all particles. The dynamical structure factor is closely related to the cross-section in the neutron scattering experiments and is also experimentally an accessible quantity.

3.1 Density-Density-Correlator

3.1.1 Dynamical Structure Factor

We start describing the dynamics of the system by introducing the density function in real space, which will be a sum of the products of delta peaks at the positions of the particles and their orientations

$$\rho\left(\vec{x},\varphi,t\right)=\sum_{j=1}^{N}\delta\left(\vec{x}-\vec{x}_j(t)\right)\delta\left(\varphi-\varphi_j(t)\right). \tag{3.1}$$

It is more convenient to transform the density function into the Fourier space

$$\rho_l(\vec{q},t)=\int_{-\infty}^{\infty}d\vec{x}\int_{-\infty}^{\infty}d\varphi \mathrm{e}^{i\vec{x}\cdot\vec{q}}\mathrm{e}^{i\varphi l}\rho\left(\vec{x},\varphi.t\right)=\sum_{j=1}^{N}\mathrm{e}^{i\vec{q}\cdot\vec{x}_j(t)}\mathrm{e}^{il\phi_j(t)}. \tag{3.2}$$

The subindex l the so-called orientational index is the Fourier counterpart of the angle φ and is the key feature of the active system. In three dimensions general rotations are described by 3 Euler angles and the corresponding density function in Fourier space contains 3 orientational indices (calculations in 3D are performed in great detail in [38–40]). The Fourier-transform of the coordinate vector $\vec{x}$ is the well known wave vector $\vec{q}$.
The time evolution of the density function is described by the adjoint Smoluchowski operator introduced in previous chapter

$$\Omega^{\dagger} = \sum_i D_t \left(\vec{\partial}_i + \beta \vec{F}_i \right) \cdot \vec{\partial}_i + v_0 \vec{o}_i \cdot \vec{\partial}_i + D_r \partial^2_{\varphi_i}. \tag{3.3}$$

The quantity that describes how much of the initial configuration remains unchanged after the time t, is called the "dynamical structure factor" or "time dependent density-density correlator" (in experiments also called intermediate scattering function [35]), and is closely related to the cross-section in inelastic neutron scattering experiments.

$$\boldsymbol{S}_{l,l'}(\vec{q},t) = \frac{1}{N} \Big\langle \rho_l(\vec{q},t=0)^* \, \rho_{l'}(\vec{q},t) \Big\rangle = \frac{1}{N} \Big\langle \rho_l(\vec{q})^* \, \mathrm{e}^{\Omega^{\dagger} t} \rho_{l'}(\vec{q}) \Big\rangle. \tag{3.4}$$

We point out the matrix like structure of the density correlator in the space of the orientational indices (bold letters mark matrix like functions throughout this work). In the case of passive Brownian particles where the angular motion is completely decoupled from the translation motion the density correlator is a scalar like function. This is one of the major difficulties that arises by switching on the activity. The Fourier-transform of the density correlator to the frequency domain is directly proportional to the differential cross-section in an inelastic neutron scattering experiment [35].

$$\begin{aligned} \hat{\boldsymbol{S}}_{l,l'}(\vec{q},\omega) &= \frac{1}{2\pi} \int_{-\infty}^{\infty} \mathrm{e}^{i\omega t} \boldsymbol{S}_{l,l'}(\vec{q},t) dt \\ \frac{d^2\sigma}{d\Omega d\omega} &\propto \hat{\boldsymbol{S}}_{0,0}(\vec{q},\omega), \end{aligned} \tag{3.5}$$

with σ being the cross section and $d\Omega$ the solid angle.
The density correlator $\boldsymbol{S}$ is an infinite dimensional matrix where each matrix element has different physical meaning. The $l = 0, l' = 0$ component describes the spatial structure of the system and is an important quantity by analyzing the physical properties of the system. Especially effects like "glass transition" , "caging" etc. In the Figure 3.1 typical shapes of the density correlator $\boldsymbol{S}_{0,0}$ for two different cases are presented. The fluid like phase (left panel) characterized by the correlator which decays to zero for long times, exhibits three different regimes.

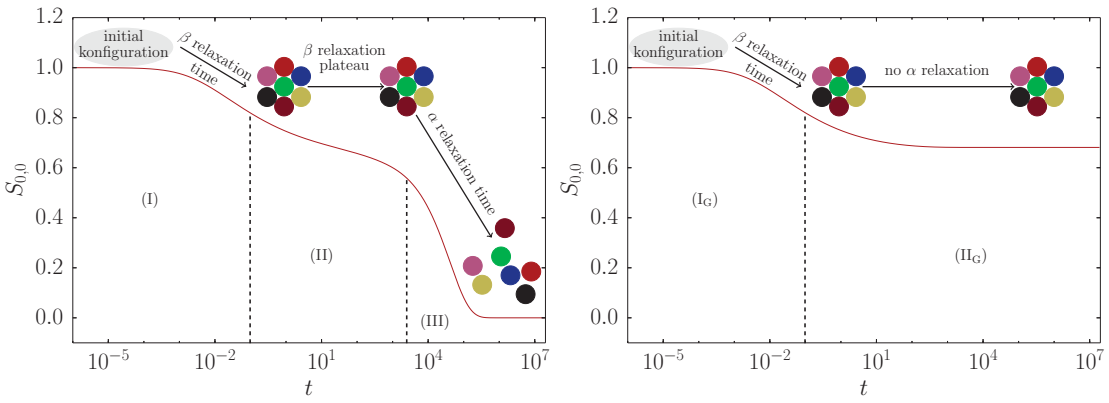

Figure 3.1: Left: Schematic plot for the normalized density correlator $\boldsymbol{S}_{0,0}(t)$ as a function of time for one wavenumber q in a fluid like phase.
Right: Schematic plot of the correlator in a solid like (glassy) phase.

- Region (I): At short time scales due to the free local motion of the particles a decay of the correlator can be observed. The time needed to decay to the first plateau is called the β-relaxation time.

- Region (II): At intermediate times if the control parameters (packing fraction, driving force) of the system are chosen properly the system shows a plateau. The slow change of the correlation function in this time range indicates the local caging of the particles. The surrounding neighbor particles form a cage which hinders the inner particle to move.

- Region (III): The fluid phase is characterized with a third region at long time scales where the cages can break and the correlator decays to zero. The time needed to destroy the cage is called the α-relaxation time. The system where the particles are able to explore the whole phase space over the time is called an "ergodic" system. A fluid like system is also ergodic.

A glassy system (right panel) is characterized by a finite long time value of the correlator $\boldsymbol{F}_{l,l'}(\vec{q}) = \lim_{t\to\infty} \boldsymbol{S}_{l,l'}(\vec{q},t)$ the so-called nonergodicity parameter. Nonergodic systems only exhibit two time regions.

- Region (I$_G$): Similarly to the fluid system at short times due to the free local motion of the particles the correlator decays to the value $\boldsymbol{F}_{0,0}$.

- Region (II$_G$): After the β-relaxation time the system forms a glass, where the particles are in local cages formed by the neighbor particles and the system never relaxes. In a glassy state the α-relaxation never occurs. The system is nonergodic and the particles are not able to explore the whole phase space

even after infinite time. In other words the system never forgets about the initial configuration.

The Mode Coupling theory predicts a critical point in control parameters separating the fluid phase and the glassy phase the so-called glass transition point. Getting closer to the glass transition makes the α-relaxation time increase until it diverges at the critical point. From a mathematical point of view the glass transition point represents a bifurcation with the nonergodicity parameter having a discontinuous jump as function of control parameters.
The initial configuration of the dynamical density correlator is described by the static structure factor and is uniquely determined by the particle-particle interaction potential.

3.1.2 Static Structure Factor

In this section we will introduce the equilibrium static structure factor and the static structure factor matrix describing the structure of the system at initial time. The symbol for the structure factor matrix is the same as for the density correlator. To distinguish those the density correlator will always have the explicit time dependence in parenthesis.

$$\begin{aligned}
&\underbrace{\boldsymbol{S}_{l,l'}(\vec{q})}_{\substack{\text{static structure}\\ \text{factor matrix}}} = \overbrace{\boldsymbol{S}_{l,l'}(\vec{q},t)}^{\text{density correlator}}\Big|_{t=0} = \frac{1}{N}\Big\langle \rho_l^*(\vec{q})\,\rho_{l'}(\vec{q})\Big\rangle = \frac{1}{N}\sum_{j,k}\Big\langle \mathrm{e}^{-i\vec{q}\cdot(\vec{x}_j-\vec{x}_k)}\mathrm{e}^{-i(l\varphi_j-l'\varphi_k)}\Big\rangle,\\
&\underbrace{\tilde{S}(\vec{q})}_{\substack{\text{static structure}\\ \text{factor}}} \equiv \tilde{S}_q = \frac{1}{N}\Big\langle \rho^*(\vec{q})\rho(\vec{q})\Big\rangle = \frac{1}{N}\sum_{j,k}\Big\langle \mathrm{e}^{-i\vec{q}\cdot(\vec{x}_j-\vec{x}_k)}\Big\rangle,
\end{aligned} \tag{3.6}$$

where the isotropy of the equilibrium structure factor in the wave vector $\vec{q}$ was exploited.
We want to express the static structure factor matrix as a function of the static structure factor. To do so we have to evaluate the equilibrium average of the angular part of the equation (3.6). We split the phase space differential into spatial and angular parts

$$d\boldsymbol{\Gamma} = d\vec{x}_1\cdots d\vec{x}_N d\varphi_1\cdots d\varphi_N = d\boldsymbol{X}\,d\boldsymbol{\Phi}, \tag{3.7}$$

and use the following identities:

$$\begin{aligned}\sum_{j,k} &= \sum_{\substack{j,k\\ j\neq k}} + \sum_{j} \delta_{j,k},\\ \int_0^{2\pi} \mathrm{e}^{-il\varphi} d\varphi &= 2\pi\delta_{l,0}.\end{aligned} \tag{3.8}$$

The expression for the static structure factor matrix can be simplified to a diagonal matrix in the space spanned by the orientational index.

$$\begin{aligned}\boldsymbol{S}_{l,l'}(\vec{q}) =& \frac{1}{N}\sum_{j,k}\int d\boldsymbol{\Gamma}\mathcal{P}_{\mathrm{eq}}\mathrm{e}^{-i\vec{q}\cdot(\vec{x}_j-\vec{x}_k)}\mathrm{e}^{-i(l\varphi_j-l'\varphi_k)}\\ =& \frac{1}{N}\sum_{\substack{j,k\\ j\neq k}}\int d\boldsymbol{X}\mathcal{P}_{\mathrm{eq}}\mathrm{e}^{-i\vec{q}\cdot(\vec{x}_j-\vec{x}_k)}\int d\boldsymbol{\Phi}\mathrm{e}^{-i(l\varphi_j-l'\varphi_k)}\\ &+\frac{1}{N}\sum_{j}\int d\boldsymbol{X}\mathcal{P}_{\mathrm{eq}}\int d\boldsymbol{\Phi}\mathrm{e}^{-i\varphi_j(l-l')} = \Big(\tilde{S}(\vec{q})-1\Big)\delta_{l,0}\delta_{l',0}+\delta_{l,l'},\end{aligned} \tag{3.9}$$

or in matrix notation,

$$\boldsymbol{S}(\vec{q}) = \begin{array}{c} \begin{array}{ccccccc} & & & -1 & 0 & 1 & \\ \end{array}\\ \begin{pmatrix} 1 & & & & & & \\ & \ddots & & & & & \\ & & & 1 & & & \\ & & & & \tilde{S}_q & & \\ & & & & & 1 & \\ & & & & & & \ddots \\ & & & & & & & 1 \end{pmatrix} \end{array} \begin{array}{l} \\ \\ \\ -1\\ 0\\ 1\\ \\ \\ \end{array} \cdot \tag{3.10}$$

We point out that the orientational index formally is in the set of integer numbers $l \in \mathbb{Z}$ and will be restricted to a finite range after introducing a cutoff Λ_l in the next chapters ($l \in \{-\Lambda_l, -\Lambda_l+1, \cdots, -1, 0, 1, \cdots, \Lambda_l-1, \Lambda_l\}$). Due to the hard sphere potential being independent of the angular orientations of the particles the system exhibits only a nontrivial structure for the $l = 0, l' = 0$ mode. We reduced the static structure factor matrix to the static structure factor well known from the literature [35, 41].

The key equation for evaluating the static structure factor is the Ornstein-Zernike equation which makes a link between the direct correlation function $c(r)$ and the

radial distribution function $g(r)$ (or the total correlation function $h(r) = g(r) - 1$) as an integral equation,

$$h(r) = c(r) + \rho \int d\vec{x} c(|\vec{x} - \vec{r}|) h(|\vec{x}|). \tag{3.11}$$

With the particle density $\rho = N/V$ not to be confused with the packing fraction ϕ (in 2D $\phi = \frac{\pi}{4}\rho$).
On the other hand in Fourier space the direct correlation function and the structure factor have an algebraic dependence.

$$\tilde{S}_q = \frac{1}{1 - \rho c_q}. \tag{3.12}$$

Although computer simulations make the structure factor an accessible quantity, for theoretical calculations it is often beneficial to have an analytic expression available. To solve the Ornstein-Zernike equation 3.11 an additional closure relation for the direct correlation function is needed. There are different closure relations which depend on the interaction potential. For hard-core potentials mainly Mean-spherical approximation [42] and the Percus-Yevic approximation [43] are used.

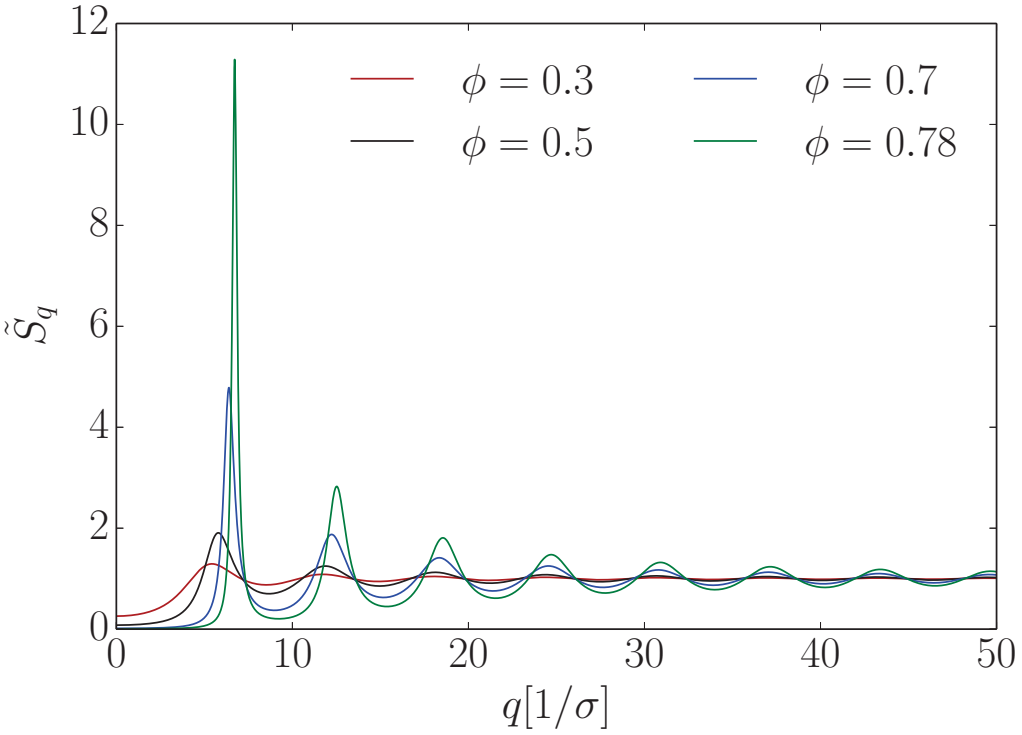

Figure 3.2: Equilibrium static structure factor for different packing fractions ϕ as a function of wavenumber q calculated by the method introduced in [44].

They both can be solved analytically in three dimensions and are in accordance with each other. Unfortunately the Percus-Yevic approximation can only be solved in closed form in odd dimensions, therefore in two dimensions numerical methods are needed to obtain the desired structure factor.
An alternative method was developed by Marc Baus and Jean-Louis Colot [44] to approximate the Percus-Yevic closure in two dimensions analytically. In the Figure 3.2 the static structure factor for different packing fractions is plotted. In this work the results for the structure factor calculated by the method by Baus and Colot will be used, making the quantity easily accessible for all packing fractions and all wavenumbers without solving the Ornstein-Zernike equation numerically.

3.1.3 Transformation Properties of the Correlator

Before introducing the projection formalism we want to discuss the transformation properties of the density correlator under the rotations of the wave vector $(\{q, \alpha_q\}) \to (\{q, \alpha_q + \beta\})$ and check if the following approximations in the next sections sustain the transformation properties. Unlike for the passive system for the active system the density correlator does not only depend on the magnitude of the wave vector, the angle of the wave vector with respect to the particle orientation also becomes important. So rotating the wave vector by an angle of β is equivalent to changing the orientation of each particle by β.

$$\begin{aligned}\boldsymbol{S}_{l,l'}(\{q, \alpha_q + \beta\}, t) &= \frac{1}{N} \sum_{i,j} \left\langle \mathrm{e}^{-i\vec{q}\cdot\vec{x}_i} \mathrm{e}^{-il(\varphi_i+\beta)} \mathrm{e}^{\Omega^\dagger t} \mathrm{e}^{i\vec{q}\cdot\vec{x}_j} \mathrm{e}^{il'(\varphi_j+\beta)} \right\rangle \\ &= \sum_{n,m} \boldsymbol{u}_{l,n}(\beta) \boldsymbol{S}_{n,m}(\{q, \alpha_q\}, t) \boldsymbol{u}^\dagger_{m,l'}(\beta),\end{aligned} \tag{3.13}$$

with the unitary transformation matrix:

$$\begin{aligned}&\boldsymbol{u}_{l_1,l_2}(\alpha) = \mathrm{e}^{-il_1\alpha} \delta_{l_1,l_2}, \\ &\boldsymbol{u}(\alpha)\, \boldsymbol{u}(\beta) \equiv \boldsymbol{u}(\alpha + \beta) \quad \forall\, \alpha, \beta, \\ &\boldsymbol{u}(\alpha)\, \boldsymbol{u}^\dagger(\alpha) \equiv \mathrm{Id} \quad \forall\, \alpha.\end{aligned} \tag{3.14}$$

In compact matrix notation the transformation property of the density correlator is given by:

$$\boxed{\boldsymbol{S}(\{q, \alpha_q + \beta\}, t) = \boldsymbol{u}(\beta) \boldsymbol{S}(\{q, \alpha_q\}, t) \boldsymbol{u}^\dagger(\beta), \qquad \text{Transformation property.}} \tag{3.15}$$

3.2 Projection Formalism

In this section we will introduce the projection formalism by Mori and Zwanzig and derive the equation of motion for the dynamical density function presented in

the previous section. The main idea of the Mori-Zwanzing (MZ) formalism is to rewrite the time evolution equation for the density correlator in a mathematically identical integro-differential equation that is better suited for further approximations. Deriving the equation of motion relies frequently on transforming from time domain to Laplace domain.

3.2.1 Laplace-Transform and its Properties

The Laplace-transform (LT) is an integral transform which transforms a function from real valued time domain to a generally complex valued frequency domain. Like in case of Fourier-transform it is a useful method to convert ordinary differential equations in an algebraic ones. We use a more common definition for the Laplace-transformation of the function f.

$$\hat{f}(z) = \int_0^\infty \mathrm{e}^{-zt} f(t) dt. \tag{3.16}$$

The frequency z is generally a complex valued frequency and if the integral exists the function $\hat{f}$ is called the Laplace transform of the function f. In the following we want to list and prove many of the properties for the Laplace-transformation successively used in latter chapters.

- The Laplace transform transforms the convolution of two general operators $\boldsymbol{M}$ and $\boldsymbol{S}$ to the product of the Laplace transform of each.

$$\begin{aligned}
\mathrm{LT}\Big[\left(\boldsymbol{M} * \boldsymbol{S}\right)(t) \Big] &= \int_0^\infty \mathrm{e}^{-zt} dt \int_0^t dt' \boldsymbol{M}\left(t-t'\right) \boldsymbol{S}\left(t'\right) \\
&= \int_0^\infty dt' \int_{t'}^\infty dt \mathrm{e}^{-zt} \boldsymbol{M}\left(t-t'\right) \boldsymbol{S}\left(t'\right) \\
&= \int_0^\infty dt' \int_0^\infty ds \mathrm{e}^{-z(s+t')} \boldsymbol{M}\left(s\right) \boldsymbol{S}\left(t'\right) \\
&= \int_0^\infty ds \mathrm{e}^{-zs} \boldsymbol{M}\left(s\right) \int_0^\infty dt' \mathrm{e}^{-zt'} \boldsymbol{S}\left(t'\right) = \hat{\boldsymbol{M}}\left(z\right) \hat{\boldsymbol{S}}\left(z\right).
\end{aligned} \tag{3.17}$$

- The LT of the derivative in time domain gets transformed to an ordinary algebraic expression in Laplace domain.

$$\mathrm{LT}\Big[\partial_t \boldsymbol{S}\left(t\right)\Big] = \int_0^\infty dt \mathrm{e}^{-zt} \partial_t \boldsymbol{S}\left(t\right) \overset{\mathrm{PI}}{=} -\boldsymbol{S}\left(0\right) + z\hat{\boldsymbol{S}}\left(z\right) \tag{3.18}$$

- LT is also very useful to analyze the long time values of an observable.

$$\lim_{z\to 0} z\hat{\boldsymbol{S}}\left(z\right) = \lim_{z\to 0} \mathrm{LT}\Big[\partial_t \boldsymbol{S}\left(t\right)\Big] + \boldsymbol{S}(0) = \int_0^\infty dt \partial_t \boldsymbol{S}\left(t\right) + \boldsymbol{S}(0) = \lim_{t\to\infty} \boldsymbol{S}\left(t\right) \tag{3.19}$$

- Es an example we present the Laplace transform of important functions frequently used in this work. For a general operator $\boldsymbol{A}$ and a real valued time variable t we write:

$$\mathrm{LT}\Big[\mathrm{e}^{\boldsymbol{A}t}\Big](z) = \int_0^t dt \mathrm{e}^{-zt}\mathrm{e}^{\boldsymbol{A}t} = \Big[z\mathbb{I} - \boldsymbol{A}\Big]^{-1}, \tag{3.20}$$

$$\mathrm{LT}\left[\left(\frac{t}{t_0}\right)^{-\alpha}\right](z) = z^{\alpha-1}\overbrace{\Gamma(1-\alpha)}^{\substack{\text{Euler gamma}\\ \text{function}}}/t_0, \quad \alpha, t_0 \in \mathbb{R} \wedge \alpha < 1. \tag{3.21}$$

By using the Laplace transform of the exponential function we can prove the Dyson decomposition formula used to evaluate exponentials of sums of noncommuting operators like the Baker-Campbell-Hausdorff formula known from quantum mechanics.

$$\begin{aligned}\mathrm{LT}\Big[\mathrm{e}^{(\boldsymbol{A}+\boldsymbol{B})t}\Big](z) =& \Big[z\mathbb{I} - \boldsymbol{A} - \boldsymbol{B}\Big]^{-1} = \Big[z\mathbb{I} - \boldsymbol{A}\Big]^{-1} + \Big[z\mathbb{I} - \boldsymbol{A}\Big]^{-1}\boldsymbol{B}\Big[z\mathbb{I} - \boldsymbol{A} - \boldsymbol{B}\Big]^{-1} \\ =& \mathrm{LT}\Big[\mathrm{e}^{\boldsymbol{A}t}\Big](z) + \mathrm{LT}\Big[\mathrm{e}^{\boldsymbol{A}t}\Big](z)\mathrm{LT}\Big[\boldsymbol{B}\mathrm{e}^{(\boldsymbol{A}+\boldsymbol{B})t}\Big](z),\end{aligned} \tag{3.22}$$

$$\boxed{\mathrm{e}^{(\boldsymbol{A}+\boldsymbol{B})t} = \mathrm{e}^{\boldsymbol{A}t} + \int_0^t \mathrm{e}^{\boldsymbol{A}t'}\boldsymbol{B}\mathrm{e}^{(\boldsymbol{A}+\boldsymbol{B})(t-t')}dt' \equiv \mathrm{e}^{\boldsymbol{A}t} + \int_0^t \mathrm{e}^{(\boldsymbol{A}+\boldsymbol{B})t'}\boldsymbol{B}\mathrm{e}^{\boldsymbol{A}(t-t')}dt'}. \tag{3.23}$$

Unlike the Baker-Campbell-Hausdorff expansion formula the Dyson decomposition is an exact conversion and is better suited for non-equilibrium problems where the time evolution operator is not nilpotent and the expansion can not be stopped after finite number of terms.

3.2.2 Mori-Zwanzig Equation of Motion

With the Dyson decomposition identity and the Laplace transform we derived sufficient tools to proceed further by analyzing the dynamics of the time dependent density correlator. The projection formalism of Mori and Zwanzig is based on separating "relevant" and "irrelevant" variables by introducing projectors $\boldsymbol{P}$ and $\boldsymbol{Q}$. In the case of active Brownian disks density function $\rho_l(\vec{q})$ is a relevant

variable and can be used to project to it. Also a product of densities is a relevant variable and will be used in the next section by performing the Mode Coupling approximation.
We recall the definition of the time dependent density correlator from the last chapter (3.4).

$$\boldsymbol{S}_{l,l'}\left(\vec{q},t\right)=\frac{1}{N}\Big\langle\rho_l\left(\vec{q}\right)^*\,\mathrm{e}^{\Omega^\dagger t}\rho_{l'}\left(\vec{q}\right)\Big\rangle. \tag{3.24}$$

To split the observable in relevant and irrelevant components we have to introduce a projector $\boldsymbol{P}$ which projects into the density state and the corresponding projector $\boldsymbol{Q}$, that is perpendicular to $\boldsymbol{P}$. In other words the projector $\boldsymbol{P}$ projects to the relevant components and the projector $\boldsymbol{Q}$ to the irrelevant components of an observable.

$$\boldsymbol{P}=\sum_{l,l',\vec{q}}\Big|\rho_l\left(\vec{q}\right)\Big\rangle\mathcal{N}_{l,l'}\Big\langle\rho_{l'}\left(\vec{q}\right)^*\Big|,\quad \boldsymbol{Q}=\mathbb{I}-\boldsymbol{P}. \tag{3.25}$$

Since $\boldsymbol{P}$ and $\boldsymbol{Q}$ are projectors they fulfill the projector properties. Applying a projector for the second time to an observable should not change the result, so the projector is idempotent and the normalization factor $\mathcal{N}_{l,l'}$ can be determined.

$$\begin{aligned}\boldsymbol{P}&\overset{!}{=}\boldsymbol{P}\boldsymbol{P}=\sum_{\substack{l_1,l_2,\vec{q}\\ l_3,l_4,\vec{p}}}\Big|\rho_{l_1}\left(\vec{q}\right)\Big\rangle\mathcal{N}_{l_1,l_2}\underbrace{\Big\langle\rho_{l_2}\left(\vec{q}\right)^*\rho_{l_3}\left(\vec{p}\right)\Big\rangle}_{N\boldsymbol{S}_{l_2,l_3}\delta_{\vec{q},\vec{p}}}\mathcal{N}_{l_3,l_4}\Big\langle\rho_{l_4}\left(\vec{p}\right)^*\Big|,\\ \Rightarrow\boldsymbol{P}&=\frac{1}{N}\sum_{l,l',\vec{q}}\Big|\rho_l\left(\vec{q}\right)\Big\rangle\boldsymbol{S}^{-1}_{l,l'}(\vec{q})\Big\langle\rho_{l'}\left(\vec{q}\right)^*\Big|.\end{aligned} \tag{3.26}$$

By construction $\boldsymbol{P}$ and $\boldsymbol{Q}$ are perpendicular to each other and both projectors applied to an observable vanish $\boldsymbol{P}\boldsymbol{Q}=\boldsymbol{Q}\boldsymbol{P}=0$.
Using the projectors $\boldsymbol{P}$, $\boldsymbol{Q}$ and the Dyson decomposition allows us to rewrite the time evolution equation for the density correlator as an integro-differential equation with a memory kernel containing all the information about the past.

$$
\begin{aligned}
\partial_t \boldsymbol{S}_{l,l'}(\vec{q},t) =& \frac{1}{N}\Big\langle \rho_l(\vec{q})^* \,\Omega^\dagger \mathrm{e}^{\Omega^\dagger t}\rho_{l'}(\vec{q})\Big\rangle = \frac{1}{N}\Big\langle \rho_l(\vec{q})^* \,\Omega^\dagger \overbrace{\Big(\boldsymbol{P}+\boldsymbol{Q}\Big)}^{\mathbb{I}} \mathrm{e}^{\Omega^\dagger t}\rho_{l'}(\vec{q})\Big\rangle \\
=& \frac{1}{N}\Big\langle \rho_l(\vec{q})^* \,\Omega^\dagger \boldsymbol{Q}\mathrm{e}^{\Omega^\dagger t}\rho_{l'}(\vec{q})\Big\rangle \\
&+ \frac{1}{N^2}\sum_{l_1,l_2} \underbrace{\Big\langle \rho_l(\vec{q})^* \,\Omega^\dagger \rho_{l_1}(\vec{q})\Big\rangle}_{-N\boldsymbol{\omega}_{l,l_1}(\vec{q})} \boldsymbol{S}^{-1}_{l_1,l_2}(\vec{q})\Big\langle \rho_{l_2}(\vec{q})^* \,\mathrm{e}^{\Omega^\dagger t}\rho_{l'}(\vec{q})\Big\rangle \\
\overset{3.22}{=}& -\sum_{l_1,l_2}\boldsymbol{\omega}_{l,l_1}(\vec{q})\,\boldsymbol{S}^{-1}_{l_1,l_2}(\vec{q})\,\boldsymbol{S}_{l_2,l'}(\vec{q},t) \\
&+ \frac{1}{N}\int_0^t dt' \Big\langle \rho_l(\boldsymbol{q})^* \,\Omega^\dagger \boldsymbol{Q}\mathrm{e}^{\Omega^\dagger \boldsymbol{Q}(t-t')}\Omega^\dagger \boldsymbol{P}\mathrm{e}^{\Omega^\dagger t'}\rho_{l'}(\boldsymbol{q})\Big\rangle \\
=& -\sum_{l_1,l_2}\boldsymbol{\omega}_{l,l_1}(\vec{q})\,\boldsymbol{S}^{-1}_{l_1,l_2}(\vec{q})\,\boldsymbol{S}_{l_2,l'}(\vec{q},t) \\
&+ \sum_{l_1,l_2}\int_0^t dt' \boldsymbol{M}_{l,l_1}(\vec{q},t-t')\,\boldsymbol{S}^{-1}_{l_1,l_2}(\vec{q})\,\boldsymbol{S}_{l_2,l'}(\vec{q},t').
\end{aligned}
\tag{3.27}
$$

The final equation can also be written in a matrix notation where the partial derivative and the integral act component wise.

$$
\boxed{\partial_t \boldsymbol{S}(\vec{q},t) = -\boldsymbol{\omega}(\vec{q})\,\boldsymbol{S}^{-1}(\vec{q})\,\boldsymbol{S}(\vec{q},t) + \int_0^t dt' \boldsymbol{M}(\vec{q},t-t')\,\boldsymbol{S}^{-1}(\vec{q})\,\boldsymbol{S}(\vec{q},t')}, \tag{3.28}
$$

where a frequency matrix $\boldsymbol{\omega}$ and the memory kernel matrix $\boldsymbol{M}$ were defined.

$$
\begin{aligned}
\boldsymbol{\omega}_{l_1,l_2}(\vec{q}) &= -\frac{1}{N}\Big\langle \rho_{l_1}(\vec{q})^* \,\Omega^\dagger \rho_{l_2}(\vec{q})\Big\rangle, \\
\boldsymbol{M}_{l_1,l_2}(\vec{q},t) &= \frac{1}{N}\Big\langle \rho_{l_1}(\vec{q})^* \,\Omega^\dagger \boldsymbol{Q}\mathrm{e}^{\boldsymbol{Q}\Omega^\dagger \boldsymbol{Q}t}\boldsymbol{Q}\Omega^\dagger \rho_{l_2}(\vec{q})\Big\rangle.
\end{aligned}
\tag{3.29}
$$

It is remarkable that although the equation (3.28) looks much more complicated than the definition from last section (3.4), from a mathematical point of view they are identical.
For deeper understanding of the equation (3.28) especially to analyze its long time behavior we transform it into the Laplace space. For better readability we omit the wavenumber dependence.

$$
\begin{aligned}
z\boldsymbol{S}(z) - \boldsymbol{S} &= -\boldsymbol{\omega}\boldsymbol{S}^{-1}\boldsymbol{S}(z) + \boldsymbol{M}(z)\boldsymbol{S}^{-1}\boldsymbol{S}(z) \\
\Rightarrow \boldsymbol{S}(z) &= \Big[z\mathbb{I} + \boldsymbol{\omega}\boldsymbol{S}^{-1} - \boldsymbol{M}(z)\boldsymbol{S}^{-1}\Big]^{-1}\boldsymbol{S}.
\end{aligned}
\tag{3.30}
$$

For very high densities when the system exhibits glassy behavior the density correlator decays to finite value for very long times. Finite long time value in real space corresponds to $1/z$ pole for the correlator in Laplace space as $z \to 0$. To achieve a $1/z$ divergence the frequency function $\boldsymbol{\omega}$ and the memory kernel $\boldsymbol{M}(z)$ have to cancel each other as $z \to 0$.

$$\text{Glassy state:} \quad \lim_{z\to 0}\Big(\boldsymbol{\omega} - \boldsymbol{M}(z)\Big) = 0, \tag{3.31}$$

this kind of condition is very unstable under further approximations of the memory kernel that will be done in the next section. In particular the expression $\boldsymbol{\omega} - \boldsymbol{M}(z)$ can become negative which is a further problem. On the other hand approximations of $\boldsymbol{M}$ are necessary to close the equation (3.28).
To describe the glassy dynamics properly we need to do a second projection of the equation (3.28), successfully performed for passive Brownian particles by Szamel and Löwen [24].
The goal is now to find a projector which generates a second type of memory kernel $\boldsymbol{m}$, with $\boldsymbol{m}^{-1}(z) \stackrel{!}{=} 0$ as $z \to 0$ in the glassy state. That kind of condition is much more stable under approximations and easily satisfied by $\lim_{t\to\infty} \boldsymbol{m}(t) = \text{const}$.
One possible projector projecting to relevant variables would be:

$$\boldsymbol{P}_1 = -\frac{1}{N}\sum_{l_1,l_2,\vec{q}} \Big|\rho_{l_1}(\vec{q})\Big\rangle \boldsymbol{\omega}^{-1}_{l_1,l_2}(\vec{q}) \Big\langle \rho_{l_2}(\vec{q})^* \Omega^\dagger\Big|, \quad \boldsymbol{Q}_1 = \mathbb{I} - \boldsymbol{P}_1, \tag{3.32}$$

with the normalization factor $-1/N\boldsymbol{\omega}^{-1}_{l_1,l_2}(\vec{q})$ chosen to fulfill the idempotency criterion. We apply the Dyson decomposition formula at the original memory kernel from (3.29).

$$\begin{aligned}
\boldsymbol{M}_{l,l'}(\vec{q},t) =& \frac{1}{N}\Big\langle \rho_l(\vec{q})^* \Omega^\dagger \mathrm{e}^{\boldsymbol{Q}\Omega^\dagger \overbrace{(\boldsymbol{P}_1+\boldsymbol{Q}_1)}^{\mathbb{I}} t} \boldsymbol{Q}\Omega^\dagger \rho_{l'}(\vec{q})\Big\rangle \\
\stackrel{3.22}{=}& \frac{1}{N}\Big\langle \rho_l(\vec{q})^* \Omega^\dagger \mathrm{e}^{\boldsymbol{Q}\Omega^\dagger \boldsymbol{Q}_1 t} \boldsymbol{Q}\Omega^\dagger \rho_{l'}(\vec{q})\Big\rangle \\
&+ \frac{1}{N}\int_0^t dt' \Big\langle \rho_l(\vec{q})^* \Omega^\dagger \mathrm{e}^{\boldsymbol{Q}\Omega^\dagger \boldsymbol{Q}_1 t'} \boldsymbol{Q}\Omega^\dagger \boldsymbol{P}_1 \mathrm{e}^{\boldsymbol{Q}\Omega^\dagger (t-t')} \boldsymbol{Q}\Omega^\dagger \rho_{l'}(\vec{q})\Big\rangle \\
=& \boldsymbol{m}_{l.l'}(\vec{q},t) - \sum_{l_1,l_2}\int_0^t dt' \boldsymbol{m}_{l,l_1}(\vec{q},t')\,\boldsymbol{\omega}^{-1}_{l_1,l_2}(\vec{q}) \boldsymbol{M}_{l_2,l'}(\vec{q},t-t'),
\end{aligned} \tag{3.33}$$

or written as a matrix

$$\boxed{\boldsymbol{M}(\vec{q},t) = \boldsymbol{m}(\vec{q},t) - \int_0^t dt' \boldsymbol{m}(\vec{q},t')\,\boldsymbol{\omega}^{-1}(\vec{q})\boldsymbol{M}(\vec{q},t-t')}. \tag{3.34}$$

The memory kernel $\boldsymbol{m}$ also called irreducible memory kernel (or friction kernel in the literature), has almost identical structure as $\boldsymbol{M}$, the only difference is the appearance of the irreducible Smoluchowski operator instead of the full Smoluchowski operator.

$$\begin{aligned}\boldsymbol{m}_{l_1,l_2}(\vec{q},t) &= \frac{1}{N}\Big\langle \rho_{l_1}(\vec{q})^* \,\Omega^\dagger \boldsymbol{Q} \mathrm{e}^{\boldsymbol{Q}\Omega^{\dagger,\mathrm{irr}}\boldsymbol{Q}t}\boldsymbol{Q}\Omega^\dagger \rho_{l_2}(\vec{q})\Big\rangle,\\ \underbrace{\Omega^{\dagger,\mathrm{irr}}}_{\substack{\text{Irreducible Smoluchowski}\\ \text{operator}}} &= \Omega^\dagger \boldsymbol{Q}_1 = \Omega^\dagger + \frac{1}{N}\sum_{l_1,l_2,\vec{q}} \Omega^\dagger \Big|\rho_{l_1}(\vec{q})\Big\rangle \boldsymbol{\omega}^{-1}_{l_1,l_2}(\vec{q}) \Big\langle \rho_{l_2}(\vec{q})^* \,\Omega^\dagger\Big|.\end{aligned} \tag{3.35}$$

In order to rewrite the equation of motion (3.28) in terms of the irreducible memory kernel, the integral equation (3.34) has to be transformed to the Laplace domain (the wavenumbers will be omitted).

$$\boldsymbol{M}(z) = \boldsymbol{m}(z) - \boldsymbol{m}(z)\boldsymbol{\omega}^{-1}\boldsymbol{M}(z) \quad \Rightarrow \quad \boldsymbol{M}(z) = \Big[\boldsymbol{m}^{-1}(z) + \boldsymbol{\omega}^{-1}\Big]^{-1}, \tag{3.36}$$

inserting above expression in (3.28) leads to:

$$\begin{aligned} z\boldsymbol{S}(z) - \boldsymbol{S} &= -\boldsymbol{\omega}\boldsymbol{S}^{-1}\boldsymbol{S}(z) + \Big[\boldsymbol{m}^{-1}(z) + \boldsymbol{\omega}^{-1}\Big]^{-1}\boldsymbol{S}^{-1}\boldsymbol{S}(z)\\ \Rightarrow\; z\boldsymbol{S}(z) - \boldsymbol{S} &= -\boldsymbol{\omega}\boldsymbol{S}^{-1}\boldsymbol{S}(z) - \boldsymbol{m}(z)\boldsymbol{\omega}^{-1}\Big[z\boldsymbol{S}(z) - \boldsymbol{S}\Big], \end{aligned} \tag{3.37}$$

in the time domain corresponding to

$$\boxed{\partial_t \boldsymbol{S}(\vec{q},t) = -\boldsymbol{\omega}(\vec{q})\,\boldsymbol{S}^{-1}(\vec{q})\,\boldsymbol{S}(\vec{q},t) - \int_0^t dt' \boldsymbol{m}(\vec{q},t-t')\,\boldsymbol{\omega}^{-1}(\vec{q})\,\partial_{t'}\boldsymbol{S}(\vec{q},t')}. \tag{3.38}$$

The key equation describing the dynamics of the density correlator as an integro-differential equation containing the irreducible memory kernel that will be approximated in the next section by applying the Mode Coupling theory was derived.
To check that the second projection into the relevant variables corresponds to the more stable condition for $\boldsymbol{m}$ we again analyze the long time behavior of the correlator.

$$\boldsymbol{S}(z) = \Big[\mathbb{I}z + \boldsymbol{\omega}\boldsymbol{S}^{-1} - \big(\boldsymbol{m}^{-1}(z) + \boldsymbol{\omega}^{-1}\big)^{-1}\boldsymbol{S}^{-1}\Big]^{-1}\boldsymbol{S} \tag{3.39}$$

The correlator will have a $1/z$ pole as $z \to 0$ if:

$$\lim_{z\to 0}\Big[\boldsymbol{\omega} - \big(\boldsymbol{m}^{-1} + \boldsymbol{\omega}^{-1}\big)^{-1}\Big] \stackrel{!}{=} 0 \quad \Rightarrow \quad \lim_{z\to 0}\boldsymbol{m}(z) \to \infty. \tag{3.40}$$

Indeed the irreducible memory kernel needs to have a finite long time value to exhibit glassy behavior of the system. As shown in later chapters using the irreducible memory kernel is sufficient to describe glassy behavior. So the translational

degrees of freedom will "freeze" but simultaneously the rotations will also freeze, which is not the desired result by working with hard disks with zero surface friction. To avoid those problems the memory kernel will need to get splitted in its translational and rotational parts before making the MCT approximations. The tensorial structure of the frequency matrix allows us to achieve the splitting of translational and rotational relaxation the first being nonergodic and latter ergodic. The splitting will be done in detail in the next section.
The equation of motion (3.28) contains four tensorial quantities.

- Static structure factor matrix $\boldsymbol{S}(\vec{q})$: An accessible quantity derived in last section.
- Dynamical density correlator $\boldsymbol{S}(\vec{q},t)$: The quantity we want to determine.
- Frequency matrix $\boldsymbol{\omega}(\vec{q})$: Time independent quantity can be calculated analytically by evaluating the equilibrium average over the density function.
- Irreducible memory kernel $\boldsymbol{m}(\vec{q},t)$. Up to now not an accessible quantity having a very complicated mathematical structure.

To close the equation of motion (3.28) introducing a meaningful approximation for $\boldsymbol{m}$ ideally as a function of the density correlator is needed.

3.3 Mode Coupling Theory

3.3.1 Approximation of the Memory Kernel

The irreducible memory kernel defined in the last section contains an exponential of the Smoluchowski operator acting on the density function. It is not clear how the memory kernel can be approximated by standard techniques like expanding the exponential function in power series. A nonperturbative approximation of the memory kernel was introduced by Götze [23] for glassy systems, the so-called Mode Coupling approximation. The approximation is based on a second projection into the space spanned by a product of two density functions and a simulations approximation of the irreducible Smoluchowski operator by the original one. This kind of approximation is not a controlled approximation and it is very difficult to estimate the error related to the simplifications. On the other hand the Mode coupling theory describes many phenomena related to dense systems qualitatively and quantitatively precisely (like the caging effect).
From now on the multiindex notation popularized by Rolf Schilling [38–40] in his work about molecular liquids will be used, with the following conventions.

- $\rho_i \equiv \rho_{l_i}(\vec{q}_i)$ with $i \in \mathbb{N}$.

- $\boldsymbol{S}_{i,j} \equiv \boldsymbol{S}_{l_i,l_j}(\vec{q}_i,\vec{q}_j) = \boldsymbol{S}_{l_i,l_j}(\vec{q}_i)\delta_{\vec{q}_i,\vec{q}_j}$ with $i,j \in \mathbb{N}$.
- $\boldsymbol{S}_{i,j}(t) \equiv \boldsymbol{S}_{l_i,l_j}(\vec{q}_i,\vec{q}_j,t) = \boldsymbol{S}_{l_i,l_j}(\vec{q}_i,t)\delta_{\vec{q}_i,\vec{q}_j}$ with $i,j \in \mathbb{N}$.
- $\sum_i \equiv \sum_{l_i,\vec{q}_i}$ with $i \in \mathbb{N}$.

The projector projecting to the product state of two density functions can be defined as,

$$\boldsymbol{P}_2 = \sum_{1,2,3,4} \Big|\rho_1\rho_2\Big\rangle \boldsymbol{g}_{1,2,3,4} \Big\langle\rho_3^*\rho_4^*\Big|, \tag{3.41}$$

with the normalization tensor $\boldsymbol{g}$ to be chosen such that $\boldsymbol{P}_2$ will become idempotent. To achieve that the normalization tensor should satisfy the following condition written in a symmetrized form.

$$\sum_{3,4} \boldsymbol{g}_{1,2,3,4} \Big\langle \rho_3^*\rho_4^*\rho_{1'}\rho_{2'}\Big\rangle = \frac{1}{2}\Big[\delta_{1,1'}\delta_{2,2'} + \delta_{1,2'}\delta_{2,1'}\Big]. \tag{3.42}$$

Using the two state projector the memory kernel can be projected into the product state, where the exponential function gets "sandwiched" by two projectors.

$$\begin{aligned}
\boldsymbol{m}_{l,l'}(\vec{q},t) &\overbrace{\approx}^{\substack{\text{First}\\ \text{approximation}}} \frac{1}{N}\Big\langle \rho_l(\vec{q})^*\,\Omega^\dagger \boldsymbol{Q}\boldsymbol{P}_2 \mathrm{e}^{\Omega^{\dagger,\mathrm{irr}}t}\boldsymbol{P}_2\boldsymbol{Q}\Omega^\dagger\rho_{l'}(\vec{q})\Big\rangle \\
&= \frac{1}{N}\sum_{\substack{1,\cdots 4\\ 1',\cdots 4'}} \underbrace{\Big\langle\rho_l(\vec{q})^*\Omega^\dagger\boldsymbol{Q}\rho_1\rho_2\Big\rangle \boldsymbol{g}_{1,2,3,4}}_{\substack{:=\mathrm{L}\\ \text{Left Vertex}}} \underbrace{\Big\langle\rho_3^*\rho_4^*\mathrm{e}^{\Omega^{\dagger,\mathrm{irr}}t}\rho_{1'}\rho_{2'}\Big\rangle}_{\text{Four point function}} \underbrace{\boldsymbol{g}_{1',2',3',4'}\Big\langle\rho_{3'}^*\rho_{4'}^*\boldsymbol{Q}\Omega^\dagger\rho_{l'}(\vec{q})\Big\rangle}_{\substack{:=\mathrm{R}\\ \text{Right Vertex}}}.
\end{aligned} \tag{3.43}$$

The four point function is approximated by the Kawasaki factorization [45] by expressing the averages of products as products of averages.

$$\begin{aligned}
\Big\langle\rho_3^*\rho_4^*\mathrm{e}^{\Omega^{\dagger,\mathrm{irr}}t}\rho_{1'}\rho_{2'}\Big\rangle &\approx \Big\langle\rho_3^*\mathrm{e}^{\Omega^\dagger t}\rho_{1'}\Big\rangle\Big\langle\rho_4^*\mathrm{e}^{\Omega^\dagger t}\rho_{2'}\Big\rangle + \Big\langle\rho_3^*\mathrm{e}^{\Omega^\dagger t}\rho_{2'}\Big\rangle\Big\langle\rho_4^*\mathrm{e}^{\Omega^\dagger t}\rho_{1'}\Big\rangle \\
&= N^2\Big[\boldsymbol{S}_{3,1'}(t)\,\boldsymbol{S}_{4,2'}(t) + \boldsymbol{S}_{3,2'}(t)\,\boldsymbol{S}_{4,1'}(t)\Big].
\end{aligned} \tag{3.44}$$

Evaluating the later equation at time zero and making use of the condition (3.42) allows us to determine the normalization tensor $\boldsymbol{g}$.

$$\boldsymbol{g}_{1,2,3,4} \approx \frac{1}{2N^2}\boldsymbol{S}^{-1}_{1,3}\boldsymbol{S}^{-1}_{2,4}. \tag{3.45}$$

To calculate the left and right vertex defined in equation (3.43) is very cumbersome but straightforward and is performed in great detail in the appendix A. After

evaluating the vertices the memory kernel can be written in its final form depending only on statical structure factor and the dynamical density correlator. For a more concise way of writing we change the wave vector to the corresponding tuple $\vec{q} \to \{q, \alpha_q\}$ with the magnitude q and the angle with respect to the x-axis α_q, and introduce a shorthand operator $\pm_{l_2}^{l_1} \equiv l_1 - l_2$.

$$\boldsymbol{\omega}_{l_1,l_2}(\vec{q}) = \left(D_r {l_2}^2 + D_t q^2\right)\delta_{l_1,l_2} - \frac{iv_0}{2} q \mathrm{e}^{\pm_{l_1}^{l_2} i\alpha_q} \boldsymbol{S}_{l_1,l_1}(q)\,\delta_{|l_1-l_2|,1}, \tag{3.46a}$$

$$\begin{aligned}\mathbf{L}^{l}_{l_1,l_2}\left(\vec{k},\vec{p},\vec{q}\right) = -D_t\Bigg(\vec{q}\cdot\left[\vec{k}\boldsymbol{S}^{-1}_{l_1,l_1}(k) + \vec{p}\boldsymbol{S}^{-1}_{l_2,l_2}(p)\right] - q^2\Bigg)\delta_{l,l_1+l_2} \\ + \frac{iv_0}{2}\boldsymbol{S}_{l,l}(q)\Bigg(k\mathrm{e}^{\pm_l^{l_1,l_2} i\alpha_k}\boldsymbol{S}_{l-l_2,l-l_2}(k)\,\boldsymbol{S}^{-1}_{l_1,l_1}(k) \\ + p\mathrm{e}^{\pm_l^{l_1,l_2} i\alpha_p}\boldsymbol{S}_{l-l_1,l-l_1}(p)\,\boldsymbol{S}^{-1}_{l_2,l_2}(p) - q\mathrm{e}^{\pm_l^{l_1,l_2} i\alpha_q}\Bigg)\delta_{|l-l_1-l_2|,1},\end{aligned} \tag{3.46b}$$

$$\mathbf{R}^{l_3,l_4}_{l'}\left(\vec{k},\vec{p},\vec{q}\right) = -D_t\Bigg(\vec{q}\cdot\left[\vec{k}\boldsymbol{S}^{-1}_{l_3,l_3}(k) + \vec{p}\boldsymbol{S}^{-1}_{l_4,l_4}(p)\right] - q^2\Bigg)\delta_{l_3+l_4,l'}, \tag{3.46c}$$

$$\boldsymbol{m}_{l,l'}(\vec{q},t) \approx \frac{1}{2N}\sum_{\substack{\vec{p}\\ l_1\cdots l_4}} \mathbf{L}^{l}_{l_1,l_2}(\vec{q}-\vec{p},\vec{p},\vec{q})\,\boldsymbol{S}_{l_1,l_3}(\vec{q}-\vec{p},t)\,\boldsymbol{S}_{l_2,l_4}(\vec{p},t)\,\mathbf{R}^{l_3,l_4}_{l'}(\vec{q}-\vec{p},\vec{p},\vec{q})\,. \tag{3.46d}$$

The equations (3.46) include all the quantities needed to close the equation of motion for the dynamical density correlator, and can be solved uniquely under the knowledge of the static structure factor. By taking a close look to the above equations one notices that the rotational diffusion D_r enters the EOM only in the diagonal components of frequency matrix $\boldsymbol{\omega}$ apart from the $l = 0, l' = 0$ mode, therefore the dependence of the translational part of the correlator $\boldsymbol{S}_{0,0}(\vec{q},t)$ to the rotational diffusion is only possible by back coupling of other components of $\boldsymbol{S}(\vec{q},t)$ to the translational part. The frequency matrix is a tridiagonal matrix where the $l \pm 1$ shift in the orientational indices is a consequence of the orientational vector $\vec{o}$ entering the Smoluchowski operator. Having no $l \pm 2$ terms in the frequency matrix will later encourage to choose the orientational cutoff to be $\Lambda_l = 1$, as higher modes will barely influence the translational motion we are mainly interested in. We also point out the covariant and contravariant index notation for the vertices

that will become important in the next section by investigating the transformation properties of the memory kernel.
Although the static structure factor is isotropic in q and the wave vector can be replaced by its magnitude the dynamic density correlator does depend on the wave vector. The anisotropy is a consequence of the orientational vector $\vec{o}_i$ making the direction of the wave vector distinguishable. To be still able of reducing a two dimensional problem to a single dimension it is necessary to analyze the transformation properties of the correlator after the MCT approximation, especially how it changes under the rotation of the wave vector $\{q, \alpha_q\} \to \{q, \alpha_q + \beta\}$.

3.3.2 Transformation Properties after MCT Approximation

In the section 3.1.3 the transformation behavior of the density correlator under the rotation of the wave vector $\vec{q}$ was shown. It is important to prove that the MCT approximations did not destroy the transformation property (3.15) of $\boldsymbol{S}(\vec{q}, t)$. The prove can be done by rotating the wave vector $\vec{q}$ in the EOM (3.28) by an angle β and checking how $\boldsymbol{S}$ changes by the transformation. It is useful first to derive the transformation rules for the frequency matrix $\boldsymbol{\omega}$ and the memory kernel $\boldsymbol{m}$.

$$\begin{aligned}\left(\boldsymbol{u}\left(\beta\right)\boldsymbol{\omega}\left(\{q,\alpha\}\right)\boldsymbol{u}^{\dagger}\left(\beta\right)\right)_{l_1,l_2} =& \sum_{l,l'} \mathrm{e}^{i(l_2-l_1)\beta}\delta_{l,l_1}\delta_{l',l_2}\boldsymbol{\omega}_{l,l'}\left(\{q,\alpha\}\right) \\ =& \left(D_r l_2^2 + D_t q^2\right)\delta_{l_1,l_2} - \frac{iv_0}{2} q \mathrm{e}^{\pm_{l1}^{l2} i(\alpha+\beta)} \boldsymbol{S}_{l_1,l_1}\left(q\right)\delta_{|l_1-l_2|,1} \\ =& \boldsymbol{\omega}_{l_1,l_2}\left(\{q,\alpha+\beta\}\right).\end{aligned} \tag{3.47}$$

The frequency matrix obeys the same transformation rule like the correlator. To check how the memory kernel transforms we have to take a close look at the vertices. The left and right vertex are rank three tensors and therefore three unitary $\boldsymbol{u}$ matrices are needed to rotate all wave vectors.

$$\begin{aligned}&\sum_{i,j,k} \boldsymbol{u}_{l,i}\left(\beta\right)\mathbf{L}^{i}_{j,k}\left(\{k,\alpha_k\},\{p,\alpha_p\},\{q,\alpha_q\}\right)\boldsymbol{u}^{\dagger}_{j,l_1}\left(\beta\right)\boldsymbol{u}^{\dagger}_{k,l_2}\left(\beta\right) \\ &= \mathrm{e}^{i(l_1+l_2-l)\beta}\mathbf{L}^{l}_{l_1,l_2}\left(\{k,\alpha_k\},\{p,\alpha_p\},\{q,\alpha_q\}\right) \\ &= \mathbf{L}^{l}_{l_1,l_2}\left(\{k,\alpha_k+\beta\},\{p,\alpha_p+\beta\},\{q,\alpha_q+\beta\}\right).\end{aligned} \tag{3.48}$$

For every contravariant index a $\boldsymbol{u}$ and for every covariant index $\boldsymbol{u}^{\dagger}$ is used (that was the reason to introduce the super- and subindex notation at first place). The

right vertex obeys the same transformation rules as the left vertex.

$$\begin{aligned}
&\sum_{i,j,k} \boldsymbol{u}_{l_3,i}\left(\beta\right) \boldsymbol{u}_{l_4,j}\left(\beta\right) \mathbf{R}_{k}^{i,j}\left(\{k,\alpha_k\},\{p,\alpha_p\},\{q,\alpha_q\}\right) \boldsymbol{u}^{\dagger}_{l',k}\left(\beta\right) \\
&= \mathrm{e}^{i(l'-l_3-l_4)\beta} \mathbf{R}_{l'}^{l_3,l_4}\left(\{k,\alpha_k\},\{p,\alpha_p\},\{q,\alpha_q\}\right) \\
&= \mathbf{R}_{l'}^{l_3,l_4}\left(\{k,\alpha_k+\beta\},\{p,\alpha_p+\beta\},\{q,\alpha_q+\beta\}\right).
\end{aligned} \tag{3.49}$$

To derive the transformation rule for $\boldsymbol{m}$ we assume the dynamical density correlator that enters the memory kernel to have the desired transformation property (3.15) and prove it in the next step.

$$\begin{aligned}
\boldsymbol{m}_{l,l'}\left(\{q,\alpha_q+\beta\},t\right) \approx & \frac{1}{2N} \sum_{\substack{\boldsymbol{p} \\ l_1\cdots l_4}} \Big[\mathbf{L}^{l}_{l_1,l_2}\left(\{k,\alpha_k+\beta\},\{p,\alpha_p+\beta\},\{q,\alpha_q+\beta\}\right) \\
& \times \boldsymbol{S}_{l_1,l_3}\left(\{k,\alpha_k+\beta\},t\right) \boldsymbol{S}_{l_2,l_4}\left(\{p.\alpha_p+\beta\},t\right) \\
& \times \mathbf{R}_{l'}^{l_3,l_4}\left(\{k,\alpha_k+\beta\},\{p.\alpha_p+\beta\},\{q,\alpha_q+\beta\}\right) \Big] \\
= & \frac{1}{2N} \sum_{\substack{\vec{p} \\ l_1\cdots l_4}} \Big[\sum_{i,j,s} \boldsymbol{u}_{l,i}\left(\beta\right) \mathbf{L}^{i}_{j,s}\left(\{k,\alpha_k\},\{p,\alpha_p\},\{q,\alpha_q\}\right) \boldsymbol{u}^{\dagger}_{j,l_1}\left(\beta\right) \boldsymbol{u}^{\dagger}_{s,l_2}\left(\beta\right) \\
& \times \sum_{n,m} \boldsymbol{u}_{l_1,n}\left(\beta\right) \boldsymbol{S}_{n,m}\left(\{k,\alpha_k\},t\right) \boldsymbol{u}^{\dagger}_{m,l_3}\left(\beta\right) \\
& \times \sum_{n',m'} \boldsymbol{u}_{l_2,n'}\left(\beta\right) \boldsymbol{S}_{n',m'}\left(\{p,\alpha_p\},t\right) \boldsymbol{u}^{\dagger}_{m',l_4}\left(\beta\right) \\
& \times \sum_{i',j',s'} \boldsymbol{u}_{l_3,i'}\left(\beta\right) \boldsymbol{u}_{l_4,j'}\left(\beta\right) \mathbf{R}_{s'}^{i',j'}\left(\{k,\alpha_k\},\{p.\alpha_p\},\{q,\alpha_q\}\right) \boldsymbol{u}^{\dagger}_{s',l'}\left(\beta\right) \Big] \\
= & \frac{1}{2N} \sum_{i,j,s} \boldsymbol{u}_{l,i}\left(\beta\right) \mathbf{L}^{i}_{j,s}\left(\{k,\alpha_k\},\{p,\alpha_p\},\{q,\alpha_q\}\right) \\
& \times \sum_{n,m,i'} \boldsymbol{S}_{n,m}\left(\{k,\alpha_k\},t\right) \delta_{j,n}\delta_{m,i'} \sum_{n',m',j'} \boldsymbol{S}_{n',m'}\left(\{p,\alpha_p\},t\right) \delta_{s,n'}\delta_{m',j'} \\
& \times \sum_{s'} \mathbf{R}_{s'}^{i',j'}\left(\{k,\alpha_k\},\{p.\alpha_p\},\{q,\alpha_q\}\right) \boldsymbol{u}^{\dagger}_{s',l'}\left(\beta\right) \\
= & \frac{1}{2N} \sum_{\substack{i,j,s \\ i',j',s'}} \boldsymbol{u}_{l,i}\left(\beta\right) \mathbf{L}^{i}_{j,s}\left(\{k,\alpha_k\},\{p,\alpha_p\},\{q,\alpha_q\}\right) \\
& \times \boldsymbol{S}_{j,i'}\left(\{k,\alpha_k\},t\right) \boldsymbol{S}_{s,j'}\left(\{p,\alpha_p\},t\right) \\
& \times \mathbf{R}_{s'}^{i',j'}\left(\{k,\alpha_k\},\{p.\alpha_p\},\{q,\alpha_q\}\right) \boldsymbol{u}^{\dagger}_{s',l'}\left(\beta\right)
\end{aligned}$$

$$= \sum_{i,s'} \boldsymbol{u}_{l,i}(\beta) \boldsymbol{m}_{i,s'}(\{q,\alpha_q\},t)\, \boldsymbol{u}^{\dagger}_{s',l'}(\beta) = \Big(\boldsymbol{u}(\beta)\, \boldsymbol{m}(\{q,\alpha_q\},t)\, \boldsymbol{u}^{\dagger}(\beta)\Big)_{l,l'}. \tag{3.50}$$

The assumption made to prove the transformation relation of the memory kernel can be validated in the next step.

$$\begin{aligned}
\boldsymbol{S}(\{q,\alpha_q+\beta\},t) &= -\boldsymbol{S}(q)\,\boldsymbol{u}(\beta)\,\boldsymbol{\omega}^{-1}(\{q,\alpha_q\})\,\boldsymbol{u}^{\dagger}(\beta)\,\boldsymbol{u}(\beta)\,\partial_t \boldsymbol{S}(\{q,\alpha_q\},t)\,\boldsymbol{u}^{\dagger}(\beta) \\
&\quad -\boldsymbol{S}(q)\,\boldsymbol{u}(\beta)\,\boldsymbol{\omega}^{-1}(\{q,\alpha_q\})\,\boldsymbol{u}^{\dagger}(\beta)\int_0^t dt' \boldsymbol{u}(\beta)\,\boldsymbol{m}(\{q,\alpha_q\},t-t')\,\boldsymbol{u}^{\dagger}(\beta) \\
&\quad \times \boldsymbol{u}(\beta)\,\boldsymbol{\omega}^{-1}(\{q,\alpha_q\})\,\boldsymbol{u}^{\dagger}(\beta)\,\boldsymbol{u}(\beta)\,\partial_{t'}\boldsymbol{S}(\{q,\alpha_q\},t')\,\boldsymbol{u}^{\dagger}(\beta) \\
= \boldsymbol{u}(\beta)\Bigg[&- \boldsymbol{S}(q)\boldsymbol{\omega}^{-1}(\{q,\alpha_q\})\Bigg(\partial_t \boldsymbol{S}(\{q,\alpha_q\},t) + \int_0^t dt' \boldsymbol{m}(\{q,\alpha_q\},t-t') \\
&\quad \times \boldsymbol{\omega}^{-1}(\{q,\alpha_q\})\,\partial_{t'}\boldsymbol{S}(\{q,\alpha_q\},t')\Bigg)\Bigg]\boldsymbol{u}^{\dagger}(\beta) \\
&= \boldsymbol{u}(\beta)\,\boldsymbol{S}(\{q,\alpha_q\},t)\,\boldsymbol{u}^{\dagger}(\beta).
\end{aligned} \tag{3.51}$$

Finally the transformation relations for the density correlator after the MCT approximations could be proven. Being able of determining the density function of a wave vector pointing in any direction from a single wave vector, makes it possible to simplify the EOM 3.38 significantly. Making use of the transformation tensor we can fix the direction of the wave vector $\vec{q}$ of the Density correlator to any specific direction and express all other wave vectors as a rotation of it.

3.3.3 Defining the Coordinate System

In the previous section a method to transform density correlators of any wave vector $\vec{q}$ into each other, by applying the unitary transformation matrix $\boldsymbol{u}$ was developed. In this section a coordinate system will be introduced where the direction of the wave vector $\vec{q}$ will be chosen to point into positive y direction. All quantities depending on other orientation of the wave vector get aligned into the desired direction by using the transformation properties from last section. The orientation of the wave vector is denoted as a superscript e.g. $\boldsymbol{S}^{\frac{\pi}{2}}(q,t)$ is the density correlator with the wave vector pointing into positive y direction and having a magnitude of q. The summation over the wave vector appearing in the memory kernel can be changed to a double integral well known from thermodynamics.

$$\sum_{\vec{p}} \cong \frac{V}{(2\pi)^2}\int d^2p \equiv \frac{V}{(2\pi)^2}\int dp_x \int dp_y, \tag{3.52}$$

with the total volume of the system V. After the change of variables $(p_x, p_y) \to (p, k)$ with $p = |\vec{p}|$, $k = \left|\vec{k}\right|$ and $\vec{q} = \vec{k} + \vec{p}$,

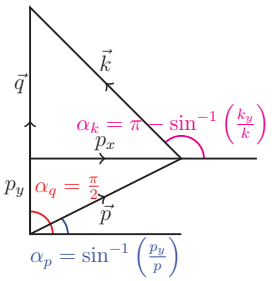

$$
\begin{aligned}
p_y &= \frac{q^2 + p^2 - k^2}{2q}, & p_x &= \sqrt{p^2 - p_y^2} \\
\partial_p p_y &= \frac{p}{q}, & \partial_k p_y &= -\frac{k}{q} \\
\partial_p p_x &= \frac{p - \frac{p_y p}{q}}{p_x}, & \partial_k p_x &= \frac{p_y k}{p_x q},
\end{aligned}
\tag{3.53}
$$

and calculating the Jacobian of the transformation,

$$
\mathcal{J} = \begin{pmatrix} \frac{p - \frac{p_y p}{q}}{p_x} & \frac{p_y k}{p_x q} \\ \frac{p}{q} & -\frac{k}{q} \end{pmatrix}, \qquad |\det(\mathcal{J})| = \frac{pk}{q p_x} = \frac{2pk}{\sqrt{4q^2p^2 - \left(q^2 + p^2 - k^2\right)^2}}, \tag{3.54}
$$

the two dimensional sum can be expressed.

$$
\sum_{\vec{p}} \cong \frac{V}{(2\pi)^2} \int d^2p = \frac{4V}{(2\pi)^2} \int_0^\infty dp \int_{|q-p|}^{q+p} dk \frac{pk}{\sqrt{4q^2p^2 - \left(q^2 + p^2 - k^2\right)^2}}. \tag{3.55}
$$

The extra factor 2 in the last equality is a consequence of integrating over $(0, \infty)$ instead of $(-\infty, \infty)$. It should be noticed that the above transformation can not be performed for zero wavenumber limit and needs to be treated differently. Also for finite wavenumbers the integrand in the equation (3.55) can diverge and possibly be an issue evaluating the integrals numerically (to avoid the problems with the divergent integrand at the boundaries during numerical calculations open Newton-Cotes formulas are used). The equations (3.46) can be expressed in the above coordinates.

$$
\begin{aligned}
\mathbf{L}_{l_1,l_2}^{l,\frac{\pi}{2}}(k,p,q) = -D_t \Bigg(& \frac{q^2 + k^2 - p^2}{2} \boldsymbol{S}_{l_1,l_1}^{-1}(k) + \frac{q^2 + p^2 - k^2}{2} \boldsymbol{S}_{l_2,l_2}^{-1}(p) - q^2 \Bigg) \delta_{l,l_1+l_2} \\
& + \frac{iv_0}{2} \boldsymbol{S}_{l,l}(q) \Bigg[k \mathrm{e}^{\pm_l^{l_1,l_2} i\alpha_k} \boldsymbol{S}_{l-l_2,l-l_2}(k) \boldsymbol{S}_{l_1,l_1}^{-1}(k) \\
& \qquad + p \mathrm{e}^{\pm_l^{l_1,l_2} i\alpha_p} \boldsymbol{S}_{l-l_1,l-l_1}(p) \boldsymbol{S}_{l_2,l_2}^{-1}(p) \mp_l^{l_1,l_2} iq \Bigg] \delta_{|l-l_1-l_2|,1},
\end{aligned}
\tag{3.56a}
$$

$$
\mathbf{R}_{l'}^{l_3,l_4,\frac{\pi}{2}}(k,p,q) = -D_t \Bigg(\frac{q^2 + k^2 - p^2}{2} \boldsymbol{S}_{l_3,l_3}^{-1}(k) + \frac{q^2 + p^2 - k^2}{2} \boldsymbol{S}_{l_4,l_4}^{-1}(p) - q^2 \Bigg) \delta_{l_3+l_4,l'}, \tag{3.56b}
$$

$$\begin{aligned}\boldsymbol{m}^{\frac{\pi}{2}}_{l,l'}(q,t) \approx & \frac{2}{n\,(2\pi)^2}\sum_{l_1\cdots l_4}\int_0^\infty dp\int_{|q-p|}^{q+p} dk \frac{pk\mathbf{L}^{l,\frac{\pi}{2}}_{l_1,l_2}(k,p,q)\,\mathbf{R}^{l_3,l_4,\frac{\pi}{2}}_{l'}(k,p,q)}{\sqrt{4q^2p^2-\left(q^2+p^2-k^2\right)^2}} \\ & \times \mathrm{e}^{-il_1\left(\alpha_k-\frac{\pi}{2}\right)}\mathrm{e}^{il_3\left(\alpha_k-\frac{\pi}{2}\right)}\boldsymbol{S}^{\frac{\pi}{2}}_{l_1,l_3}(k,t) \\ & \times \mathrm{e}^{-il_2\left(\alpha_p-\frac{\pi}{2}\right)}\mathrm{e}^{il_4\left(\alpha_p-\frac{\pi}{2}\right)}\boldsymbol{S}^{\frac{\pi}{2}}_{l_2,l_4}(p,t)\,,\end{aligned} \tag{3.56c}$$

$$\boldsymbol{\omega}^{\frac{\pi}{2}}_{l_1,l_2}(q) = \left(D_r {l_2}^2 + D_t q^2\right)\delta_{l_1,l_2} + \frac{v_0 q}{2}(l_2-l_1)\boldsymbol{S}_{l_1,l_1}(q)\,\delta_{|l_1-l_2|,1}, \tag{3.56d}$$

$$\partial_t \boldsymbol{S}^{\frac{\pi}{2}}(q,t) = -\boldsymbol{\omega}^{\frac{\pi}{2}}(q)\,\boldsymbol{S}^{-1}(q)\,\boldsymbol{S}^{\frac{\pi}{2}}(q,t) - \int_0^t dt' \boldsymbol{m}^{\frac{\pi}{2}}(q,t-t')\,\boldsymbol{\omega}^{\frac{\pi}{2}\,-1}(q)\,\partial_{t'}\boldsymbol{S}^{\frac{\pi}{2}}(q,t')\,. \tag{3.56e}$$

From now on we skip the superscript denoting the orientation of the wave vector $\vec{q}$. The equation of motion (3.56e) in its final form is a self-consistent (the memory kernel depends only on the density correlator) itegro differential equation describing the dynamics of the density correlator uniquely (after the knowledge of the static structure factor).

The EOM (3.56e) can be solved numerically by the methods developed in the appendix B over many orders of magnitude in time (that is important by analyzing the glassy dynamics). The matrix component $\boldsymbol{S}_{0,0}(\vec{q},t)$ is the key quantity in the theory allowing us to investigate many important phenomena like glass transition and caging.

For the orientational index the cutoff $\Lambda_l = 1$ will be chosen ($l \in \{-1,0,1\}$). Setting the cutoff to one is motivated by the structure of the frequency matrix containing only $l\pm1$ shifts, thus higher modes of the correlator enter the equation for $\boldsymbol{S}_{0,0}(\vec{q},t)$ not directly and only by back-coupling in the memory kernel $\boldsymbol{m}$. Choosing a higher orientational cutoff is also very demanding from the numerical point of view (more details about the complexity in appendix B).

$$\boldsymbol{\omega}(q) = \begin{pmatrix} D_r + D_t q^2 & \frac{v_0 q}{2} & 0 \\ -\frac{v_0 q}{2}\tilde{S}_q & D_t q^2 & \frac{v_0 q}{2}\tilde{S}_q \\ 0 & -\frac{v_0 q}{2} & D_r + D_t q^2 \end{pmatrix}, \quad \boldsymbol{S}(t) = \begin{pmatrix} \boldsymbol{S}_{-1,-1} & \boldsymbol{S}_{-1,0} & \boldsymbol{S}_{-1,1} \\ \boldsymbol{S}_{0,-1} & \boldsymbol{S}_{0,0} & \boldsymbol{S}_{0,1} \\ \boldsymbol{S}_{1,-1} & \boldsymbol{S}_{1,0} & \boldsymbol{S}_{1,1} \end{pmatrix}. \tag{3.57}$$

To demonstrate that the higher $\boldsymbol{S}$ modes ($l\pm2$) do not couple to $\boldsymbol{S}_{0,0}$ directly we consider again the case of a single active Brownian disk in a solvent. For a single swimmer there is no interaction potential and the memory kernel will vanish (since

it is a force-force correlator). The static structure factor matrix also simplifies to unity and the equation (3.56e) can be solved analytically.

$$\partial_t \boldsymbol{S}\left(q,t\right) = -\boldsymbol{\omega}\left(q\right)\boldsymbol{S}\left(q,t\right), \quad \Rightarrow \quad \boldsymbol{S}\left(q,t\right) = \mathrm{e}^{-\boldsymbol{\omega}(q)t}. \tag{3.58}$$

To calculate the matrix exponential of the frequency matrix it needs to be diagonalized first. The frequency matrix $\boldsymbol{\omega}$ in the space of restricted orientational indices ($l \in \{-1.0.1\}$) can be diagonalized with the transformation matrices $\boldsymbol{U}$ having the eigenvectors as rows.

$$\boldsymbol{\omega}(q) = \boldsymbol{U}\hat{\boldsymbol{\omega}}(q)\boldsymbol{U}^{-1}, \quad \Rightarrow \quad \mathrm{e}^{-\boldsymbol{\omega}(q)t} = \boldsymbol{U}\mathrm{e}^{-\hat{\boldsymbol{\omega}}(q)t}\boldsymbol{U}^{-1}, \tag{3.59}$$

where $\hat{\boldsymbol{\omega}}$ is the diagonalized frequency matrix. To calculate matrix exponential of a diagonal matrix one has to calculate the exponential of each entry.
The density correlator of a single particle can be related to the mean-squared displacement by taking the $q \to 0$ limit.

$$\begin{aligned} &\boldsymbol{S}_{0,0}(\vec{q},t) = \left\langle \mathrm{e}^{-i\vec{q}\cdot(\vec{x}(t)-\vec{x}(0))}\right\rangle \equiv \left\langle \mathrm{e}^{-i\vec{q}\cdot\vec{r}(t)}\right\rangle = \mathrm{e}^{-\frac{1}{4}q^2\left\langle \delta r^2(t)\right\rangle} = 1 - \frac{1}{4}q^2\left\langle \delta r^2(t)\right\rangle + \mathcal{O}\left(q^4\right) \\ &\Rightarrow \quad \left\langle \delta r^2(t)\right\rangle = \lim_{q\to 0}\frac{4}{q^2}\Big(1 - \boldsymbol{S}_{0,0}(q,t)\Big). \end{aligned} \tag{3.60}$$

The solution of equation (3.58) for $\boldsymbol{S}_{0,0}(q,t)$ can be expanded in powers of q.

$$\boldsymbol{S}_{0,0}(q,t) = 1 - \frac{q^2}{2D_r^2}\Big(\left(-1+\mathrm{e}^{-D_r t}\right)v_0^2 + D_r\left(2D_rD_t + v_0^2\right)t\Big) + \mathcal{O}\left(q^3\right). \tag{3.61}$$

The corresponding time dependent mean-squared displacement:

$$\left\langle \delta r^2(t)\right\rangle = \frac{2}{D_r^2}\Big(\left(-1+\mathrm{e}^{-D_r t}\right)v_0^2 + D_r\left(2D_rD_t + v_0^2\right)t\Big). \tag{3.62}$$

We recognize the formula for the mean-squared displacement from the last chapter where it got determined by using the Langevin equation for a single Brownian particle. So for a model where the memory kernel vanishes trivially higher modes of $\boldsymbol{S}(q,t)$ do not couple to $\boldsymbol{S}_{0,0}(t)$ and thus it is sufficient to consider only the orientations of $l \in \{-1,0,1\}$.
We turn back to the full EOM (3.56e) and present numerical results for different matrix elements of the density correlator to motivate a further splitting of the memory kernel in rotational and translational parts. It is convenient to introduce a normalized density correlator (also referred as density correlator) $\boldsymbol{\Phi}(q,t) \equiv \boldsymbol{S}(q,t)\boldsymbol{S}^{-1}(q)$.
The packing fraction will be chosen such, that the passive system is in a glassy

state and it gets molten by continuous increase of the activity at a constant rotational diffusion. The top panel of the Figure (3.3) shows the typical shape of a correlator in two different states. The black and blue lines denote a fluid phase where the correlator decays to zero after some time. The red and green lines correspond to a glassy state characterized by a nonvanishing long time value the so-called nonergodicity parameter. As illustrated in the figure increasing the activity force softens the system and if it exceeds some critical value it melts the glass. The critical value for the activity for this parameters is $3 < v_0^{\text{crit}} < 4$. The critical point or the glass transition point is characterized by a discontinuous jump (from finite value to zero) of the nonergodicity parameter by an infinitesimal change of the activity force. In other words the glass transition has bifurcation properties. If we choose the packing fraction to be below the critical packing fraction for the passive system, the system will exhibit a fluid like behavior for all activity forces as shown in the bottom part of Figure (3.3). Similarly to the previous system also for smaller packing fractions the system gets softened by the activity. So below the critical packing the system remains always ergodic independent of the activity. The activity only changes the time scale the system needs to relax.
Taking the plot 3.3 into consideration the theory describes the glassy behavior and the influence of the activity on the system, qualitatively correctly (in agreement with the simulation studies [13]).
Up to now we only looked at the numerical results for the specific matrix element of the density correlator $\mathbf{\Phi}_{0,0}(q,t)$ that describes the structural properties of the system and does not say anything about the rotational behavior of the particles. To analyze the rotational properties of the particles we take a close look at $\mathbf{\Phi}_{1,1}(q,t)$ that not only depends on the structure of the system it also contains information about the angular correlation. As active Brownian hard disks with no friction on the surface are considered, for long times a completely uncorrelated directions of the particles with the initial orientations is expected. The time needed for the system to forget about the initial directions of the particles, depends on the rotational diffusion (inverse proportional).

$$\boldsymbol{S}_{1,1}(q,t) = \frac{1}{N}\sum_{i,j}\left\langle \mathrm{e}^{-i\vec{q}\cdot(\vec{x}(t)-\vec{x}(0))}\mathrm{e}^{-i(\varphi(t)-\varphi(0))}\right\rangle . \tag{3.63}$$

For the correlator $\mathbf{\Phi}_{1,1}(q,t)$ it means that it remains always ergodic as long $D_r > 0$. In contradiction to the expectations the Figure 3.4 illustrates a nonergodic behavior for both matrix elements $\mathbf{\Phi}_{0,0}$ and $\mathbf{\Phi}_{1,1}$ of the correlator above the glass transition point.

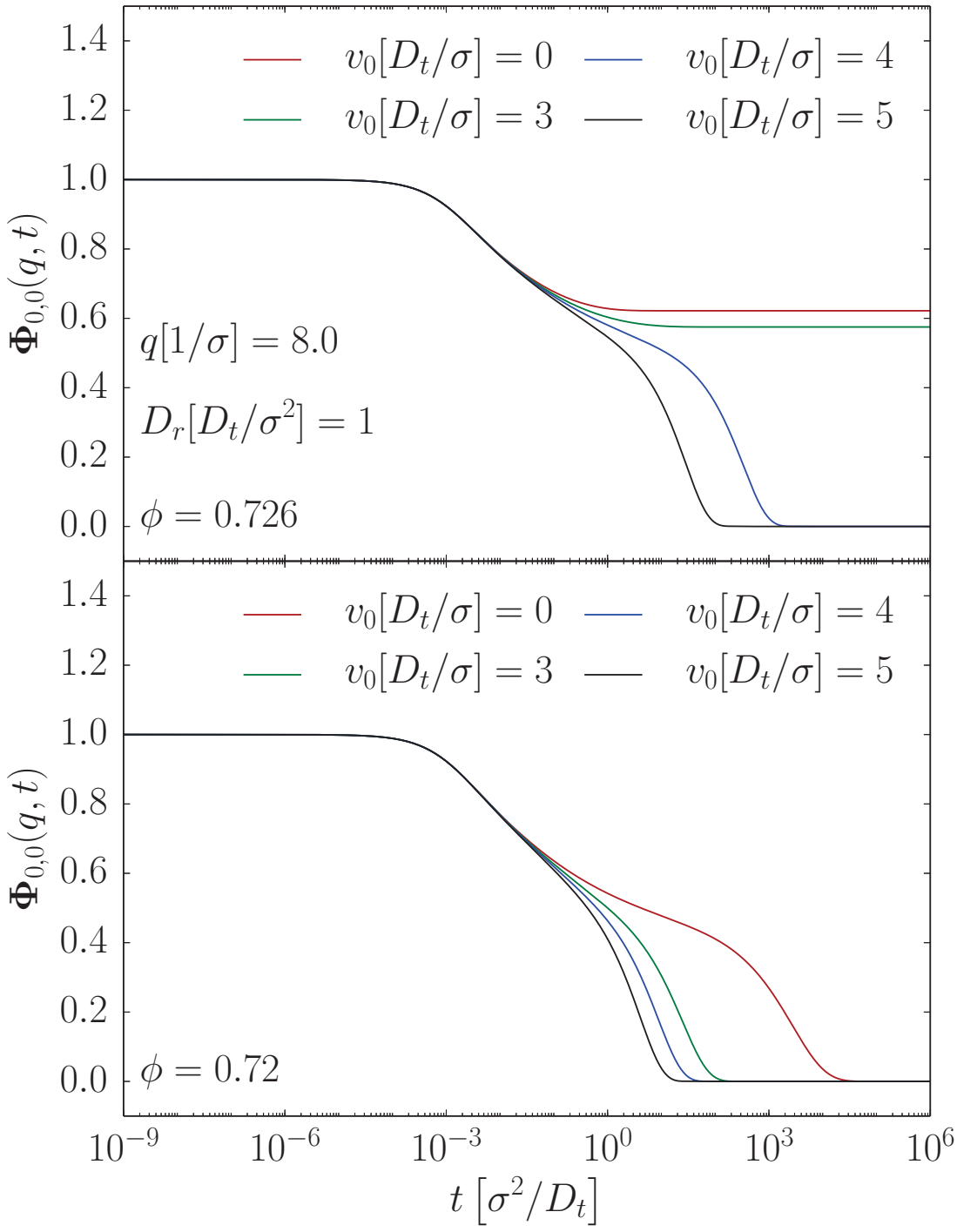

Figure 3.3: The $(0,0)$ mode of the dynamical density correlator $\mathbf{\Phi}_{0,0}(q,t)$ as a function of time for a single wavenumber q. In the top panel the packing fraction ϕ is above the critical packing fraction of the passive system. The rotational diffusion is fixed. Different colors denote different activity velocities. For the bottom panel the packing fraction is chosen to be slightly below the packing fraction of the passive system.

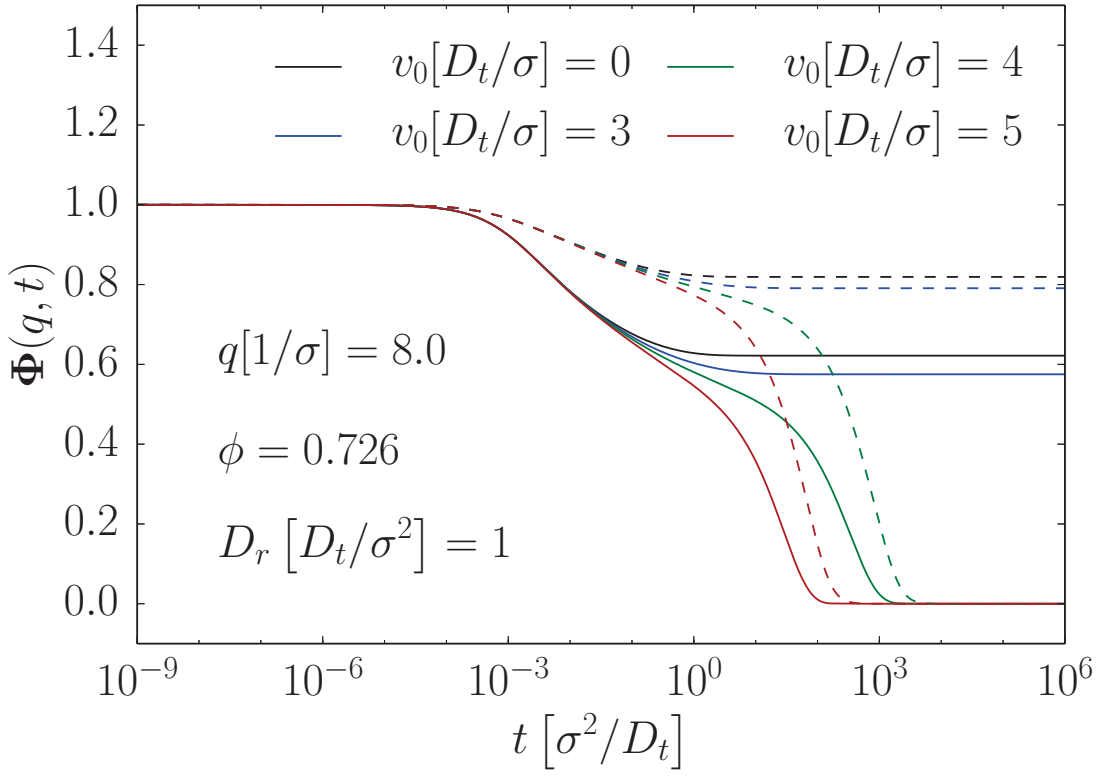

Figure 3.4: Two different matrix elements of the density correlator, $\mathbf{\Phi}_{0,0}(q,t)$ and $\mathbf{\Phi}_{1,1}(q,t)$ as a function of time for a single wavenumber q. The packing fraction ϕ is above the critical packing fraction of the passive system. The rotational diffusion is fixed. Solid lines correspond to $\mathbf{\Phi}_{0,0}$ and dashed lines to $\mathbf{\Phi}_{1,1}$. Different colors denote different activity velocities.

3.4 Nonergodicity Parameter

Sometimes it is not useful to determine the whole transient dynamics of the correlator to understand the long time behavior of the system. The long time values of the correlator are called the nonergodicity parameter $\boldsymbol{F}(q) = \lim_{t\to\infty} \boldsymbol{S}(q,t)$ (like mentioned in the previous section). To determine the long time values of the correlator it is more convenient to transform the EOM (3.56e) to the Laplace space, where the integro-differential equation gets converted to an algebraic matrix equation (wavenumbers omitted for better readability) that can be solved iteratively.

$$z\boldsymbol{S}(z) - \boldsymbol{S} = -\boldsymbol{\omega}\boldsymbol{S}^{-1}\boldsymbol{S}(z) - \boldsymbol{m}(z)\boldsymbol{\omega}^{-1}\Big[z\boldsymbol{S}(z) - \boldsymbol{S}\Big]. \tag{3.64}$$

For finite long time values the correlator can be expanded in powers of the Laplace variable z.

$$\boldsymbol{S}(z) = \frac{\boldsymbol{F}}{z} + \boldsymbol{F}_0 + \mathcal{O}(z), \qquad \boldsymbol{m}(z) = \frac{\boldsymbol{m}[\boldsymbol{F}]}{z} + \boldsymbol{m}_0 + \mathcal{O}(z). \tag{3.65}$$

The $1/z$ poles for $z \to 0$ is responsible for the finite long time value in time domain. After inserting the expansion formulas into the Laplace transformed EOM a recursive expression for the nonergodicity parameter $\boldsymbol{F}$ can be found.

$$\boldsymbol{F} = \Big[\boldsymbol{\omega}\boldsymbol{m}^{-1}[\boldsymbol{F}]\boldsymbol{\omega}\boldsymbol{S}^{-1} + \mathbb{I}\Big]^{-1}\boldsymbol{S}. \tag{3.66}$$

$\boldsymbol{\omega}$ is a fully occupied matrix and if the memory matrix is not identical to the zero matrix the expression in square brackets will also be a fully occupied matrix, thus the recursive equation for $\boldsymbol{F}$ can have a trivial solution when the nonergodicity parameter is a zero matrix (e.g. in fluid state) or all matrix elements of $\boldsymbol{F}$ are nonvanishing because of the structure of the equation.
The simultaneous freezing of the orientational and translational degrees of freedom for hard disks is an evidence that the irreducible memory kernel obtained by the second projection step is sufficient to describe the structural properties (e.g. glass transition, caging) of the system qualitatively correctly but is not well suited to understand the rotational properties of the particles and thus the influence of the rotational diffusion at the system properly. That encourages us to make a further modification of the memory kernel that will fix the problems of the "naive" theory ("naive" $\simeq$ without splitting the memory kernel in translational and rotational parts).

3.5 Translational and Rotational Splitting of the Memory Kernel

Following the steps of the Mori-Zwanzig projection formalism we did rewrite the equations such that the irreducible memory kernel needed to diverge like $1/z$ for $z \to 0$ in Laplace domain to exhibit glassy dynamics. But we did not take into account the tensorial structure of the theory (not all components need to have a finite long time value). The translational and rotational behavior are completely different and also need to be treated differently. To make the memory kernel more robust under the MCT approximations we have to put in more knowledge about the correlators by introducing the irreducible memory kernel.
The Smoluchowski operator and all related quantities formally can be splitted in its translational and rotational parts.

$$\Omega^\dagger = \underbrace{\sum_i D_t \left(\vec{\partial}_i + \beta \vec{F}_i\right) \cdot \vec{\partial}_i + v_0 \vec{o}_i \cdot \vec{\partial}_i}_{\Omega^\dagger_{\mathrm{T}}} + \underbrace{\sum_i D_r \partial^2_{\phi_i}}_{\Omega^\dagger_{\mathrm{R}}} = \Omega^\dagger_{\mathrm{T}} + \Omega^\dagger_{\mathrm{R}}, \tag{3.67}$$

the translational and rotational parts are denoted by a sub- or superscript T and R respectively.

$$\boldsymbol{\omega}_{l,l'}(\vec{q}) = -\frac{1}{N}\left\langle \rho^*_l(\vec{q}) \left(\Omega^\dagger_{\mathrm{T}} + \Omega^\dagger_{\mathrm{R}}\right) \rho_{l'}(\vec{q}) \right\rangle = \boldsymbol{\omega}^{\mathrm{T}}_{l,l'}(\vec{q}) + \boldsymbol{\omega}^{\mathrm{R}}_{l,l'}(\vec{q}). \tag{3.68}$$

The rotational part of the frequency matrix $\boldsymbol{\omega}^{\mathrm{R}}_{l,l'}(\vec{q}) = D_r l^2 \delta_{l,l'}$ is diagonal in orientational indices and has a trivial entry for $l = 0, l' = 0$, therefore it is not invertible.
To derive an irreducible memory kernel better suited for the ABD system, the steps from the section 3.2.2 need to be repeated for quantities intrinsically splited in translational and rotational parts. Using the fact that the final form of the irreducible memory kernel $\boldsymbol{m}$ is completely independent of the rotational diffusion, one can conclude that the rotational part of the memory kernel vanishes.

$$\boldsymbol{M}(\vec{q},t) = \boldsymbol{M}^{\mathrm{T}}(\vec{q},t) + \boldsymbol{M}^{\mathrm{R}}(\vec{q},t) = \boldsymbol{M}^{\mathrm{T}}(\vec{q},t). \tag{3.69}$$

The translational part of the memory kernel is related to its irreducible memory kernel by the integral equation derived by using the Dyson decomposition formula.

$$\begin{aligned} &\boldsymbol{M}^{\mathrm{T}}(\vec{q},t) = \boldsymbol{m}^{\mathrm{T}}(\vec{q},t) - \int_0^t dt' \boldsymbol{M}^{\mathrm{T}}(\vec{q},t')\, \boldsymbol{\omega}^{-1}_{\mathrm{T}}(\vec{q})\, \boldsymbol{m}^{\mathrm{T}}(\vec{q},t-t'), \\ \Leftrightarrow \\ &\boldsymbol{M}^{\mathrm{T}}(\vec{q},z) = \left[\boldsymbol{m}^{T^{-1}}(\vec{q},z) + \boldsymbol{\omega}^{-1}_{\mathrm{T}}(\vec{q})\right]^{-1}. \end{aligned} \tag{3.70}$$

After making use of the 3.28 and the properties of the Laplace transform a modified equation of motion for the density correlator will be obtained.

$$\begin{aligned} & z\boldsymbol{S}(z) - \boldsymbol{S}(\boldsymbol{q}) = -\boldsymbol{\omega}\boldsymbol{S}^{-1}\boldsymbol{S}(z) + \boldsymbol{M}(z)\boldsymbol{S}^{-1}\boldsymbol{S}(z) \\ \Leftrightarrow\ & \boldsymbol{S}(z) = \left[z + \left(\boldsymbol{\omega} - \left(\boldsymbol{m}_{\mathrm{T}}^{-1}(z) + \boldsymbol{\omega}_{\mathrm{T}}^{-1}\right)^{-1}\right)\boldsymbol{S}^{-1}\right]^{-1}\boldsymbol{S} \\ \Leftrightarrow\ & z\boldsymbol{S}(z) - \boldsymbol{S} = -\boldsymbol{\omega}\boldsymbol{S}^{-1}\boldsymbol{S}(z) - \boldsymbol{m}^{\mathrm{T}}(z)\boldsymbol{\omega}_{\mathrm{T}}^{-1}\left[z\boldsymbol{S}(z) - \boldsymbol{S} + \boldsymbol{\omega}^{\mathrm{R}}\boldsymbol{S}^{-1}\boldsymbol{S}(z)\right] \end{aligned} \tag{3.71}$$

$$\Leftrightarrow\ \boxed{\partial_t \boldsymbol{S}(t) = -\boldsymbol{\omega}\boldsymbol{S}^{-1}\boldsymbol{S}(t) - \int_0^t dt' \boldsymbol{m}^{\mathrm{T}}(t-t')\boldsymbol{\omega}_{\mathrm{T}}^{-1}\left[\partial_{t'}\boldsymbol{S}(t') + \boldsymbol{\omega}^{\mathrm{R}}\boldsymbol{S}(t')\right]} \tag{3.72}$$

The latter equation 3.72 is the final EOM for the density correlator. From mathematical point of view that EOM is identical to the previous equation 3.56e, but it has a modified structure. The convolution integral contains an extra term in the square brackets the so-called hopping term $\boldsymbol{\omega}^{\mathrm{R}}\boldsymbol{S}(t)$. The translational part of the irreducible memory kernel $\boldsymbol{m}^{\mathrm{T}}$ does not need to be calculated, it is identical to $\boldsymbol{m}$ that was already evaluated in previous sections.
To demonstrate the benefits of the EOM 3.72 over the previous EOM 3.56e we again analyze the long time behavior of the correlator in Laplace space, where the expansion formulas for $\boldsymbol{S}$ and $\boldsymbol{m}^{\mathrm{T}}$ in powers of the Laplace variable will be used.

$$\begin{aligned} \boldsymbol{S}(z) &= \frac{\boldsymbol{F}}{z} + \boldsymbol{F}_0 + z\boldsymbol{F}_1 + \mathcal{O}\left(z^2\right), \\ \boldsymbol{m}^{\mathrm{T}}(z) &= \frac{\boldsymbol{m}^{\mathrm{T}}[\boldsymbol{F}]}{z} + \boldsymbol{m}_0^{\mathrm{T}} + z\boldsymbol{m}_1^{\mathrm{T}} + \mathcal{O}\left(z^2\right). \end{aligned} \tag{3.73}$$

After inserting 3.73 in 3.71 the following equation can be derived:

$$\begin{aligned} & \boldsymbol{F} + z\boldsymbol{F}_0 + z^2\boldsymbol{F}_1 - \boldsymbol{S} = -\boldsymbol{\omega}\boldsymbol{S}^{-1}\left[\frac{\boldsymbol{F}}{z} + \boldsymbol{F}_0 + z\boldsymbol{F}_1\right] \\ & - \left[\frac{\boldsymbol{m}^{\mathrm{T}}[\boldsymbol{F}]}{z} + \boldsymbol{m}_0^{\mathrm{T}} + z\boldsymbol{m}_1^{\mathrm{T}}\right]\boldsymbol{\omega}_{\mathrm{T}}^{-1}\left[\boldsymbol{F} + z\boldsymbol{F}_0 + z^2\boldsymbol{F}_1 - \boldsymbol{S} + \boldsymbol{\omega}^{\mathrm{R}}\left[\frac{\boldsymbol{F}}{z} + \boldsymbol{F}_0 + z\boldsymbol{F}_1\right]\right]. \end{aligned} \tag{3.74}$$

We collect terms in different powers of z and take the limit $z \to 0$ to get a recursive equation for the long time value $\boldsymbol{F}$.

$\boxed{\frac{1}{z^2}}$

$$0 = \frac{1}{z^2}\boldsymbol{m}^{\mathrm{T}}[\boldsymbol{F}]\boldsymbol{\omega}^{\mathrm{R}}\boldsymbol{F}. \tag{3.75}$$

$\boxed{\frac{1}{z}}$

$$0 = -\boldsymbol{\omega}\boldsymbol{S}^{-1}\frac{\boldsymbol{F}}{z} - \frac{\boldsymbol{m}[\boldsymbol{F}]}{z}\boldsymbol{\omega}_{\mathrm{T}}^{-1}\left[\boldsymbol{F} - \boldsymbol{S} + \boldsymbol{\omega}^{\mathrm{R}}\boldsymbol{F}_0\right] - \boldsymbol{m}_0^{\mathrm{T}}\boldsymbol{\omega}^{\mathrm{R}}\frac{\boldsymbol{F}}{z}. \tag{3.76}$$

So there are two equations that have to be satisfied by the nonergodicity parameter. In the first equation (3.75) the structure of the rotational diffusion plays a key role, being a not fully occupied matrix. One possible solution of the equation 3.75 is given by $\boldsymbol{\omega}^{\mathrm{R}}\boldsymbol{F} = 0$. The latter is not a unique solution because of the structure of the memory kernel that itself depends on the nonergodicity parameter.

$$0 = \sum_k \boldsymbol{\omega}^R_{i,k}\boldsymbol{F}_{k,j} = \boldsymbol{\omega}^R_{i,i}\boldsymbol{F}_{i,j} \;\; \forall\,\{i,j\} \;\; \Rightarrow \;\; \boldsymbol{F}_{i,j} = 0 \;\; \forall\,\{i,j\}_{i\neq 0}\,. \tag{3.77}$$

If the solution is given by $\boldsymbol{\omega}^{\mathrm{R}}\boldsymbol{F} = 0$ than all $\boldsymbol{F}_{0,j}$ can have an finite value with a simultaneous vanish of all other components. That kind of condition would allow the system to have frozen translations $\boldsymbol{F}_{0,0} > 0$ with relaxing rotations $\boldsymbol{F}_{1,1} = 0$. The finite values of $\boldsymbol{F}_{0,j}$ have to obey the condition (3.76). The disadvantage of the equation (3.76) compared to the previous recursive equation (3.66) (without the hopping term) is the extra term $\boldsymbol{F}_0$. To get an expression for $\boldsymbol{F}_0$ it is necessary to solve the transient dynamics first.

$$\boldsymbol{F}_0 = \lim_{z\to 0}\partial_z\Big[z\boldsymbol{S}(z)\Big] = \lim_{z\to 0}\partial_z\int_0^\infty z\mathrm{e}^{-zt}\boldsymbol{S}(t)dt = \int_0^\infty \boldsymbol{S}(t)dt. \tag{3.78}$$

The necessity of having to evaluate the time integral over the whole interval of the density correlator to close the recursive equation for the nonergodicity parameter ruins the elegance of the equation (3.76) being not self-consistent.
In the next chapter we will show the numerical results for the density correlator and the nonergodicity parameter by solving the equations (3.72) and (3.76) respectively. The numerical methods needed to solve integro-differential equations with a hopping term in the convolution integral are presented in the appendix B.

3.6 Summary

This chapter is the key chapter in this thesis that includes all important quantities needed for further numerical calculations. The dynamical density correlator matrix was defined, and the importance of each matrix component emphasized. Calculating the density correlator is a handy way for analyzing the dynamics of the system without keeping track of all particle trajectories. To describe the initial structure of the system the statical structure factor was introduced, being isotropic in wave vector and numerically easily accessible quantity by using the approximations from Baus and Colot. To derive the equation of motion for the density correlator in a form which is better suited for approximations than the initial definition, the projection formalism of Mori and Zwanzig for ABD systems was used. The main idea behind the projection formalism was to separate “relevant” and “irrelevant”

variables, the first being conserved quantities and the later not. After following the steps of the projection formalism an EOM for the correlator was derived that is from the mathematical point of view identical to the initial definition. The EOM represents an integro-differential equation with the memory kernel in the convolution integral. To make the memory kernel more robust under approximations second projection step was used. The knowledge from the Mode Coupling Theory of the glass transition was used to approximate the memory kernel. After the approximations the memory kernel became an accessible quantity depending only on the density correlator and the static structure factor as an input. After analyzing the long time behavior of the correlator, that allowed a simultaneous freezing of the translational and rotational degrees for hard disks a further splitting was encouraged. Finally the equation of motion for the density correlator was derived, as a self-consistent integro-differential equation solved numerically in the next chapter. The extra hopping term in the convolution integral allows the correlator to have frozen translational degrees by a simultaneous relaxation of the rotations.

Chapter 4

Numerical Results

In the last chapter the equation of motion for the density correlator was derived. Since it is an integro-differential equation for matrix like functions determining an analytic solution is hopeless and numerical methods are needed. The tools to solve that kind of equations numerically are provided in the appendix B. We recall the EOM the numerical results are based on.

$$\partial_t \boldsymbol{S}(t) = -\boldsymbol{\omega}\boldsymbol{S}^{-1}\boldsymbol{S}(t) - \int_0^t dt' \boldsymbol{m}^{\mathrm{T}}(t-t')\,\boldsymbol{\omega}_{\mathrm{T}}^{-1}\Big[\partial_{t'}\boldsymbol{S}(t') + \boldsymbol{\omega}^{\mathrm{R}}\boldsymbol{S}(t')\Big]. \tag{4.1}$$

In this chapter we present numerical results for the normalized density correlator $\boldsymbol{\Phi}$ for different set of parameters. Effectively the influence of three different parameters $\{\phi, v_0, D_r\}$ can be studied, the other two parameters $\{D_t, \sigma\}$ are used to define the units (so all quantities are measured in units of D_t and σ or combinations of those). The packing fraction ϕ enters the equilibrium static structure factor, the activity force v_0 enters the memory kernel as well as the frequency function, and the rotational diffusion D_r only influences $\boldsymbol{\omega}^R$.

4.1 Dynamical Density Correlator

The dynamical density correlator is a matrix in space of the orientational indices. Different components provide insight to different physical properties.

4.1.1 $\boldsymbol{\Phi}_{0,0}$

The most important matrix element of the correlator is the $l = 0, l' = 0$ element. Setting the orientational indices to zero removes any angular dependence. So $\boldsymbol{\Phi}_{0,0}$ is perfectly suited for studying structural properties of the system. So the correlator $\boldsymbol{\Phi}_{0,0}$ will be used to investigate the glassy dynamics and the influence of

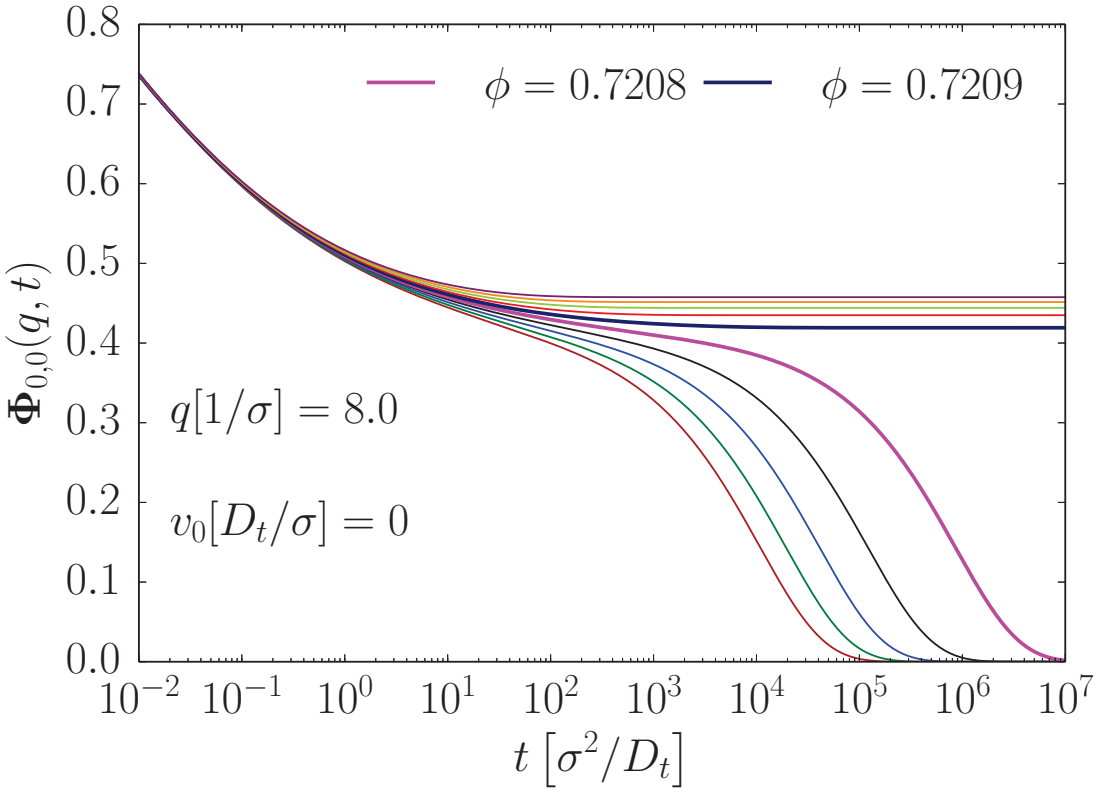

Figure 4.1: Density correlator $\mathbf{\Phi}_{0,0}$ as a function of time for a passive system. The packing fraction is chosen in the range of $0.7204 < \phi < 0.7213$.

different parameters at the system. To study the influence of the activity at the glass transition point, it is useful to have the critical packing fraction ϕ^c_{passive} of the passive system available. The critical packing fraction denotes the bifurcation point in the system that separates the glassy state from the fluid state. In the Figure 4.1 the correlation function $\mathbf{\Phi}$ of the passive system for many different packing fractions can be observed. From that figure the location of the critical point can be estimated $0.7208 < \phi^c_{\text{passive}} < 0.7209$. One should notice that the critical packing fraction depends on the discretization accuracy of the double integral over the wavenumber space. The details about the numerical settings are presented in the Appendix B. The current discretization used for all the plots in this chapter is a good compromise of acceptable performance speed and accurate results. Doubling the number of discrete q points changes only the last digit of ϕ^c_{passive} but the calculations take 8 times longer. If the packing fraction is chosen below ϕ^c_{passive} the correlator decays to zero and above it remains finite and reaches the value of the

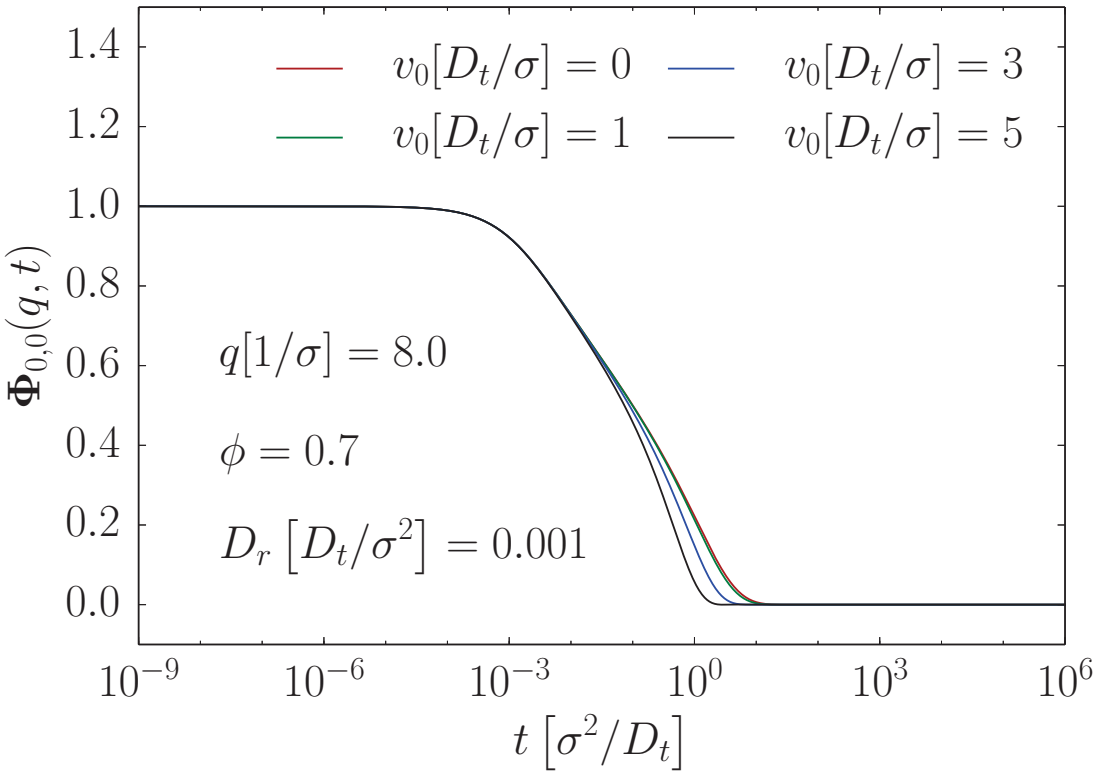

Figure 4.2: Density correlator $\mathbf{\Phi}_{0,0}$ as a function of time for different activity velocities v_0 at fixed rotational diffusion D_r. The packing fraction is chosen below the critical passive packing $\phi < \phi^c_{\text{passive}}$.

nonergodicity parameter. The Figures 4.2 and 4.3 illustrate the influence of the activity at the system for two different packing fractions. In the first figure 4.2 the packing fraction is below ϕ^c_{passive}, so all curves remain ergodic. The increase of the velocity only forces the correlator do decay faster. The particles with a higher self-propulsion velocity can break the intermediate cage faster. In the second figure 4.3 the packing fraction is above ϕ^c_{passive}, and thus there exists a critical velocity needed to destroy the glass. In contradiction to systems under shear a nonzero activity force is not sufficient to melt the glass. For a given packing fraction and rotational diffusion there exist a critical velocity $v^c_0(\phi, D_r)$ that separates a glass from fluid. The precise dependence of the glass transition point at the parameters will be investigated in the next sections. From the Figure 4.3 the critical velocity for the given settings can be estimated being in the range $2 < v^c_0 < 4$.
From the physical point of view it is logical that the increase of activity lets the particles break the neighboring cages faster and the systems becomes softer. The

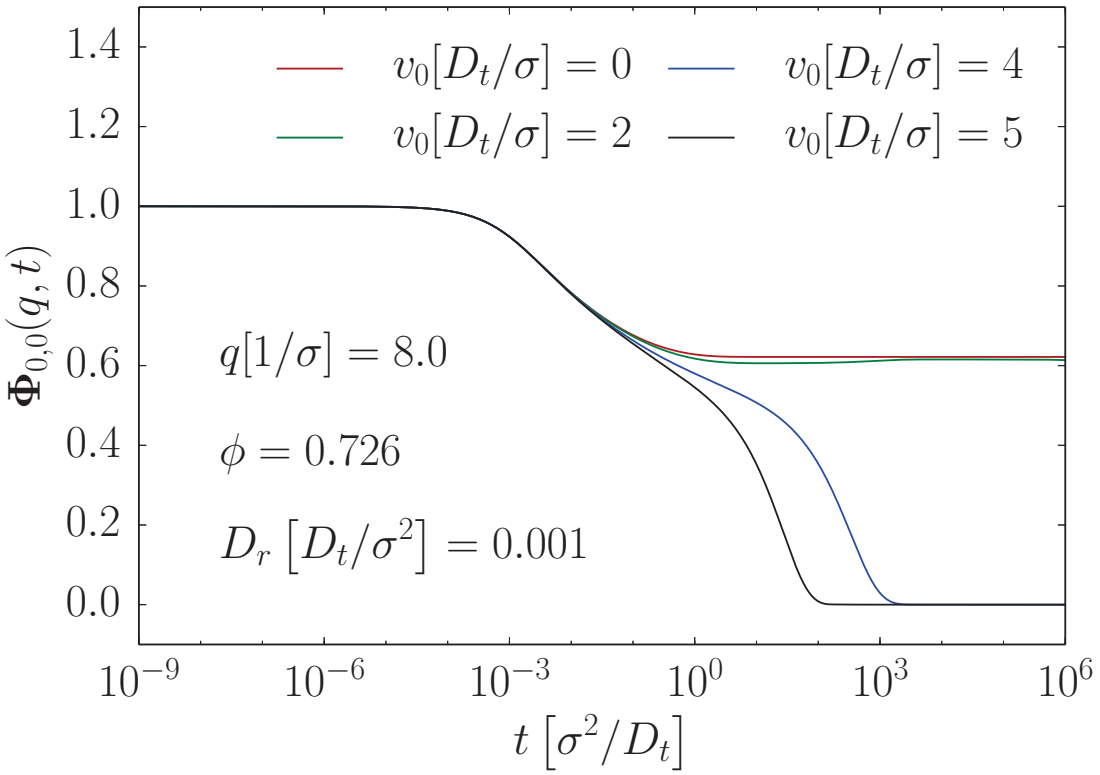

Figure 4.3: Density correlator $\mathbf{\Phi}_{0,0}$ as a function of time for different activity velocities v_0 at fixed rotational diffusion D_r. The packing fraction is chosen above critical passive packing $\phi > \phi^c_{\text{passive}}$.

influence of activity on the system was also described qualitatively correctly by the theory without an additional hopping term in the convolution integral (before splitting in translational and rotational parts). The hopping term will become important by studying the influence of the rotational diffusion D_r on the system, which is not obvious. The rotational diffusion describes the rate of the random changes of the direction of each particle. Having a zero rotational diffusion corresponds to a system of nonrotating particles. If one considers a nail in a wall which needs to be pulled out, the surface fraction of the nail can be decreased by rotating it and the nail can be pulled out more easily than without rotating. So in that case increasing the rotational capability of the nail softens the system. As a second example we consider a crowded place with people, where one wants to escape the crowd. Maintaining the direction in which one pushes makes it easier to leave the crowd than first pushing in one direction and than changing the direction and pushing into another direction. So in that case increasing the rotational capability

makes the system more stable (it is more difficult to break the cage). In that two examples the rate of rotations affect the stability of the system differently. In the following we want to analyze the influence of the rotational diffusion on the system of active Brownian disks. If we take a close look at the EOM 4.1 we

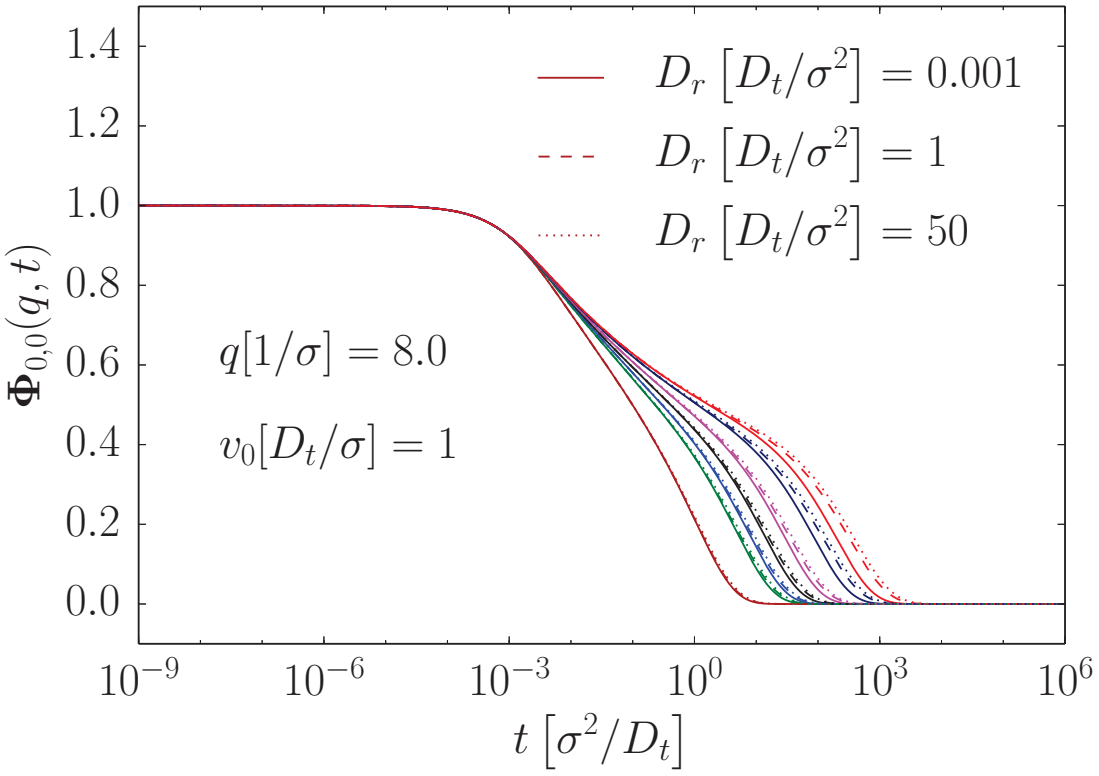

Figure 4.4: Correlation function $\mathbf{\Phi}_{0,0}$ as a function of time for a fixed activity force (smaller value) but different rotational diffusion constant D_r. Different colors mark different packing fractions (increasing from left to right). Different line shapes denote different D_r.

notice that the only term depending on the rotational diffusion is the rotational part of the frequency matrix $\boldsymbol{\omega}^{\mathrm{R}}$ (and thus the total frequency matrix). Due to the shape of $\boldsymbol{\omega}^{\mathrm{R}}$ the rotational diffusion does not affect $l = 0, l' = 0$ part of the correlator directly, it enters the equation only by back coupling of other matrix elements of the correlator. The dependence of $\mathbf{\Phi}_{0,0}$ on the rotational diffusion for different densities and activity forces is illustrated in Figures 4.4 and 4.5. In the first Figure 4.4 the system experiences a smaller activity force v_0 than in the second Figure 4.5. In both cases the system relaxes later by increasing the rotational diffusion, but for higher v_0 the effect is larger. It is obvious that for vanishing

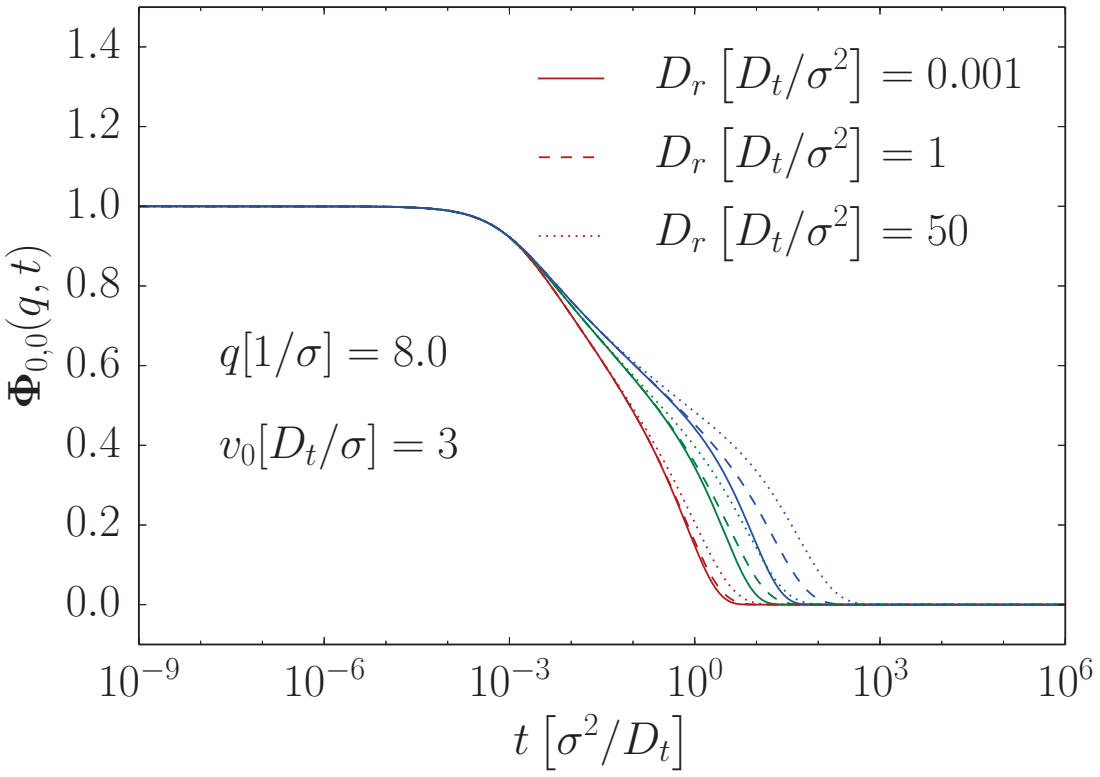

Figure 4.5: Correlation function $\mathbf{\Phi}_{0,0}$ as a function of time for a fixed activity force (higher value) but different rotational diffusion constant D_r. Different colors mark different packing fractions (increasing from left to right).

activity $v_0 = 0$, changing D_r will not affect the correlator, since the translational and rotational motion will be completely decoupled. It is also interesting to consider the limit of very high rotational diffusion. From a physical point of view one would expect in the limit of infinite rotational diffusion $D_r \to \infty$ the system to be described by the passive system again. For very high D_r the self-propulsion velocity on average, will influence the system only at the timescales of $t \sim 1/D_r$ and can be completely neglected for infinite D_r. The approach of the active system by very high rotational diffusion to the passive system is illustrated in the Figure 4.6. The correlator of the active system with $D_r = 1000$ almost coincides with the correlator with zero activity. For the system of a single active Brownian disk there exists an effective parameter D_{eff} that describes the system at long time scales. so the system does not depend on the activity v_0 and the rotational diffusion D_r separately, but on the fraction v_0^2/D_r. That kind of effective parameter (The Péclet number) was also successfully used to describe the system of a single

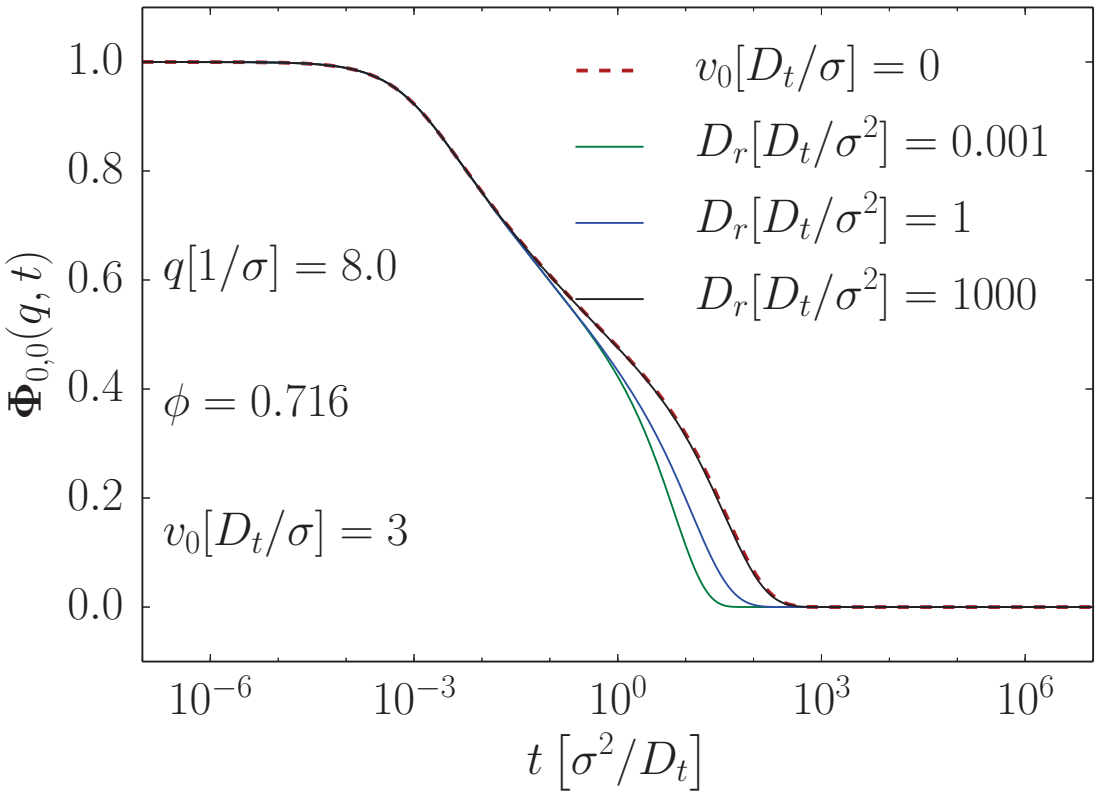

Figure 4.6: Correlation functions $\mathbf{\Phi}_{0,0}$ as a function of time for a fixed activity force (solid lines) but different rotational diffusion D_r. Dashed line corresponds to the passive system. The packing fraction is below the glass transition point of a passive system.

anisotropic active Brownian particle in a solvent [22]. It is interesting to analyze if the ABD system also can be described by a dimensionless quantity v_0^2/D_r (measured in units of D_t). The dimensionless number v_0^2/D_rD_t is also called in the literature the Péclet number (sometimes with a factor of 2). So we want to analyze the transformation $(\phi, v_0, D_r) \to (\phi, \mathrm{Pe})$ that would allow us to reduce the number of independent parameters. The Figure 4.7 shows the correlation function by fixed Péclet number $\mathrm{Pe} = 32$ for different activities. It is clear that in this case the Péclet number is not a sufficient parameter to describe the system, and both v_0 and D_r are needed. For very high activities one can observe an undershoot of the correlation function for the wavenumber $q[1/\sigma] = 8$. To better understand the meaning of the negative part of the correlator it is convenient not to plot only a single wavenumber, but the whole range of it. In the Figure 4.8 the correlation

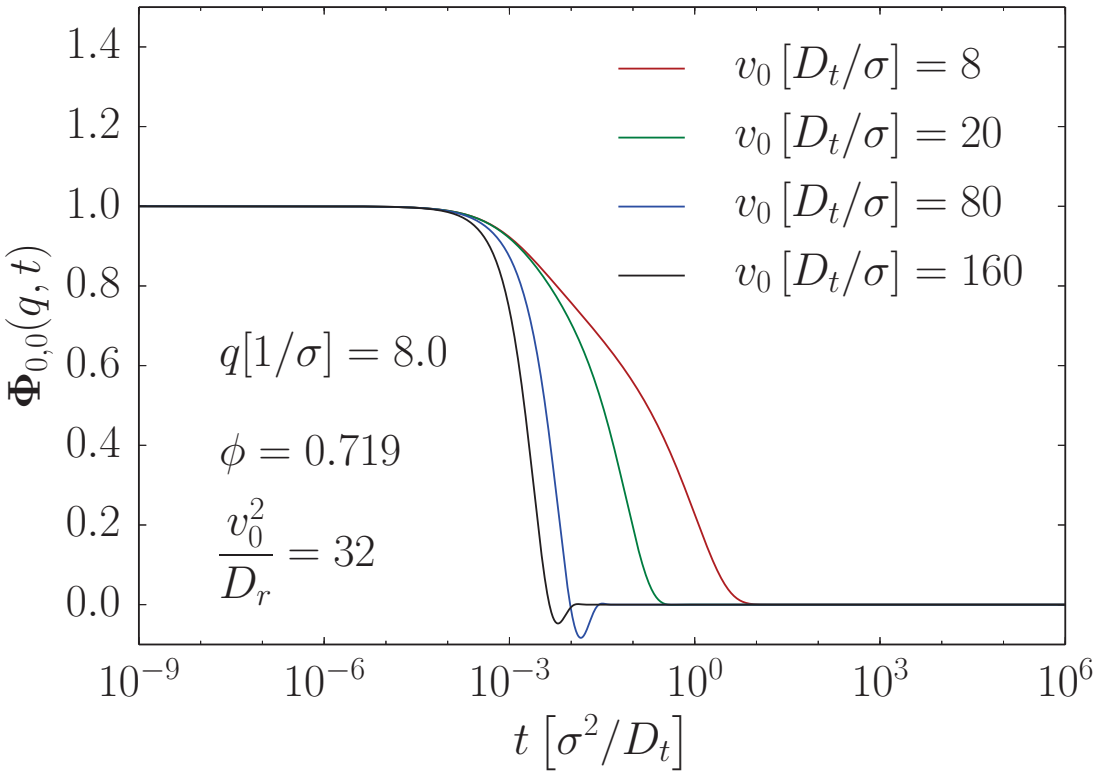

Figure 4.7: Correlation function $\mathbf{\Phi}_{0,0}$ as a function of time for a fixed Péclet number $\mathrm{Pe} = \frac{v_0^2}{D_r}$. Different colors mark different activity values.

functions for all available wavenumbers by a constant Péclet number are plotted. The opacity of the lines marks the value of q. The darker lines correspond to higher q values (the highest wavenumber is $q[1/\sigma] = 50$). Above certain activity correlators stop to be monotonically decreasing and show oscillation patterns for some wavenumbers. The strength of the undershoot depends on the activity and on the time interval. The wavenumber is the Fourier-transform of the position vector in real space and describes the resolution of the length. High wavenumbers allow to look into small length scales. The length the particle can travel without changing the direction is characterized by the persistence length (similarly to [22]) $\mathrm{L} = v_0\tau_{\mathrm{rot}}$ with the rotational time scale $\tau_{\mathrm{rot}} = 1/D_r$. Using the persistence length it is useful to define a dimensionless wavenumber $\tilde{q} = \mathrm{L}q/2\pi$. The condition $\tilde{q} \gtrsim 1$ needs to be fulfilled to be able to resolve the persistence length of the particles.

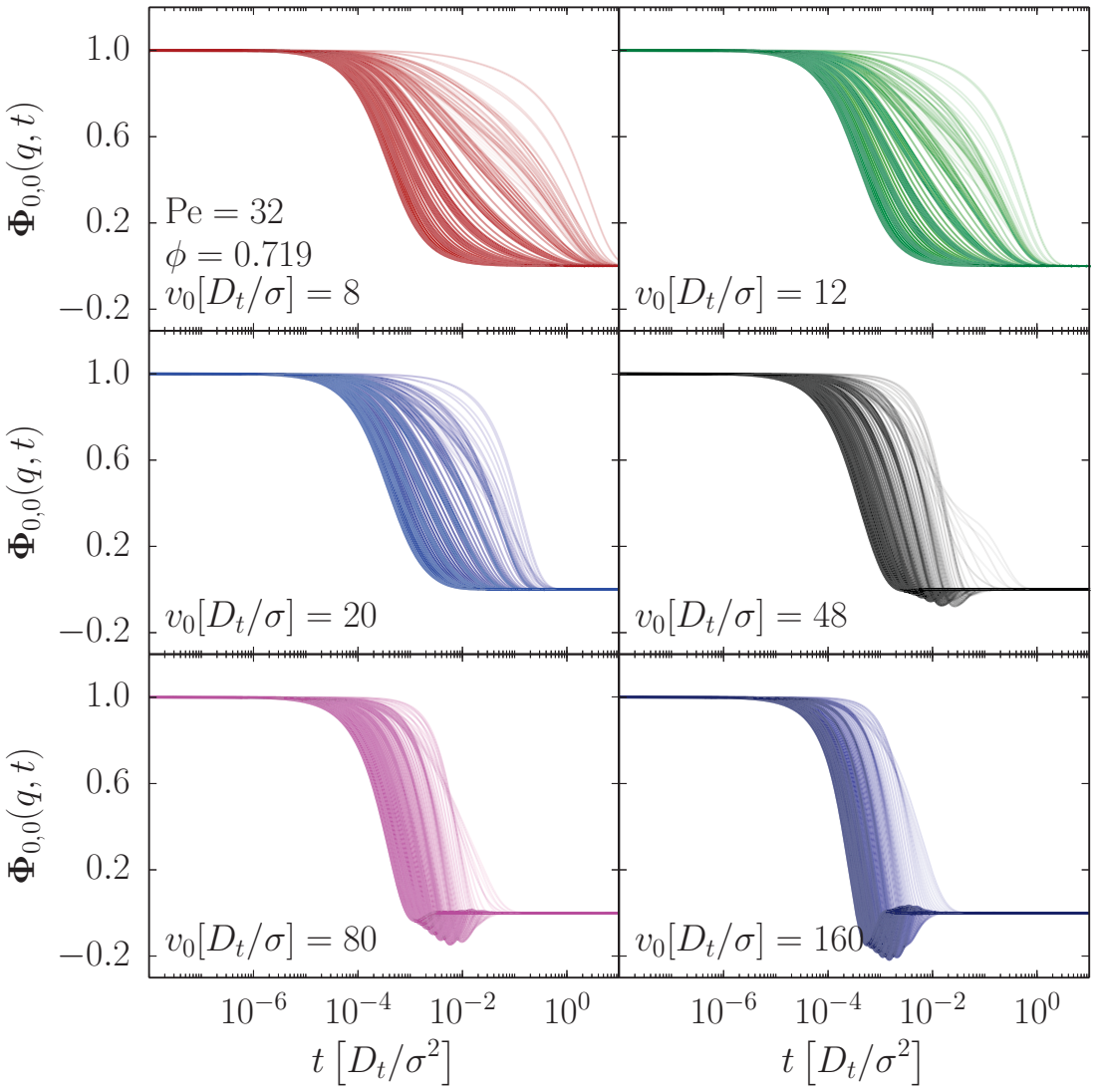

Figure 4.8: Density correlator $\mathbf{\Phi}_{0,0}$ as a function of time for all wavenumbers for different activities. The opacity of the line marks the value of q (darker lines correspond to higher q). The ratio $\mathrm{Pe} = v_0^2/D_r$ is kept constant.

The Figure 4.9 illustrates the correlation function $\mathbf{\Phi}_{0,0}$ as a function of time normalized by the rotational time scale for different wavenumbers at a constant Péclet number. From top to bottom the activity gets increased. If the activity is bigger than a certain value and the wavenumber is big enough to resolve the persistence length of the particle, the short time diffusion can be ignored and one observes oscillations for the correlator (middle right panel and the bottom panel in 4.9).

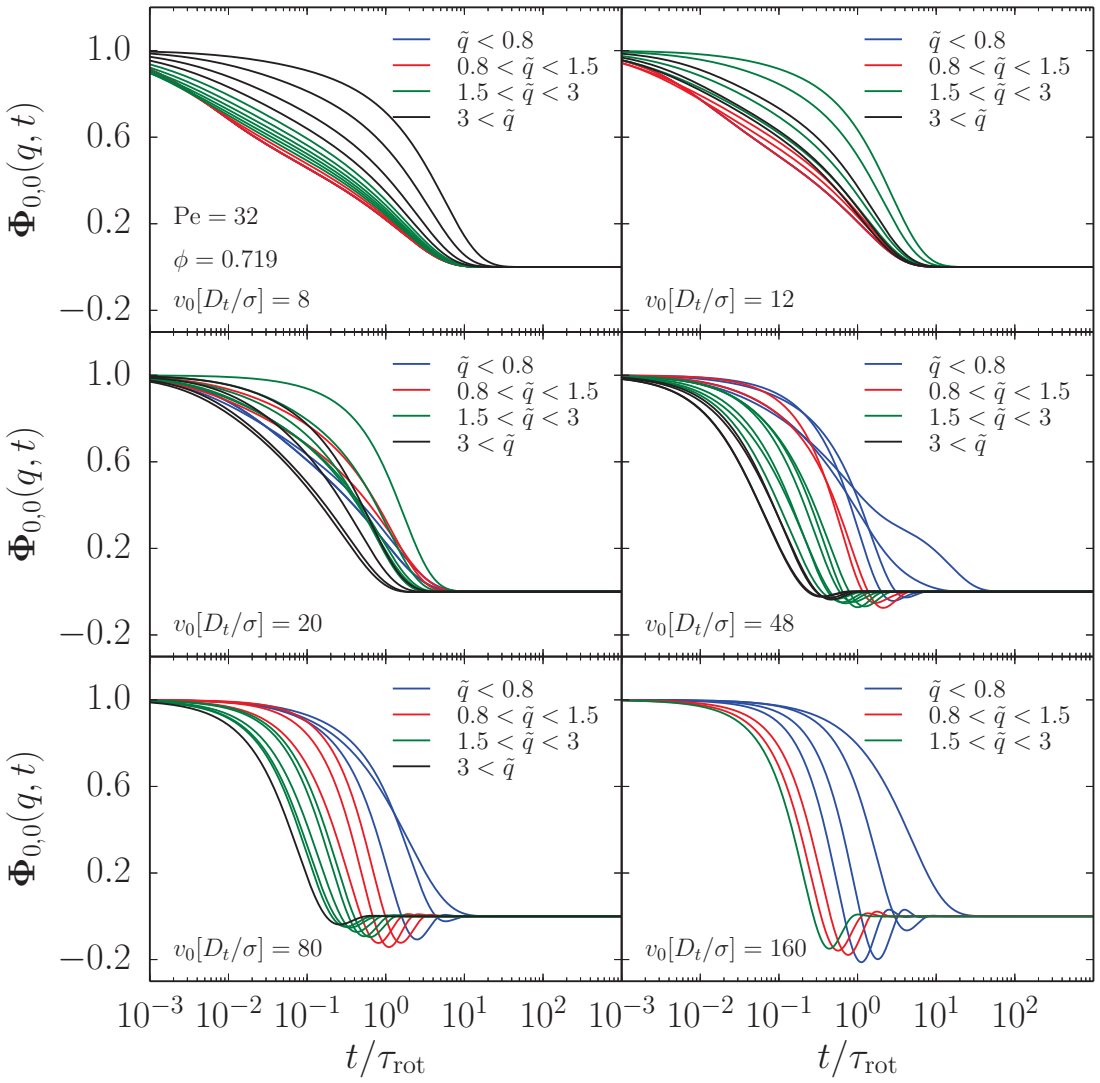

Figure 4.9: Density correlator $\mathbf{\Phi}_{0,0}$ as a function of time normalized by the rotational time scale $\tau_{\mathrm{rot}} = \frac{1}{D_r}$ at constant Péclet number. Different colors denote different range of the dimensionless wavenumber $\tilde{q} = \frac{\mathrm{L}q}{2\pi}$ with the persistence length $\mathrm{L} = \frac{v_0}{D_r}$. The activity v_0 gets increased from top to bottom.

Is the wavenumber too big the short time diffusion becomes important and the correlator decays monotonously again. The two regimes for the wavenumber can be seen in the middle right panel of the Figure 4.9. If the wavenumber is big enough to resolve the persistence length but not too big that the short time diffusion becomes important, than rotational and translational diffusion can be neglected

and only the ballistic motion $v_0 t$ will be observed. For the ballistic motion the density correlator $\mathbf{\Phi}_{0,0}(q,t) \propto \mathrm{sinc}(v_0 q t)$ behaves like a sinc function [22], which explains the oscillations.
As a final part in this section we want to look at the behavior of the system at different time scales in a glassy state, where the recursive equations of the nonergodicity parameter presented in the previous chapter will be used. In the

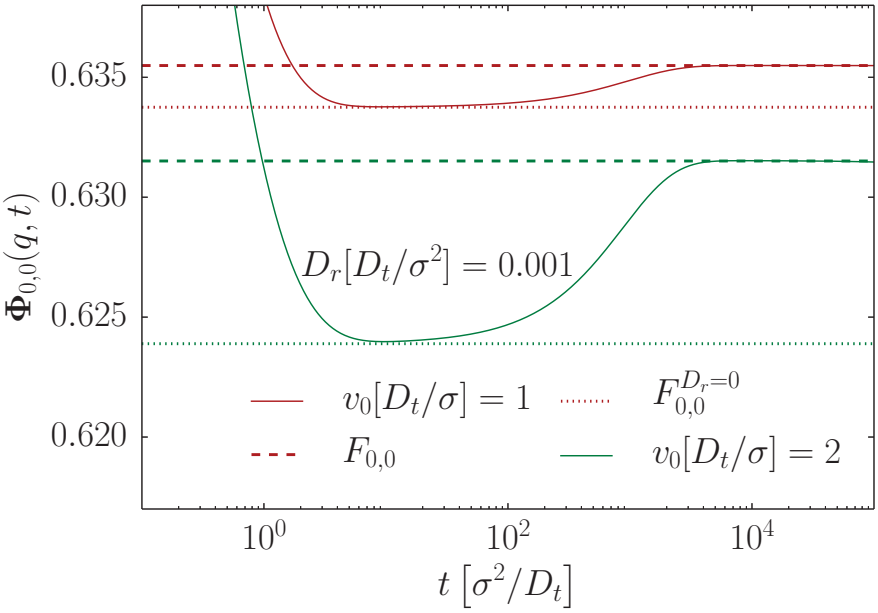

Figure 4.10: Density correlator $\mathbf{\Phi}_{0,0}$ (solid line) as function of time for different activities at a small rotational diffusion $D_r = 0.001$. Dashed lines correspond to the nonergodicity parameter and dotted lines correspond to the nonergodicity parameter for vanishing rotations. The packing fraction is chosen above the critical packing $\phi = 0.726$.

Figure 4.10 the correlation functions $\mathbf{\Phi}_{0,0}$ as function of time for two different activities at a constant D_r are plotted. The dashed lines mark the nonergodicity parameter obtained from the recursive equation 3.75 and 3.76. The dotted lines correspond to the nonergodicity parameter without the integral term $\boldsymbol{F}_0$. The system exhibits three different time regimes.

- Times $t \lesssim \min(1, 1/D_r)$: Initial decay of the correlator due to the short time diffusion of the particles. The rotational diffusion at this time scale can be neglected.
- $1 \lesssim t \lesssim 1/D_r$: Intermediate time scale only possible for small rotational diffusion constants $D_r < 1$. Local translational caging of the particles before

the rotational diffusion becomes relevant.

- $1/D_r \lesssim t$: The rotational diffusion becomes an important quantity and the correlator decays exponentially to the final long time value.

If the rotational diffusion is not small enough the system will not exhibit the intermediate time scale and it directly decays to the final long time value. The EOM in Laplace domain will provide deeper insight about the time scales of the correlator.

$$0 = -\boldsymbol{\omega}\boldsymbol{S}^{-1}\frac{\boldsymbol{F}}{z} - \frac{\boldsymbol{m}^{\mathrm{T}}[\boldsymbol{F}]}{z}\boldsymbol{\omega}_{\mathrm{T}}^{-1}\left[\boldsymbol{F} - \boldsymbol{S} + \boldsymbol{\omega}^{\mathrm{R}}\left[\frac{\boldsymbol{F}}{z} + \boldsymbol{F}_0\right]\right], \tag{4.2}$$

where it was considered the Laplace variable to be small enough that z^0 and higher terms can be neglected, but big enough that the term $D_r/z^2 \ll 1$ is negligible (or in time domain $D_r t \ll 1$). By making that assumptions we can simplify the recursive equation for the nonergodicity parameter.

$$\boldsymbol{\omega}_{\mathrm{T}}\boldsymbol{S}^{-1}\boldsymbol{F} + \boldsymbol{m}^{\mathrm{T}}[\boldsymbol{F}]\boldsymbol{\omega}_{\mathrm{T}}^{-1}\Big[\boldsymbol{F} - \boldsymbol{S}\Big] = 0. \tag{4.3}$$

The equation is completely independent on D_r and corresponds to the equation for $\boldsymbol{F}$ at $D_r = 0$. So if there exists a time $1 \ll t \ll 1/D_r$ then the intermediate plateau value of the correlator $\boldsymbol{\Phi}_{0,0}$, is given by $\boldsymbol{F}_{0,0}^{D_r=0}$, which is illustrated in the Figure 4.10.

4.1.2 Matrix Elements of the Correlator

Up to now we only considered the $l = 0, l' = 0$ component of the density correlation matrix that is a key quantity by analyzing the structural properties of the system. In this section the focus will be on other components of the correlator matrix describing also the rotational behavior of the system. The Figure 4.11 shows different matrix elements of the density correlator for different parameters. In the top panel four different matrix elements for different activities and packing fractions are plotted. The activity dependence is shown on the left plot. The packing fraction is above the critical packing of the passive system, as one can see from the lowest v_0 curve for $\boldsymbol{\Phi}_{0,0}$ which is nonergodic. Even if the particles are hindered at translational motion the rotations never freeze thus $\boldsymbol{\Phi}_{1,1}$ always remains ergodic. The time scale at which the $\boldsymbol{\Phi}_{1,1}$ decays to zero is determined by the rotational diffusion and the activity, since $\boldsymbol{\Phi}_{1,1}$ contains also translational part $\boldsymbol{\Phi}_{1,1}(t) \propto \sum_{j,k}\left\langle \mathrm{e}^{i\vec{q}\cdot(\vec{x}_j(t)-\vec{x}_k(0))}\mathrm{e}^{i(\varphi_j(t)-\varphi_k(0))}\right\rangle$. On the top right figure the activity is kept constant and the packing fraction is varied. The two lines with highest ϕ are in the glassy state. The interplay of the rotational diffusion and the activity

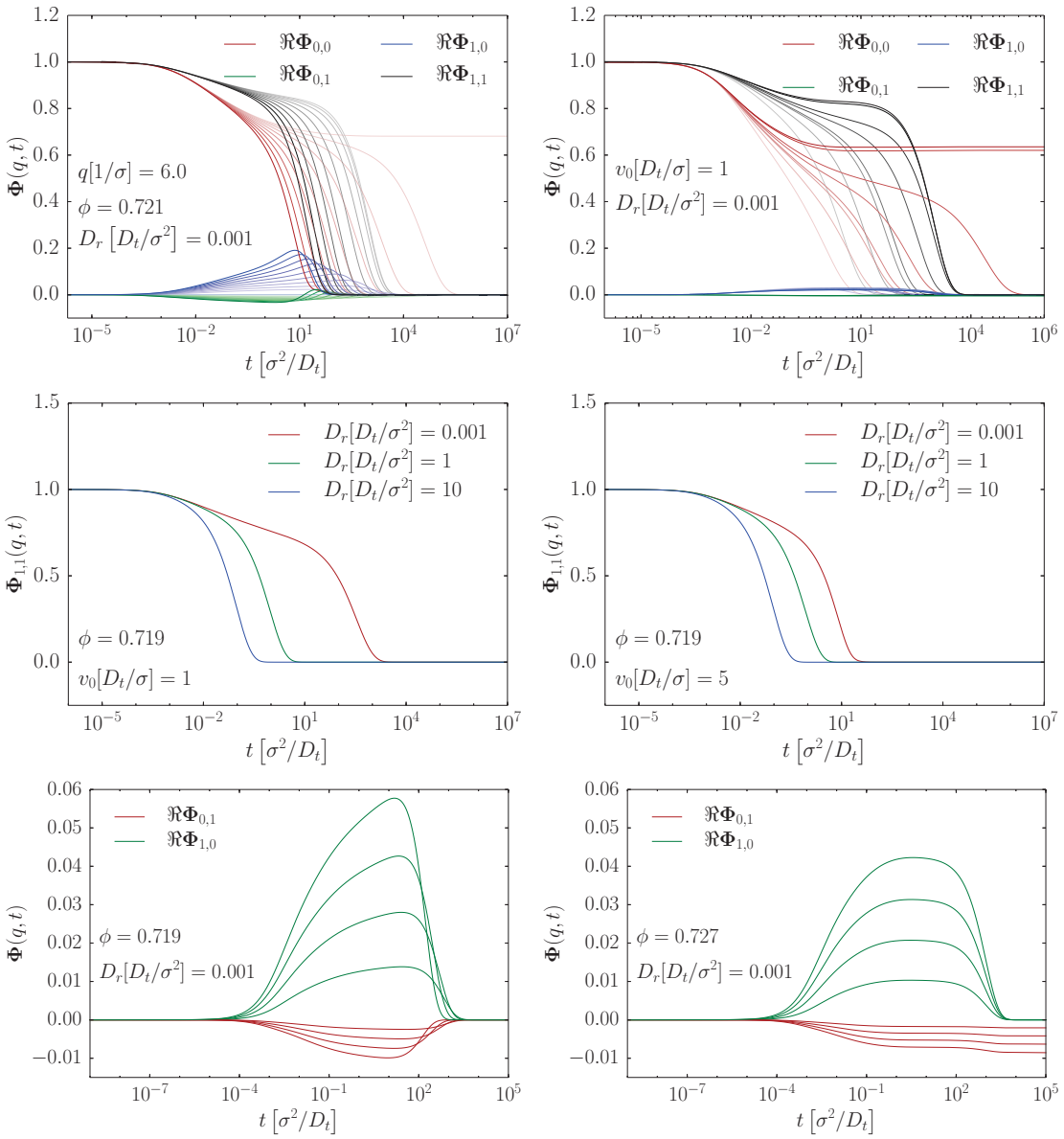

Figure 4.11: Different components of the density correlator matrix $\mathbf{\Phi}$ as a function of time. A Different opacity value denotes the value of the varied parameter (darker lines correspond to higher values). The top figures show the influence of activity and packing fraction at the density correlator matrix (left figure: change in v_0, right figure: change in ϕ). The middle panel shows figures for the $\mathbf{\Phi}_{1,1}$ for different D_r at constant activity. Lower panel shows the difference between $\mathbf{\Phi}_{0,1}$ and $\mathbf{\Phi}_{1,0}$.

at the relaxation timescale is illustrated in the middle panel. For two different activities the influence of D_r can be studied. For a higher rotational diffusion the relaxation is dominated by rotational diffusion and therefore the relaxation time does not depend on the activity. For small D_r values the relaxation is dominated by the translational motion and changing the activity shifts the relaxation time drastically. One way of getting the information only about the rotational relaxation without the additional structural relaxation is to look at the correlator at vanishing wavenumber. The bottom panel of the Figure 4.11 shows the comparison of the off-diagonal elements of the correlator for different v_0 in a fluid state (left plot) and in a glassy state (right plot). In the last chapter a condition for the nonergodicity parameter was derive.

$$0 = \boldsymbol{m}^{\mathrm{T}}[\boldsymbol{F}]\boldsymbol{\omega}^{\mathrm{R}}\boldsymbol{F}. \tag{4.4}$$

If we assume that the memory kernel is invertible the above equation would correspond to:

$$0 = \sum_k \boldsymbol{\omega}^R_{i,k}\boldsymbol{F}_{k,j} = \boldsymbol{\omega}^R_{i,i}\boldsymbol{F}_{i,j} \;\; \forall\{i,j\} \;\; \Rightarrow \;\; \boldsymbol{F}_{i,j} = 0 \;\; \forall\{i,j\}_{i\neq 0}\,. \tag{4.5}$$

That kind of asymmetry of the correlator is confirmed in the bottom right plot of 4.11 where the system is in a glassy state and $\boldsymbol{\Phi}_{1,0}$ is ergodic and the $\boldsymbol{\Phi}_{0,1}$ remains nonergodic. The physical interpretation would be that the final orientations are uncorrelated to the initial structure but the final structure is correlated to the initial orientations.

4.2 Relaxation Time

In the last section the density correlator $\boldsymbol{\Phi}_{0,0}$ for many different parameters as a function of time was presented. The correlator $\boldsymbol{\Phi}_{0,0}$ was plotted for a glassy as well as for the fluid state and the influence of different parameters studied. An important question that arises is to understand how the glass transition point depends on the parameters and to determine the phase diagram that separates the glassy and fluid state. To determine the glass transition point on a direct way is very cumbersome, due to the form of the recursive equation of the nonergodicity parameter $\boldsymbol{F}$ that is not self-consistent and also depends on the integral of the correlator itself. At the bifurcation point it is very tricky to keep the time domain algorithm stable enough to determine the time integral of the correlator precisely that is needed in the recursive equation 3.75 (small deviations for $\boldsymbol{F}_0$ will influence the final result dramatically since the equation for $\boldsymbol{F}$ is solved recursively, and the number of recursions close to the bifurcation point is very high and the error gets amplified after each recursion).

The goal in this section is to show the results for the relaxation time τ for the correlator $\mathbf{\Phi}_{0,0}$, and use the MCT prediction [46, 47] of a power low divergence of the relaxation time at the critical point to determine critical parameters and thus the glass transition point. If the system is in a fluid state the correlator decays after some time to zero. The characteristic time the correlator needs to relax is called the relaxation time τ. There are different ways to introduce the criterion that defines the relaxation time. The most common definition is the criterion:

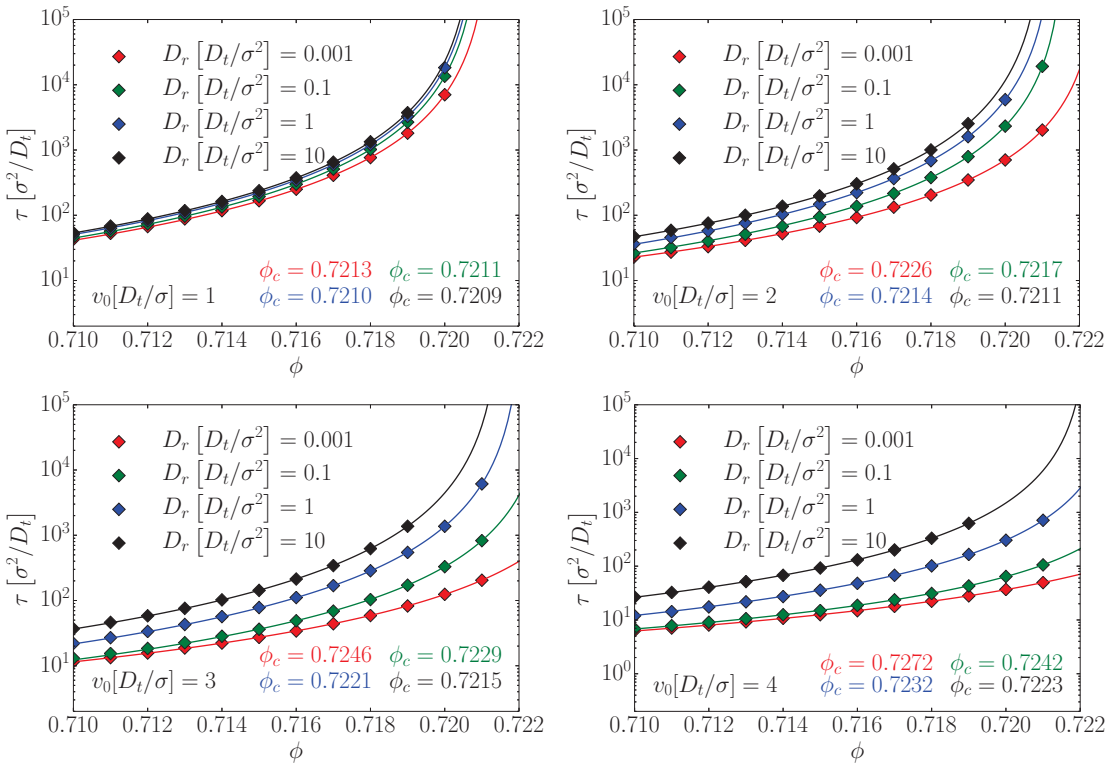

Figure 4.12: Relaxation times τ as a function of packing fraction for different rotational diffusion by fixed activity. The activity is increased from left to right and from top to bottom panel. The symbols mark the numerical values calculated from the correlator $\mathbf{\Phi}_{0,0}$, and the solid line is the MCT fit 4.6. The critical packing fraction ϕ_c values correspond to the divergence point estimated by the MCT fit.

$\mathbf{\Phi}_{0,0}(q,t) < 1/\mathrm{e}, \quad \forall t > \tau$. By using this condition one should be careful that the value of the intermediate (β-relaxation) plateau is not lower than 1/e, since than the corresponding relaxation time would be the β-relaxation time instead of α-relaxation time. The MCT predicts that close to the glass transition point the

relaxation time can be approximated by:

$$\tau(\phi, v_0, D_r) = A(\phi, v_0, D_r)\Big(\phi - \phi_c(v_0, D_r)\Big)^{-\gamma(v_0, D_r)}, \tag{4.6}$$

with two parameter dependent constants the amplitude $A(\phi, v_0, D_r)$ and the exponent $\gamma(v_0, D_r)$. At the critical packing $\phi_c(v_0, D_r)$ the relaxation time becomes divergent as expected from the glass transition point. The Figure 4.12 illustrates the relaxation times τ as a function of packing fraction ϕ close to the transition point for different rotational diffusions. The influence of the rotational diffusion

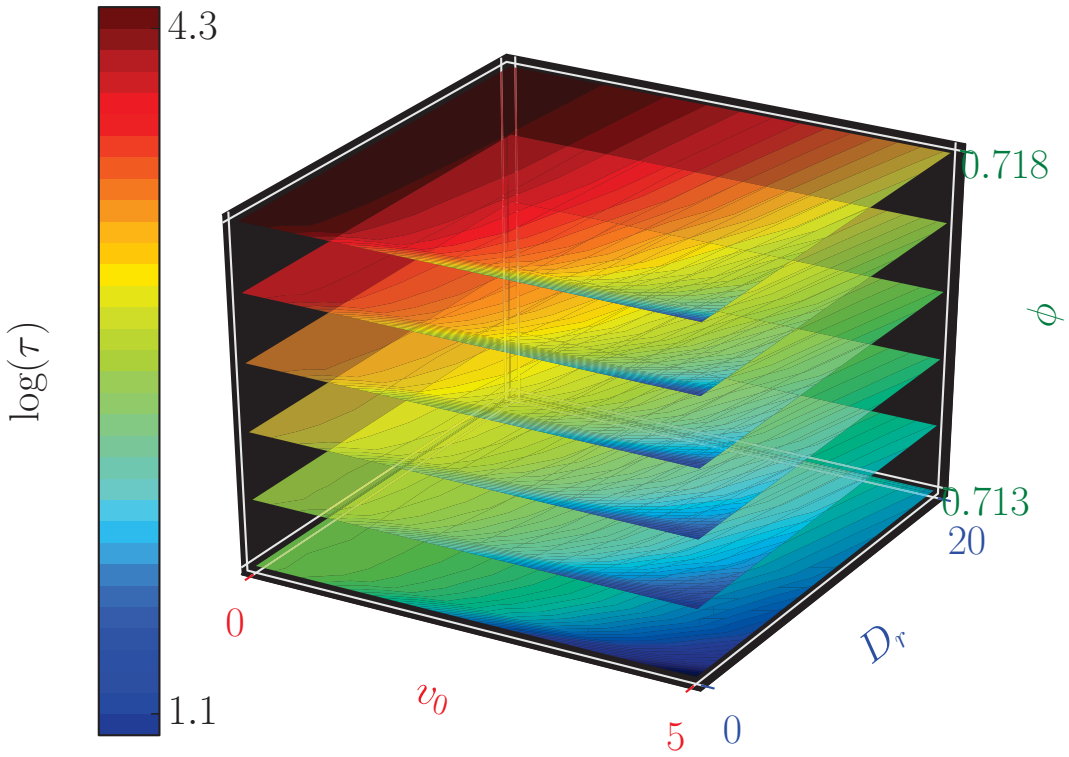

Figure 4.13: Logarithm of the relaxation time τ as a function of v_0, D_r and ϕ. Different layers in the 3D axis correspond to different packing fraction.

becomes more pronounced at higher activity velocities, but in all cases increasing D_r slows down the relaxation (increases the relaxation time). The critical values for the packing fraction ϕ_c which marks the divergence point for the relaxation time, are calculated by using the MCT fit 4.6. The relaxation time τ as a function of all control parameters (v_0, D_r, ϕ) is plotted in the so-called 4D plot 4.13 where the color represents the 4th dimension (the parameters are still measured in units

of D_t and σ but were removed for better readability). Increasing the packing fraction and rotational diffusion slows down the relaxation. Increasing the activity makes the system relax faster and thus has an opposite effect as ϕ and D_r.

4.3 Glass Transition

Based on the results from the previous section in this section the focus will be to determine the critical parameters that separate the glassy state from the fluid. To calculate the glass transition point the data for the relaxation time has to be fitted with the MCT prediction 4.6. The left panel of the Figure 4.14 shows the critical

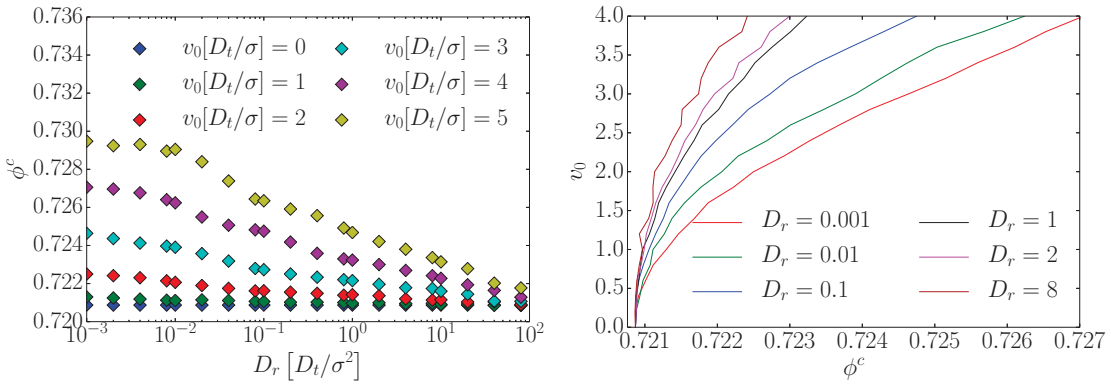

Figure 4.14: Critical packing fraction ϕ_c as a function of activity and rotational diffusion.

packing fraction ϕ^c (equivalent to ϕ_c) as a function of the rotational diffusion for different activity values. The blue symbols correspond to the passive system. It can be observed that for higher rotational diffusions the system gets closer to the passive system and as mentioned already it will coincide with the passive system for $D_r \to \infty$. On the right panel the critical packing fraction as a function of activity strength for different rotational diffusion is plotted. The lines correspond to the bifurcation point separating the glassy state from the fluid (the units of the parameters are omitted). For higher D_r the curves start to show same instabilities related to the method to determine the critical line. The MCT fit formula 4.6 is only valid close to the glass transition point and for higher D_r it was difficult to reach large relaxation times (necessary to be close to transition point) due to the numerical instabilities of the time domain algorithm. So the MCT fit was used for relaxation times that were not close enough to the transition point. Increasing the rotational diffusion further, decreases the stability even more. The Figure 4.15 illustrates the glass transition surface in the space spanned by the control

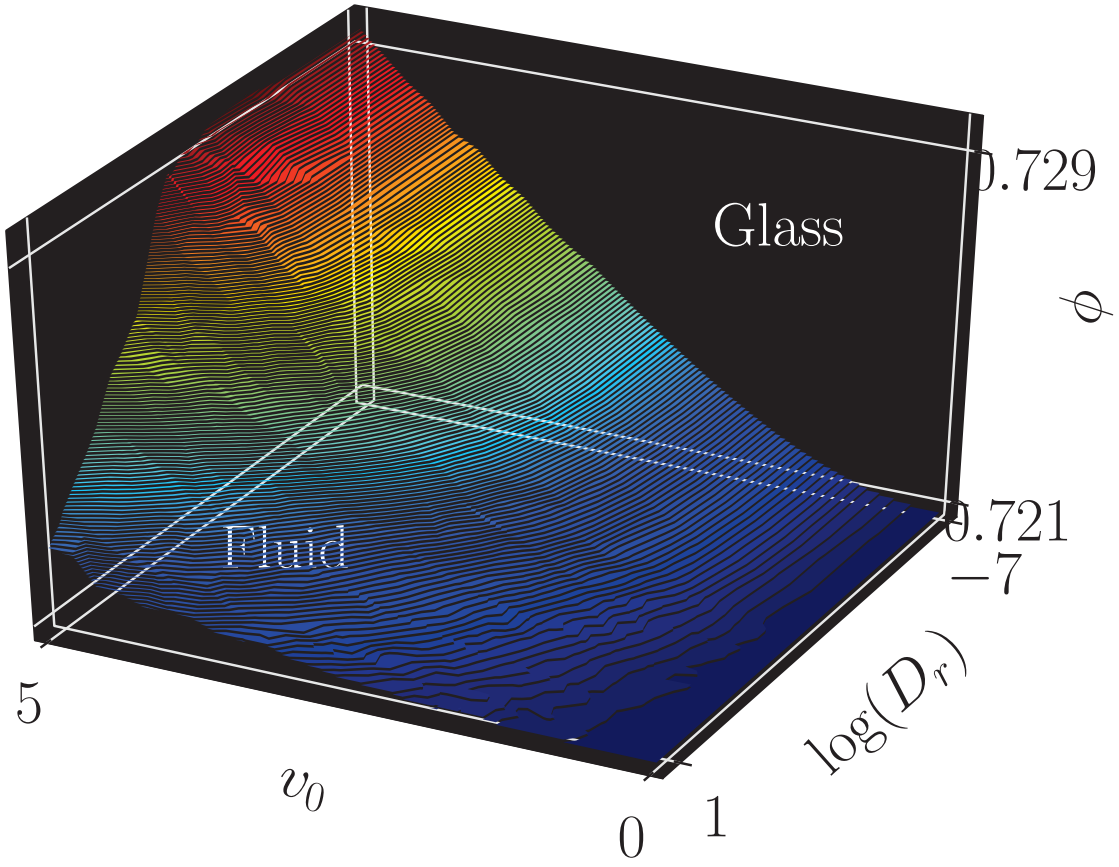

Figure 4.15: Glass transition surface in the space spanned by activity v_0, rotational diffusion D_r and the packing fraction ϕ.

parameters v_0, D_r and ϕ. The glassy state and the fluid state is marked in the color plot. If the parameters are chosen such, that the point is above the colored surface than the system is in a glassy state and if the point is below the surface than it is in a fluid state. According to the Figure 4.15 there are different ways to melt the glass.

- Increasing the activity v_0 can melt the glass. For any given packing fraction and rotational diffusion there exists a critical activity v_0^c that separates the glassy and fluid state. If the activity is bigger than the critical value $v_0 > v_0^c$ the glass gets molten.

- Decreasing of the packing fraction ϕ. Melting the system by decreasing the packing fraction is also know from passive systems. For any given activity and rotational diffusion D_r there exists a critical packing fraction ϕ_c that

corresponds to the glass transition point. If the packing fraction is chosen below the critical packing $\phi < \phi_c$ the glass gets molten.

- Decreasing the rotational diffusion D_r. In contradiction to the other two melting processes there does not always exists a critical D_r^c that separates the glassy and fluid state. If the packing fraction is higher than the critical packing of the system of non-rotating particles $\phi > \phi_c(v_0, D_r = 0)$ than the system is stable enough and can not be molten by any rotational diffusion.

4.4 Summary

In this chapter the numerical results for the density correlator matrix as a function of time for different parameters were presented. To do so the final equation of motion was solved by numerical algorithms (derived in Appendix B) in the time domain. The numerical results for the density correlator matrix were splitted in two parts, the $(0, 0)$ mode of the correlator and all other matrix components. The $(0, 0)$ mode is an important quantity being the only matrix element of the correlator with no direct angular dependence, and thus perfectly suited for studying the structural properties of the system. The influence of activity and the rotational diffusion at the system were studied in detail. The rotational behavior of the particles and their effect on the translational behavior was analyzed by looking at other matrix components of the correlator. From the decay times of $\mathbf{\Phi}_{0,0}$ for

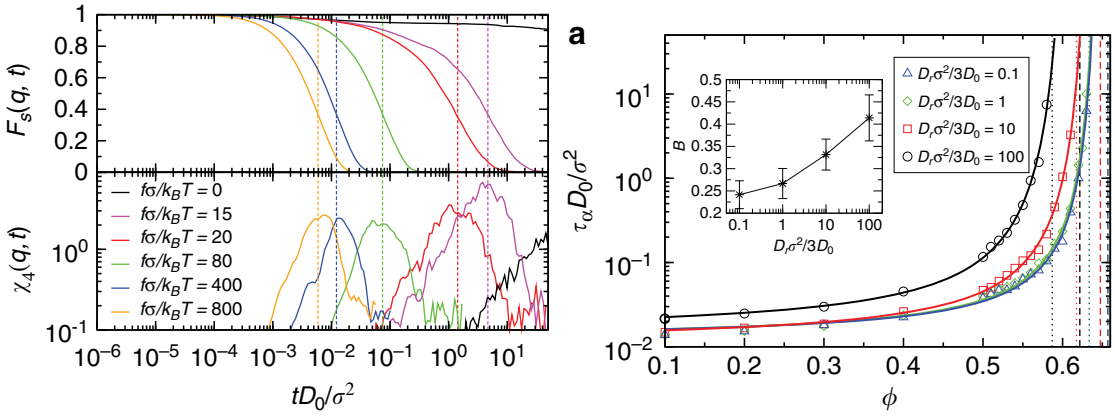

Figure 4.16: Simulation results obtained by Ran Ni et al. [13] in three dimensions. Left plot shows the correlation function $F_s(q, t)$ as a function of time for different activity forces denoted by $f\sigma/K_BT$. On the right plot the alpha relaxation time as a function of packing fraction for different rotational diffusion is presented. Symbols correspond to the simulation results and the solid lines to the MCT fit.

different parameters the alpha relaxation times were estimated, and by using the Mode Coupling prediction of the power law divergence of the relaxation time at the critical point, the glass transition surface in the space spanned by the control parameters (v_0, D_r, ϕ) was determined. The Figure 4.16 shows simulation results performed for the ABD system in 3D by Ran Ni et al. [13]. The correlation function $F_s(q,t)$ (corresponding to $\mathbf{\Phi}_{0,0}$) for different activity strength is illustrated on the left plot and qualitatively agrees to the numerical results we obtained using the MCT. The decay time for the correlator decreases by the increase of activity. Also the curves for the alpha relaxation time obtained by simulation methods (right plot) agree with our observations and show similar dependence at the rotational diffusion. The left part of the Figure 4.17 illustrates a 3D fluid-glass diagram in

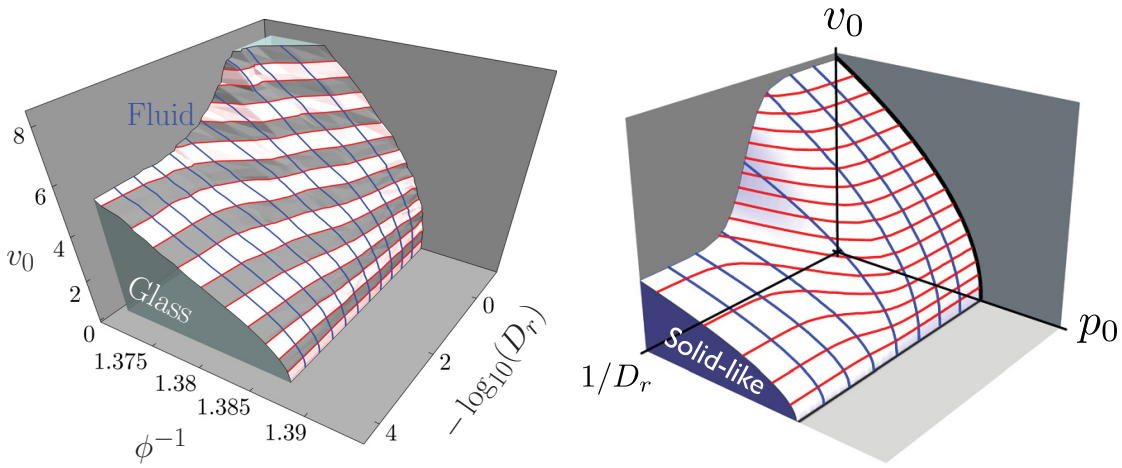

Figure 4.17: Left panel: Fluid-glass diagram in the domain $\Big(v_0, 1/\phi, \log(1/D_r)\Big)$ obtained from the data used in Figure 4.15. Right panel: 3D fluid-glass diagram for a self-propelled Voronoi liquid obtained by Bi et al. [48]. (Note: From the context of the paper [48] it is clear that $1/D_r$ is meant to be $\log(1/D_r)$).

the domain spanned by $\Big(v_0, 1/\phi, \log(1/D_r)\Big)$. The data used for the plot is the same as in Figure 4.15 only the axis are chosen differently. Choosing that kind of domain is motivated by the work done by Bi et al. [48], where the model of self-propelled Voronoi liquid is studied. The self-adhesion parameter p_0 corresponds to the inverse density in our model. The results obtained by MCT-theory are qualitatively in a very good agreement with the results obtained for the model of self-propelled Voronoi liquid (right plot of the Figure 4.17).

Chapter 5

Single Active Tracer Particle

In the last chapters we introduced in great detail the system of active Brownian hard disks. The equation of motion for the density correlator was derived and the memory kernel in the convolution integral was approximated using the Mode coupling theory of the glass transition. The EOM was solved numerically in the time domain and the influence of different control parameters at the system studied. In this chapter we want to extend the ABD system with a further degree of freedom. A single active tracer particle with the same dimensions as the bulk particles will be added. The main goal of introducing the tracer particle will be to determine the time dependent mean-squared displacement.

5.1 Theory

The theory required to calculate the tracer density correlator and thus the mean-squared displacement follows the steps done for the bulk system. First the Mori-Zwanzig formalism will be used and the memory kernel will be approximated by using Mode Coupling theory. Due to the extra tracer particle the Smoluchowski operator describing the time evolution of all observables gets additional terms. To distinguish quantities related to the bulk and to the tracer, all tracer related terms will have a super- or subscript "s" . The full adjoint Smoluchowski operator is the sum of the bulk operator introduced in previous chapters and the adjoint Smoluchowski operator for the tracer particle.

$$\Omega^\dagger = \Omega_0^\dagger + \Omega_s^\dagger, \tag{5.1}$$

with the components

$$\begin{aligned} \Omega_0^\dagger &= \sum_i D_t \left(\vec{\partial}_i + \beta \vec{F}_i\right) \cdot \vec{\partial}_i + v_0 \vec{o}_i \cdot \vec{\partial}_i + D_r \partial_{\varphi_i}^2, \\ \Omega_s^\dagger &= D_t^s \left(\vec{\partial}_s + \beta \vec{F}_s\right) \cdot \vec{\partial}_s + v_0^s \vec{o}_s \cdot \vec{\partial}_s + D_r^s \partial_{\varphi_s}^2. \end{aligned} \tag{5.2}$$

A priori the tracer particle is not the same particle as the bulk particles, so introducing it is related to have to deal with three more parameters D_t^s, v_0^s, D_r^s. The translational diffusion of the tracer particle can be eliminated by measuring D_r^s and v_0^s in units of D_t^s and the particle diameter σ that is identical for all particles. Having additional parameters for the tracer particle is important since it will allow us later to consider cases of a single passive tracer particle in an active environment or a single active tracer particle in a passive environment. The dynamics of the tracer particle will be described by the tracer density correlator.

$$\rho_l^s\left(\vec{q},t\right)=\mathrm{e}^{i\vec{q}\cdot\boldsymbol{x}_s(t)}\mathrm{e}^{il\varphi_s(t)},\qquad \boldsymbol{S}_{l,l'}^s\left(\vec{q},t\right)=\left\langle \rho_l^{s*}\left(\vec{q}\right)\rho_{l'}^s\left(\vec{q},t\right)\right\rangle, \tag{5.3}$$

with the single particle tracer density ρ_l^s. The time evolution of the tracer density function is determined by the full adjoint Smoluchowski operator.

$$\boldsymbol{S}_{l,l'}^s\left(\vec{q},t\right)=\left\langle \rho_l^{s*}\left(\vec{q}\right)\mathrm{e}^{\Omega^\dagger t}\rho_{l'}^s\left(\vec{q}\right)\right\rangle,\qquad \boldsymbol{S}_{l,l'}^s\left(\vec{q}\right)=\delta_{l,l'}. \tag{5.4}$$

The static structure factor for a single tracer particle does not depend on the wavenumber and is delta correlated in the orientational indices. The equation of motion for the tracer density correlator will be derived by using the projection formalism of Mori and Zwanzig as described in detail for the bulk correlator. The projector to the slow variables will be introduced.

$$\boldsymbol{P}_s=\sum_{l_1,l_2,\vec{q}}\left|\rho_{l_1}^s\left(\vec{q}\right)\right\rangle\boldsymbol{S}_{l_1,l_2}^{s^{-1}}\left(\vec{q}\right)\left\langle\rho_{l_2}^{s*}\left(\vec{q}\right)\right|=\sum_{l_1,\vec{q}}\left|\rho_{l_1}^s\left(\vec{q}\right)\right\rangle\left\langle\rho_{l_1}^{s*}\left(\vec{q}\right)\right|,\quad \boldsymbol{Q}_s=\mathbb{I}-\boldsymbol{P}_s. \tag{5.5}$$

The calculation of the EOM for the tracer correlator is completely identical to the bulk correlator and will be skipped. The final equation of motion after splitting into the rotational and translational parts can be written as (with omitted wavenumbers):

$$\partial_t\boldsymbol{S}^s\left(t\right)=-\boldsymbol{\omega}^s\boldsymbol{S}^s\left(t\right)-\int_0^t dt'\boldsymbol{m}_{\mathrm{T}}^s\left(t-t'\right)\boldsymbol{\omega}_{\mathrm{T}}^{s^{-1}}\left[\partial_{t'}\boldsymbol{S}^s\left(t'\right)+\boldsymbol{\omega}_{\mathrm{R}}^s\boldsymbol{S}^s(t')\right], \tag{5.6}$$

with the tracer frequency matrix $\boldsymbol{\omega}^s$ and the memory kernel $\boldsymbol{m}^s$.

$$\begin{aligned}
&\boldsymbol{\omega}_{l_1,l_2}^s\left(\vec{q}\right)=-\left\langle\rho_{l_1}^{s*}\left(\vec{q}\right)\Omega^\dagger\rho_{l_2}^s\left(\vec{q}\right)\right\rangle\\
&\boldsymbol{m}_{\mathrm{T},l_1,l_2}^s\left(t\right)=\left\langle\rho_{l_1}^{s*}\Omega^\dagger\boldsymbol{Q}_s\mathrm{e}^{\Omega^{\dagger\mathrm{irr}}t}\boldsymbol{Q}_s\Omega^\dagger\rho_{l_2}^s\right\rangle\\
&\Omega^{\dagger\mathrm{irr}}=\boldsymbol{Q}_s\left(\Omega^\dagger+\sum_{l_1,l_2,\vec{q}}\Omega^\dagger\left|\rho_{l_1}^s\left(\vec{q}\right)\right\rangle\boldsymbol{\omega}_{l_1,l_2}^{s^{-1}}\left(\vec{q}\right)\left\langle\rho_{l_2}^{s*}\left(\vec{q}\right)\Omega^\dagger\right|\right)
\end{aligned} \tag{5.7}$$

The MCT approximation of the memory kernel and evaluation of the tracer vertices is analogous to the procedure done for the bulk system and is presented in detail in appendix A. Also the transformation properties of the tracer correlator is identical to the bulk correlator. After introducing the coordinate system the final equation of motion can be calculated.

$$\boldsymbol{\omega}^{s,\frac{\pi}{2}}_{l,l'}(q) = \left[D^s_t q^2 + D^s_r l^2\right]\delta_{l,l'} + \frac{v^s_0}{2} q (l'-l)\delta_{|l-l'|,1}. \tag{5.8}$$

$$\begin{aligned}\boldsymbol{\mathcal{V}}^{s,\frac{\pi}{2}}_{l,l_1,l_2}(k,p,q) =& \frac{D^s_t}{4}\left[\delta_{l_2,0}\left(\tilde{S}^{-1}_k - 1\right) + 1\right]\tilde{S}^{\mathrm{tb}^2}_k \tilde{S}^{-1}_k \Big[D^s_t \delta_{l,l_1}\delta_{l_2,0}\left(q^2+p^2-k^2\right)^2 \\ &+ i\left(q^2+p^2-k^2\right)k\left[v_0 \mathrm{e}^{il_2\alpha_k}\delta_{l,l_1} - v^s_0 \mathrm{e}^{i(l_1-l)\alpha_k}\delta_{l_2,0}\right]\delta_{|l_1+l_2-l|,1}\Big]\end{aligned} \tag{5.9}$$

$$\begin{aligned}\boldsymbol{m}^{s,\frac{\pi}{2}}_{\mathrm{T},l,l'}(q,t) = \frac{1}{\pi^2 n}\sum_{l_1,l_2}\int_0^\infty dp \int_{|q-p|}^{q+p} dk \frac{pk\boldsymbol{\mathcal{V}}^{s,\frac{\pi}{2}}_{l,l_1,l_2}(k,p,q)}{\sqrt{4q^2p^2 - \left(q^2+p^2-k^2\right)^2}} \\ \times \mathrm{e}^{-il_1\left(\alpha_p - \frac{\pi}{2}\right)}\mathrm{e}^{il'\left(\alpha_p-\frac{\pi}{2}\right)}\boldsymbol{S}^{s,\frac{\pi}{2}}_{l_1,l'}(p,t) \\ \times \mathrm{e}^{-il_2\left(\alpha_k-\frac{\pi}{2}\right)}\boldsymbol{S}^{\frac{\pi}{2}}_{l_2,0}(k)\end{aligned} \tag{5.10}$$

$$\boxed{\partial_t \boldsymbol{S}^s(t) = -\boldsymbol{\omega}^s \boldsymbol{S}^s(t) - \int_0^t dt' \boldsymbol{m}^s_{\mathrm{T}}(t-t')\boldsymbol{\omega}^{s^{-1}}_{\mathrm{T}}\left[\partial_{t'}\boldsymbol{S}^s(t') + \boldsymbol{\omega}^s_{\mathrm{R}}\boldsymbol{S}^s(t')\right]} \tag{5.11}$$

In the final equation of motion the direction of the wave vector and the magnitude were omitted, all quantities only depend on the wavenumber q pointing in positive y direction. The full frequency function $\boldsymbol{\omega}^s$ is a sum of the rotational and translational frequency function, with the obvious splitting $\boldsymbol{\omega}^s_{\mathrm{R},l,l'} = D^s_r l^2 \delta_{l,l'}$ and $\boldsymbol{\omega}^s_{\mathrm{T}}$ with the remaining terms of $\boldsymbol{\omega}^s$. The density correlator of the tracer particle is coupled to the bath correlator (blue color in the memory kernel) in the memory kernel. The vertex function $\boldsymbol{\mathcal{V}}^s$ does not only depend on the tracer parameters, also the activity of the bulk particles enters the equation. The term $\tilde{S}^{\mathrm{tb}}_k = \langle \rho^{s*}_k \rho_k \rangle$ is the tracer bath structure factor which is directly related to the equilibrium static structure factor of the bulk as described in [25]. The direct correlation function of the tracer particle can be approximated by the direct correlation function of the bulk $c^s_q \approx c_q$, the equality holds if the tracer particle is included in the bulk particles.

$$\frac{\tilde{S}^{\mathrm{tb}}_q}{\rho \tilde{S}_q} = c^s_q \approx c_q = \frac{1}{\rho}\left(\frac{\tilde{S}_q - 1}{\tilde{S}_q}\right) \quad \Rightarrow \quad \tilde{S}^{\mathrm{tb}}_q = \tilde{S}_q - 1. \tag{5.12}$$

The mean-squared displacement of the tracer particle is directly related to the correlator.

$$\boldsymbol{S}^s_{0,0}\left(\vec{q},t\right)=\left\langle \mathrm{e}^{-i\boldsymbol{q}\cdot\boldsymbol{r}(t)}\right\rangle=\mathrm{e}^{-\frac{1}{4}q^2\left\langle r^2(t)\right\rangle}\equiv\mathrm{e}^{-\frac{1}{4}q^2\mathrm{MSD}(t)}=1-\frac{1}{4}q^2\mathrm{MSD}\left(t\right)+\mathcal{O}\left(q^4\right). \tag{5.13}$$

By evaluating the tracer correlator at zero wavenumber makes it possible to determine the mean-squared displacement.

$$\mathrm{MSD}\left(t\right)=\lim_{q\to 0}\frac{4}{q^2}\Big(1-\boldsymbol{S}^s_{0,0}(q,t)\Big). \tag{5.14}$$

5.2 Numerical Results

In this section the numerical results for the tracer density correlator and the mean-squared displacement will be presented. The algorithm for solving the equation of motion of the tracer correlator is identical to the algorithm of the bulk correlator and is shown very detailed in appendix B. The tracer memory kernel does not only depend on the tracer correlator it also depends on the correlator of the bulk, which needs to be calculated beforehand. Once the bulk correlator results are saved the tracer EOM can be solved for different sets of parameters. The result will be plotted for the matrix element $\boldsymbol{\Phi}^s_{0,0}(t)$. One should notice that in the case of a tracer particle the normalized density correlator $\boldsymbol{\Phi}^s(t)=\boldsymbol{S}^s(t)\boldsymbol{S}^{s^{-1}}$ is identical to the density correlator $\boldsymbol{S}^s(t)$, since the tracer static structure factor is unity.

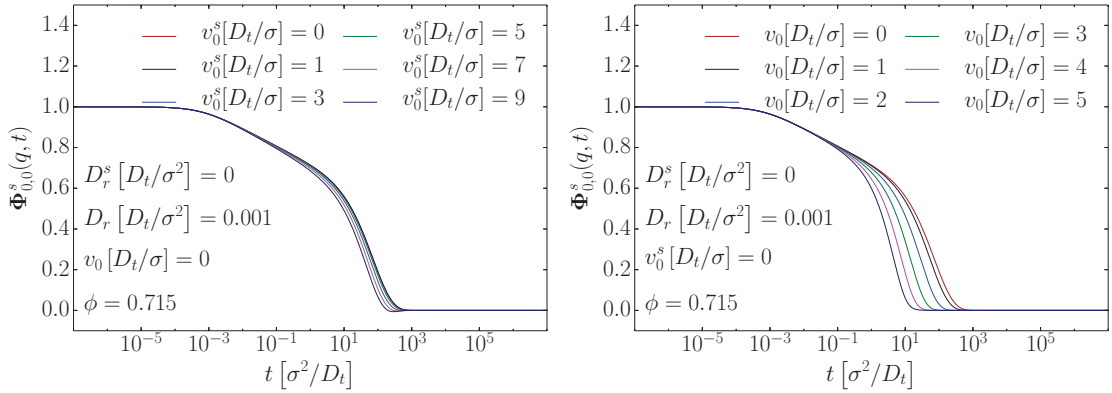

Figure 5.1: Density correlator of the tracer particle $\boldsymbol{\Phi}^s_{0,0}(q,t)$ as a function of time. Left panel: Active tracer particle in a passive environment for different tracer activities. Right panel: Passive tracer particle in an active environment for different bulk activities. The rotational diffusions and the packing fraction are kept constant.

The only reason to use the symbol $\mathbf{\Phi}$ is to be consistent in notation with previous chapters. The Figure 5.1 illustrates the single particle tracer correlator $\mathbf{\Phi}^s_{0,0}(q,t)$ as a function of time for different parameters. On the left panel the tracer is in a passive environment, so the bulk particles only undergo Brownian motion and do not have a self-propulsion velocity. The tracer particle itself is active. The time scale for the tracer and for the bulk particles were chosen to be the same $D_t = D^s_t$, which makes it possible to eliminate the free choice of one parameter and decreases the degrees of freedom by one. All the quantities are measured in units of D_t and σ and combinations thereof. Although the differences are small increasing the activity of the tracer particle makes the correlator decay faster as expected from the previous results of the bulk dynamics. The rotational diffusion of the tracer particle is chosen to vanish $D^s_r = 0$ to achieve a larger separation of the lines by increasing the velocity. $D^s_r = 0$ corresponds to a tracer particle that does not rotate. The right panel of the Figure 5.1 shows the single particle correlator $\mathbf{\Phi}^s_{0,0}(q,t)$ as a function of time for an active environment but a passive tracer particle. Increasing the bulk activity makes the correlator decay faster but in comparison to the previous case the influence is much bigger. Also the rotational diffusion for the bulk particles is chosen to be small. Therefore the tracer particle can escape the local neighbor cage easier by increasing the activity of the neighbor particles instead of its own activity.

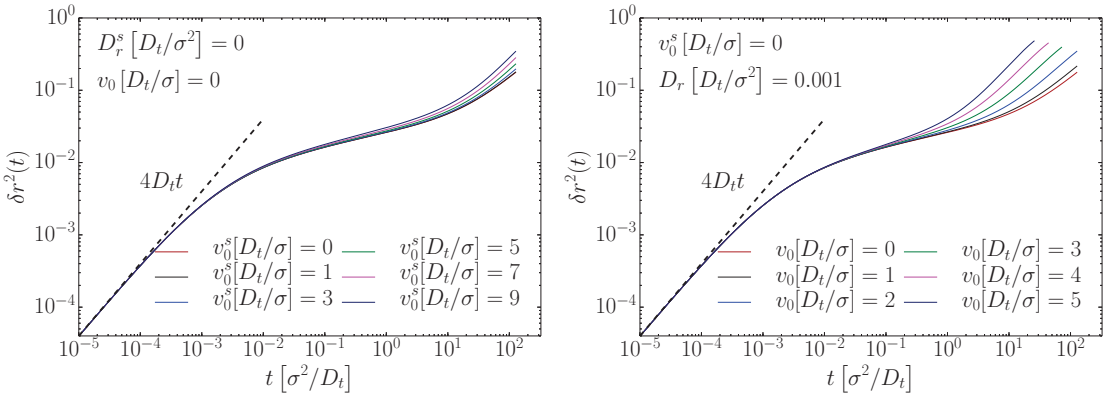

Figure 5.2: Mean-squared displacement of the single tracer particle for different activities. Left panel: active tracer particle in a passive environment, different colors denote different activities of the tracer particle. Right panel: passive tracer particle in an active environment, different colors correspond to different bulk activities. The rotational diffusion and the packing fraction are kept constant.

The Figure 5.2 emphasizes the dominance of the bulk activity over the tracer activity. The mean-squared displacement of the tracer particle gets increased much

faster by increasing the bulk activity (right panel) than the tracer activity (left panel). One should notice that in the Figure 5.2 it was only possible to display the mean-squared displacement for a certain range of time. To determine the mean-squared displacement the zero wavenumber limit is needed, but the numerical algorithm used to solve the EOM does not support vanishing wavenumbers (The Jacobian of the coordinate transformation is divergent for $q \to 0$ and needs to be treated differently). To avoid the problem a finite but small wavenumber was chosen, which limits the time resolution of the mean-squared displacement.

5.3 Summary

In this chapter a single active tracer particle in an active environment was introduced. To derive the equation of motion for the tracer correlator similar steps as for the bulk dynamics were performed. The results for the tracer density correlator and thus the mean-squared displacement in two different case were presented: firstly an active tracer particle in a passive environment and secondly a passive tracer particle in an active environment. Analyzing the numerical data showed the dominant influence of the bulk activity over the tracer activity. Increasing the activity of the environment softens the system much faster than increasing the activity of a single tracer particle. At the end the results for the mean-squared displacement were presented, that emphasized the superior influence of the bulk activity.

Chapter 6

ITT Application

Systems of active Brownian disks are intrinsically out of equilibrium Boltzmann-statistics (Boltzmann distribution) can not be applied. The integration through transients formalism provides an elegant way to be still able to calculating non-equilibrium averages. Using the ITT the non-equilibrium average gets linked to a time integral of an equilibrium correlation function. The ITT formalism was successfully applied to link transport coefficients like viscosity and diffusion constant to equilibrium correlation functions. The general ITT formula was already derived in the previous chapters (equation 2.29).

$$\langle A \rangle_{\text{non}} = \langle A \rangle - v_0 \beta \sum_i \int_0^\infty dt' \left\langle \vec{o}_i \cdot \vec{F}_i \mathrm{e}^{\Omega^\dagger t'} A(\Gamma) \right\rangle . \tag{6.1}$$

For any observable A the non-equilibrium average is linked to its equilibrium average and the time integral over the equilibrium correlator $\left\langle \vec{o}_i \cdot \vec{F}_i \mathrm{e}^{\Omega^\dagger t'} A(\Gamma) \right\rangle$. In the following $\beta = 1$ will be used.

6.1 Non-equilibrium Velocity

In this section the ITT formalism will be applied to determine the non-equilibrium velocity by approximating the relevant equilibrium correlation function by using the projection formalism. To determine the non-equilibrium velocity was already in the center of interest in other groups like A. Sharma and J.M. Brader [49]. The main difference between our work and the work done by other groups will be the way how the equilibrium correlation function gets approximated. The swim velocity is defined as the non-equilibrium average of the scalar product between the velocity vector and the orientation of each particle normalized by the number of

particles. The velocity is given by the Langevin equation 2.17 of the ABD system.

$$\bar{v} = \frac{1}{N}\left\langle \sum_i \vec{v}_i \cdot \vec{o}_i \right\rangle = \frac{1}{N}\sum_i \left[D_t \left\langle \vec{F}_i \cdot \vec{o}_i \right\rangle + v_0 \left\langle \vec{o}_i \cdot \vec{o}_i \right\rangle + \sqrt{2D_t}\left\langle \vec{\xi}_i^{\vec{x}} \cdot \vec{o}_i \right\rangle \right]. \quad (6.2)$$

All the averages are considered as a non-equilibrium average. The white noise $\vec{\xi}^{\vec{x}}$ has a Gaussian distribution, and thus is completely uncorrelated with the orientation vector of each particle and the last term in the above equation will vanish. The second term describes the expectation value of the length of the orientation vector which is by definition normalized $\sum_i \langle \vec{o}_i \cdot \vec{o}_i \rangle = N$.

$$\bar{v} = v_0 + \frac{D_t}{N}\sum_i \Big\langle \underbrace{\vec{F}_i \cdot \vec{o}_i}_{\widetilde{F}_i} \Big\rangle. \quad (6.3)$$

The non-equilibrium velocity can be written as the equilibrium expectation value plus the non-equilibrium average of the force projected into the particle orientation $\widetilde{F}_i$. The latter will be determined by the ITT formula to get rid of the non-equilibrium average.

$$\sum_i \left\langle \widetilde{F}_i \right\rangle_{\text{non}} = \overbrace{\sum_i \left\langle \widetilde{F}_i \right\rangle_{\text{eq}}}^{=0} - v_0 \sum_{i,j} \int_0^\infty dt' \left\langle \widetilde{F}_i \mathrm{e}^{\Omega^\dagger t'} \widetilde{F}_j \right\rangle_{\text{eq}}. \quad (6.4)$$

One should notice that the in equilibrium the force and the orientation are not correlated and the first term in the last equation can be dropped.

$$\bar{v} = v_0 \left(1 - \frac{D_t}{N}\int_0^\infty dt' C(t') \right), \qquad C(t') = \sum_{i,j} \left\langle \widetilde{F}_i \mathrm{e}^{\Omega^\dagger t'} \widetilde{F}_j \right\rangle_{\text{eq}}. \quad (6.5)$$

By using the ITT we linked the non-equilibrium velocity to an equilibrium force-force autocorrelation function $C(t)$. The force-force correlator will be determined by using the projection formalism. To make the equation 6.5 robust under the MCT approximation and avoid getting negative values for the swim velocity it is convenient to rewrite the equation into a different form (motivated in the work by Gazuz and Fuchs [37]). To achieve the rewriting it is useful to transform the relevant quantities into the Laplace space and use a definition of the irreducible Smoluchowski operator.

$$\Omega^{\dagger,\text{irr}} = \Omega^\dagger + \sum_{i,j} \left| \widetilde{F}_i \right\rangle \frac{D_t}{N} \left\langle \widetilde{F}_j \right|, \quad (6.6)$$

$$C(z) = \sum_{i,j} \left\langle \widetilde{F}_i \Big(z - \Omega^\dagger \Big)^{-1} \widetilde{F}_j \right\rangle_{\text{eq}}, \quad (6.7)$$

$$\left(z-\Omega^{\dagger}\right)^{-1}=\left(z-\Omega^{\dagger,\mathrm{irr}}\right)^{-1}-\sum_{i,j}\left(z-\Omega^{\dagger}\right)^{-1}\left|\widetilde{F}_i\right\rangle\frac{D_t}{N}\left\langle\widetilde{F}_j\right|\left(z-\Omega^{\dagger,\mathrm{irr}}\right)^{-1}. \quad (6.8)$$

Using the last operator splitting identity the force-force correlator can be written in terms of the irreducible counterpart of $C(z)$.

$$\begin{aligned} C(z)&=C^{\mathrm{irr}}(z)-\sum_{\substack{i,j\\k,l}}\left\langle\widetilde{F}_i\left(z-\Omega^{\dagger}\right)^{-1}\widetilde{F}_k\right\rangle\frac{D_t}{N}\left\langle\widetilde{F}_l\left(z-\Omega^{\dagger,\mathrm{irr}}\right)^{-1}\widetilde{F}_j\right\rangle\\ &=\frac{C^{\mathrm{irr}}(z)}{1+\frac{D_t}{N}C^{\mathrm{irr}}(z)}. \end{aligned} \quad (6.9)$$

By taking the limit of a vanishing Laplace variable the time integral of the correlator will be determined.

$$\int_0^{\infty}C(t)dt=\frac{\int_0^{\infty}C^{\mathrm{irr}}(t)dt}{1+\frac{D_t}{N}\int_0^{\infty}C^{\mathrm{irr}}(t)dt}. \quad (6.10)$$

Introducing the irreducible force-force correlator allows us to rewrite the swim velocity.

$$\bar{v}=\frac{v_0}{1+\frac{D_t}{N}\int_0^{\infty}C^{\mathrm{irr}}(t)dt},\qquad C^{\mathrm{irr}}(t)=\sum_{i,j}\left\langle\widetilde{F}_i\mathrm{e}^{\Omega^{\dagger,\mathrm{irr}}t}\widetilde{F}_j\right\rangle_{\mathrm{eq}}. \quad (6.11)$$

To guarantee positive values for the average swim velocity it is sufficient that the time integral of the irreducible force-force correlator remains positive, that is a big advantage over the reducible form of the average swim velocity. The integral term $\int_0^{\infty}C(t')dt'$ for large v_0 can become very large and produce negative $\bar{v}$. The irreducible force-force correlator will be determined by introducing a two state projector $\boldsymbol{P}_2$ and using the MCT approximation, a similar procedure was applied by approximating the irreducible memory kernel.

$$\boldsymbol{P}_2=\sum_{1,2,3,4}\left|\rho_1\rho_2\right\rangle\boldsymbol{g}_{1,2,3,4}\left\langle\rho_3^*\rho_4^*\right|,\qquad \boldsymbol{g}_{1,2,3,4}\approx\frac{1}{2N^2}\boldsymbol{S}_{1,3}^{-1}\boldsymbol{S}_{2,4}^{-1}. \quad (6.12)$$

The four point function will be approximated by the Kawasaki factorization.

$$\begin{aligned} &\sum_{i,j}\left\langle\widetilde{F}_i\mathrm{e}^{\Omega^{\dagger,\mathrm{irr}}t}\widetilde{F}_j\right\rangle\approx\sum_{i,j}\left\langle\widetilde{F}_iP_2\mathrm{e}^{\Omega^{\dagger,\mathrm{irr}}t}P_2\widetilde{F}_j\right\rangle\\ &=\left(\frac{1}{2N^2}\right)^2\sum_{\substack{i,j\\1,2,3,4}}\left\langle\widetilde{F}_i\rho_1\rho_2\right\rangle\boldsymbol{S}_{1,1}^{-1}\boldsymbol{S}_{2,2}^{-1}\left\langle\rho_1^*\rho_2^*\mathrm{e}^{\Omega^{\dagger,\mathrm{irr}}t}\rho_3\rho_4\right\rangle\boldsymbol{S}_{3,3}^{-1}\boldsymbol{S}_{4,4}^{-1}\left\langle\rho_3^*\rho_4^*\widetilde{F}_j\right\rangle\\ &=\frac{1}{2N^2}\sum_{\substack{i,j\\1,2,3,4}}\left\langle\widetilde{F}_i\rho_1\rho_2\right\rangle\boldsymbol{S}_{1,1}^{-1}\boldsymbol{S}_{2,2}^{-1}\boldsymbol{S}_{1,3}(t)\boldsymbol{S}_{2,4}(t)\boldsymbol{S}_{3,3}^{-1}\boldsymbol{S}_{4,4}^{-1}\left\langle\rho_3^*\rho_4^*\widetilde{F}_j\right\rangle. \end{aligned} \quad (6.13)$$

The two vertex functions need to be calculated, where it is sufficient to calculate only one since the second vertex is obtained by negating the orientational indices.

$$\begin{aligned}\sum_i \left\langle \widetilde{F}_i \rho_1 \rho_2 \right\rangle &= \sum_i \left\langle \boldsymbol{o}_i \cdot \boldsymbol{F}_i \rho_{l_1}(-\vec{q}_2)\rho_{l_2}(\vec{q}_2) \right\rangle \delta_{\vec{q}_1,-\vec{q}_2} \\ &= N\left(1-\tilde{S}(q_2)\right)\frac{i\vec{q}_2}{2}\cdot\left[\delta_{l_1,0}\begin{pmatrix}1\\ il_2\end{pmatrix}\delta_{|l_2|,1} - \delta_{l_2,0}\begin{pmatrix}1\\ il_1\end{pmatrix}\delta_{|l_1|,1}\right]\delta_{\vec{q}_1,-\vec{q}_2} \\ &\equiv N\boldsymbol{\mathcal{V}}^{\text{non}}_{l_1,l_2}(\vec{q}_2)\delta_{\vec{q}_1,-\vec{q}_2}.\end{aligned} \tag{6.14}$$

To simplify the notation it is convenient to define

$$\begin{aligned}\tilde{\boldsymbol{\mathcal{V}}}^{\text{non}}_{l_1,l_2}(\vec{q}_1) &\equiv \boldsymbol{\mathcal{V}}^{\text{non}}_{l_1,l_2}(\vec{q}_1)\boldsymbol{S}^{-1}_{l_1,l_1}(\vec{q}_1)\boldsymbol{S}^{-1}_{l_2,l_2}(\vec{q}_1) \\ &= \frac{i\vec{q}_1}{2}\cdot\left(\tilde{S}^{-1}(q_1)-1\right)\left[\delta_{l_1,0}\begin{pmatrix}1\\ il_2\end{pmatrix}\delta_{|l_2|,1} - \delta_{l_2,0}\begin{pmatrix}1\\ il_1\end{pmatrix}\delta_{|l_1|,1}\right].\end{aligned} \tag{6.15}$$

The final form of the force-force correlator depends only on the density correlator matrix and can be calculated by using the data for the density correlator obtained in previous chapters.

$$\sum_{i,j}\left\langle \widetilde{F}_i \mathrm{e}^{\Omega^{\dagger,\text{irr}}t}\widetilde{F}_j\right\rangle = \frac{1}{2}\sum_{\substack{l_1,\cdots,l_4\\ \vec{p}}}\tilde{\boldsymbol{\mathcal{V}}}^{\text{non}}_{l_1,l_2}(-\vec{p})\boldsymbol{S}_{l_1,l_3}(\vec{p},t)\boldsymbol{S}_{l_2,l_4}(-\vec{p},t)\tilde{\boldsymbol{\mathcal{V}}}^{\text{non}}_{-l_3,-l_4}(\vec{p}). \tag{6.16}$$

The summation over the two dimensional wavevector $\vec{p}$ can be changed to a 2D integral $\sum_{\boldsymbol{p}} \cong \frac{V}{(2\pi)^2}\int_0^{2\pi} d\alpha_p \int_0^\infty pdp$, and the angular part of the wavevector can be integrated analytically.

$$\bar{v} = \frac{v_0}{1+\frac{D_t}{8\pi n}\int_0^\infty dt' \int_0^\infty dpp^3\left(\tilde{S}^{-1}(p)-1\right)^2 W^{\frac{\pi}{2}}(p,t')}, \tag{6.17}$$

with

$$\begin{aligned}W^{\frac{\pi}{2}}(p,t) = &\left(\boldsymbol{S}^{\frac{\pi}{2}}_{0,-1}(p,t)-\boldsymbol{S}^{\frac{\pi}{2}}_{0,1}(p,t)\right)\left(\boldsymbol{S}^{\frac{\pi}{2}}_{-1,0}(p,t)-\boldsymbol{S}^{\frac{\pi}{2}}_{1,0}(p,t)\right) \\ &+\boldsymbol{S}^{\frac{\pi}{2}}_{0,0}(p,t)\left(\boldsymbol{S}^{\frac{\pi}{2}}_{-1,-1}(p,t)-\boldsymbol{S}^{\frac{\pi}{2}}_{1,-1}(p,t)-\boldsymbol{S}^{\frac{\pi}{2}}_{-1,1}(p,t)+\boldsymbol{S}^{\frac{\pi}{2}}_{1,1}(p,t)\right).\end{aligned} \tag{6.18}$$

6.2 Numerical Results

The equation 6.17 and the data for density correlator matrix calculated in the previous chapters will be used to determine the average swim velocity numerically. The Figure 6.1 shows the influence of self-propulsion velocity and the rotational

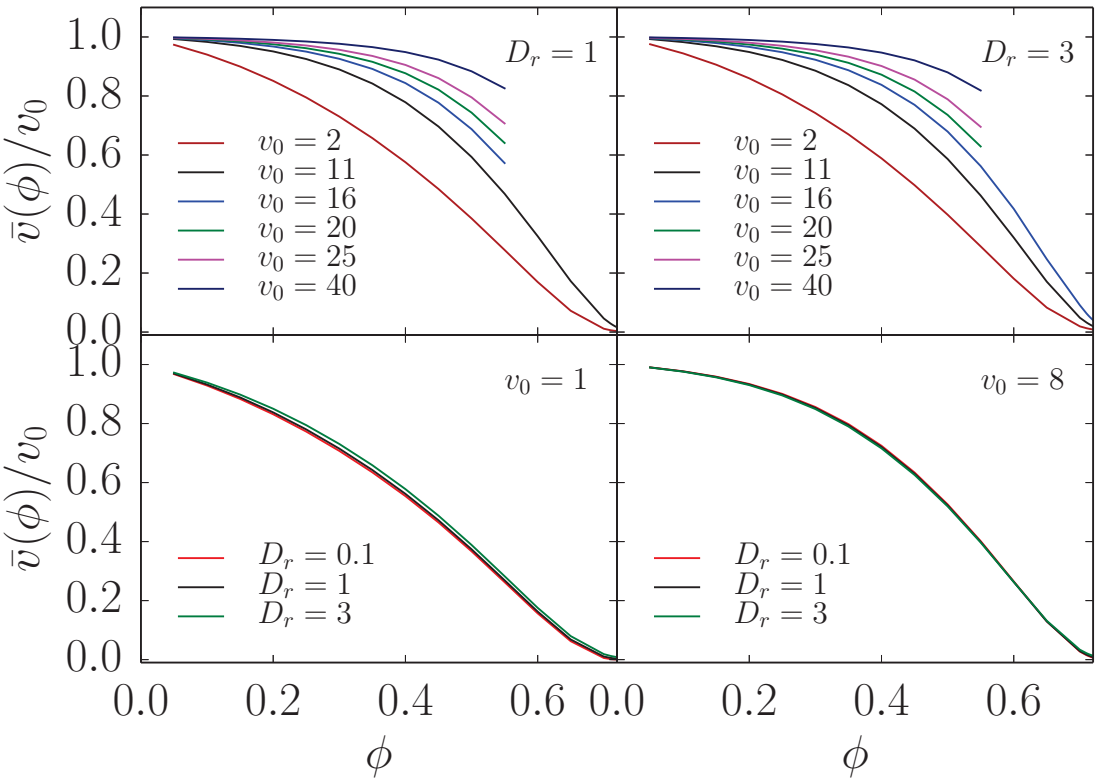

Figure 6.1: Average swim velocity $\bar{v}$ normalized by the activity strength v_0 as a function of packing fraction. On the top plots different colors correspond to different activities and on the bottom plots the activity is kept constant and the rotational diffusion is varied. For high activities not all packing fractions are plotted because of the numerical instabilities at high densities.

diffusion at the average swim velocity as a function of the packing fraction. In the top plots the rotational diffusion is kept constant and the self-propulsion velocity is varied. The average swim velocity is normalized by the equilibrium self-propulsion velocity v_0. The highest value for the fraction $\bar{v}/v_0 = 1$ is achieved for zero packing fraction where the particles do not interact with each other. After increasing the packing fraction the average swim velocity decreases continuously until it drops to zero at the glass transition point. It turns out (as shown in the top figures) that the normalized average swim speed $\bar{v}/v_0$ increases by increasing the activity. That behavior can be understood by looking at the results from previous chapters, where we showed that systems for higher activities are more fluidized than for smaller. From the top left plot to the top right plot the rotational diffusion got increased, where the tendency remains the same also for higher D_r. The influence of the

rotational diffusion at a constant velocity is shown in the bottom plots. The dependence of the swim velocity on D_r is much weaker than on the activity and the effect is getting even small by increasing the activity.

6.2.1 Motility Induced Phase Separation

At the end of this chapter we want to investigate the so-called motility induced phase separation introduced and described in great detail by Cates et al. in [50]. When the speed of particles decreases very quickly by increasing the packing fraction the suspension can become unstable and lead to a phase separation where a dense and dilute fluid phase coexist. The criterion for phase separation is given in [50] as concavity of the free energy $f(\phi)$.

$$f(\phi) = \phi\Big(\log(\phi) - 1\Big) + \int_0^{\phi} \frac{1}{2}\log\left(\frac{\bar{v}^2(\phi')}{D_r} + 2D_t\right) d\phi'. \tag{6.19}$$

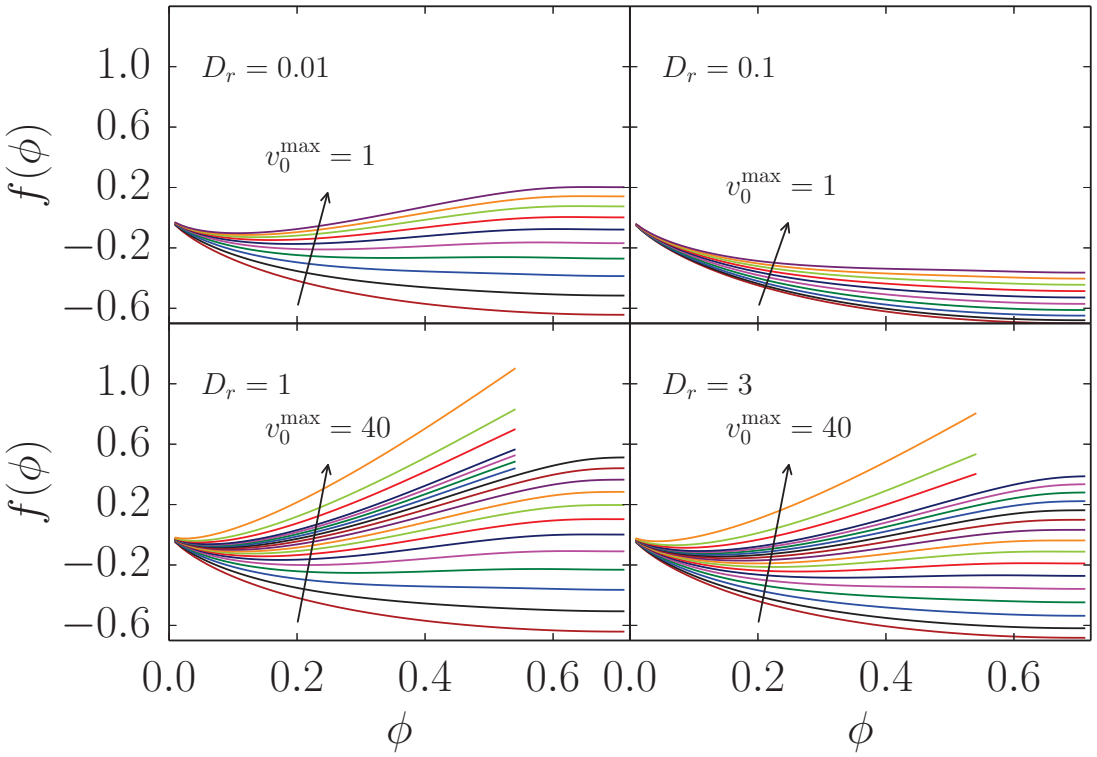

Figure 6.2: Free energy as a function of packing fraction for different velocities. From top to bottom and left to right panel the rotational diffusion gets increased.

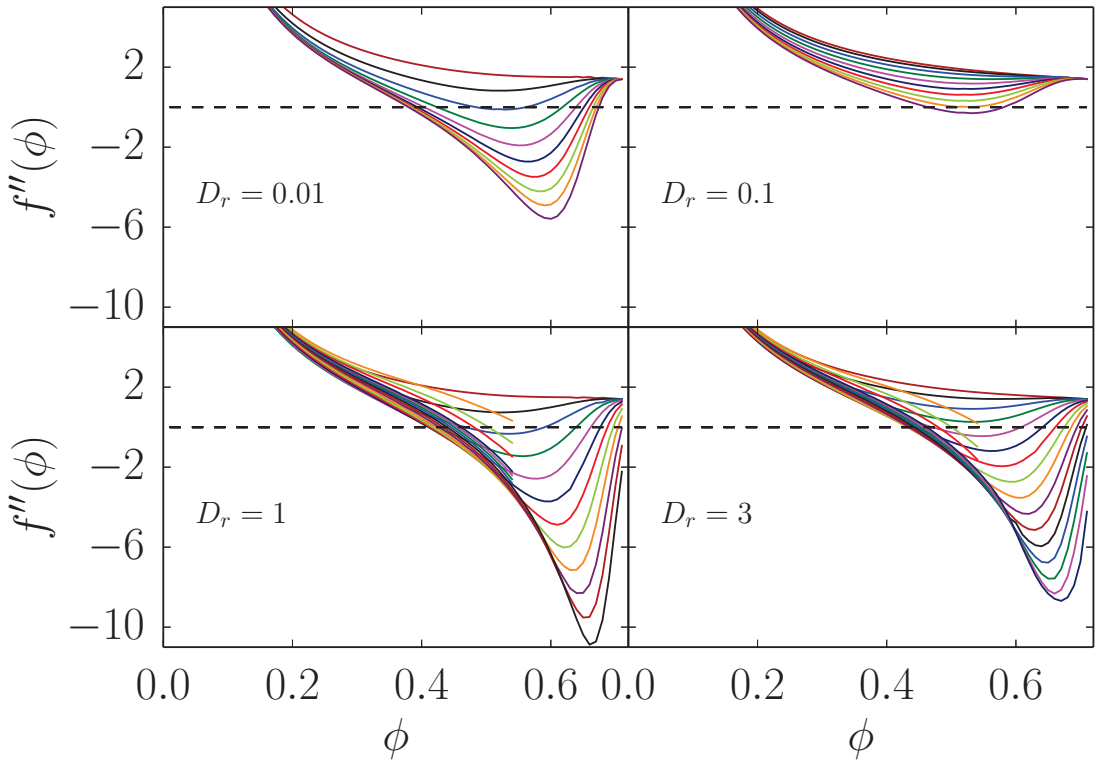

Figure 6.3: Second derivative of the free energy as a function of packing fraction for different velocities. From top to bottom and left to right panel the rotational diffusion gets increased. The black dashed line marks the zero point. The colors for the activity match the colors of the previous plot.

The condition for the instability is $f''(\phi) < 0$. The Figures 6.2,6.3 show the numerical results for the free energy as a function of packing fraction and the second derivative with respect to ϕ respectively. From top to bottom panels the rotational diffusion gets increased. The curvature of the free energy determines if the instability condition is fulfilled or not. If $f''(\phi)$ becomes negative the theory suggests a phase separation. For very small D_r smaller activities are sufficient to have a range of packing fractions where the phase separation occurs as shown on the top plots of the figure 6.3. By increasing the rotational diffusion higher activities are needed to have a phase separated region. The area of phase separation in the $(\phi, v_0/D_r\sigma)$ plane for different rotational diffusion can be observed in the Figure 6.4. The area surrounded by the dashed line corresponds to the region where the phase separation occurs. The motility induced phase separation for active Brownian disks was also found by numerical simulation methods as illustrated

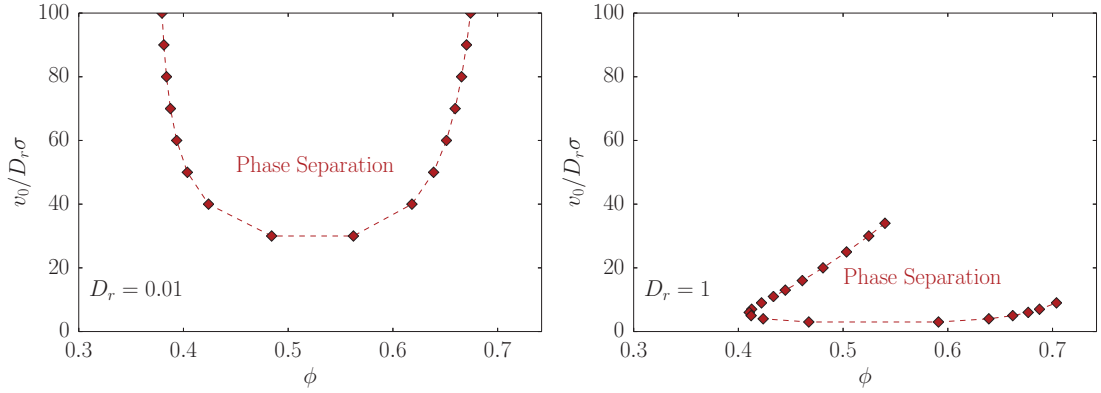

Figure 6.4: Phase separation diagram in the $(\phi, v_0/D_r\sigma)$ plane for different rotational diffusion. The area enclosed by the dashed line corresponds to the phase separated fluid.

in [51–53]. The simulation results are shown in the Figure 6.5. The numerical results are qualitatively in good accordance with the simulation results for small D_r (note the swapped axis by comparing the numerical results with the simulation results).

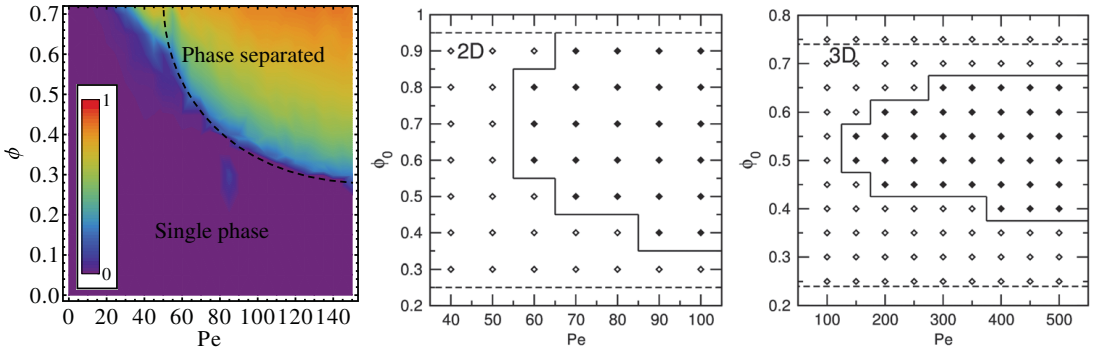

Figure 6.5: Phase separation diagrams obtained by computer simulation methods. The left plot is from the PRL paper by Gabriel S. Redner et al. [52]. The middle and right plots were presented by Joakim Stenhammar et al. in Soft matter journal [53]. Note Pe $\cong v_0/D_r\sigma$.

The Figure 6.6 shows the comparison of the ITT-MCT results for the phase separation and the simulation results for Brownian disks performed by Fily et al [15]. The red area marks the region where the phase separation occurs. For high packing fractions the glassy state is shown in both plots as a blue area. Qualitatively the ITT-MCT and the simulation results are in a good agreement. It is remark-

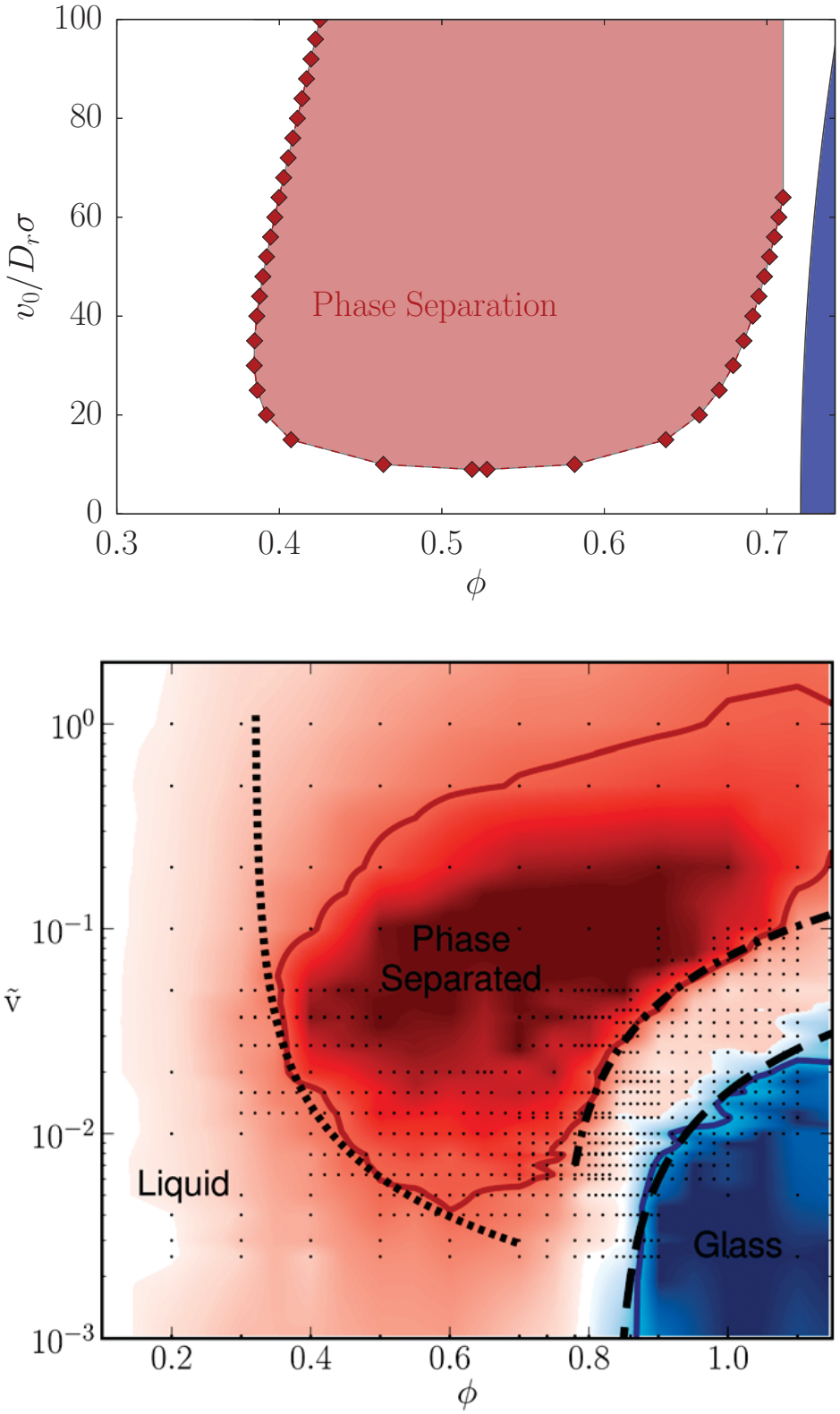

Figure 6.6: Top: phase separation diagram in the (ϕ,$v_0/D_r\sigma$) plane for ITT-MCT method at fixed rotational diffusion constant $D_r = 0.1$. Bottom: Simulation results by Fily et al. [15] for Brownian disks.

able that the ITT-MCT formalism, that is based on a purely microscopic theory is able of making the right predictions about the phase separation which is mainly a macroscopic phenomenon. One should also mention that the only approximation made to get the average swim speed using the ITT-MCT formalism was, to approximate the four point functions in the memory kernel.

Chapter 7

Conclusion and Outlook

7.1 Conclusion

In this thesis systems of active Brownian hard disks are investigated, by using the Mode Coupling theory of the glass transition, and the influence of the activity and the rotational diffusion at the glassy behavior is studied. MCT has already been applied to passive systems and the separation of glassy and fluid phases by increased packing fraction observed. The main goal in this work was to determine the dependence of the glass transition point on the additional parameters v_0 and D_r relevant for the active systems. The collective behavior of the particles is characterized by a dynamical density density correlation matrix, which is the key quantity throughout this work. The relevant equations of motion for the density correlator are derived in Chapter 3 and solved numerically. The results are presented in Chapter 4 for different sets of control parameters. By analyzing the $\mathbf{\Phi}_{0,0}$ mode of the correlator matrix it could be proven that the glass transition can be caused by the change of activity and in contradiction of systems under shear a critical activity is needed to achieve the melting of a glass. So if the packing fraction is high enough and the activity below $v_0^c > 0$ the system is robust enough to maintain the glassy state even after very long times.
Opposite to the passive systems where the rotational diffusion does not influence the structural properties of the system, by switching on the activity it is necessary also to take the rotational diffusion into account. By studying the numerical results, continuous strengthening of the fluid by the increase of rotational diffusion can be observed. By setting D_r to very high values the system can even be approximated by the passive case. The glass transition point as a function of different parameters is determined by exploiting the power law divergence of the α-relaxation time as predicted by the MCT. The numerical values for the α-relaxation time are in good agreement with the simulation results and show the

same tendency by varying v_0 and D_r. By calculating the decay time of the density correlator, and by using the power law fits the glass transition plane in the space spanned by the control parameters can be determined. The glass transition plots show three different ways to melt the glass.

- Decreasing the packing fraction.
- Increasing the activity.
- Reducing the rotational diffusion (only by sufficiently large activity).

Since increasing the activity and the rotational diffusion shows opposite influence at the system, there is a strong indication of having a dimensionless effective parameter that is sufficient to characterize the system, the so-called Péclet number $\mathrm{Pe} = \frac{v_0^2}{D_r D_t}$. Introducing the Péclet number corresponds to the transformation $(\phi, v_0, D_r) \to (\phi, \mathrm{Pe})$, with the degrees of freedom reduced by one. Numerical results show that the transformation can not be done without the loss of information and it is necessary to have the knowledge about all three parameters.
To study the influence of the activity at the mean-squared displacement a single active tracer particle is added to the system in chapter 5. The mean-squared displacement is determined for different tracer and bulk activities, and the superior influence of the bulk activity is observed.
In the final chapter the application of the ITT formalism using the MCT approximation for the transient correlator is presented. The goal was to determine the non-equilibrium velocity or average swim speed of the particles at different system settings. For small packing fractions the average swim speed is close to the single particle velocity value v_0 as the particles do not interact with each other very frequently. The average swim speed decreases continuously by increasing the packing fraction, and at the glass transition point it vanishes completely, as the particles are surrounded by neighbor particles and can not leave the cage.
At the end of chapter 6 the results for the free energy of the system are presented. By determining the curvature of the free energy it is possible to find the instability of the system that corresponds to a phase separation into two phases, a dense and a dilute fluid phase. The increase of the rotational diffusion makes it more difficult to achieve the phase separation and higher activity strength is needed. The so-called motility induced phase separation for active Brownian hard disks was also found by using numerical simulation methods. The ITT-MCT results are qualitatively in good agreement with the simulations results, which emphasizes the strength of the ITT-MCT formalism, which is based on purely microscopic theory and is able of making right predictions about macroscopic quantities.

7.2 Outlook

By dealing with the mode coupling approximation of the memory kernel for ABD system it was necessary to perform a second projection of the memory kernel to the translational and rotational parts to make it robust under the approximations, and to make sure that the rotations never freeze (the $(1, 1)$ mode of the correlator always decays).

By expanding the model of active Brownian hard disks to hard ellipses the second projection would not be necessary, since for very dense packing the ellipses can stuck to each other and stop rotating, so rotational freezing would make physical sense. A hard ellipse is characterized by two radii a and b. One could perform the MCT calculation for hard ellipses without projecting to translational and rotational parts and take the limit $a \to b$, which should coincide with the hard disk model. By doing so the convolution integral would not contain the hopping term which produces numerical instabilities at glass transition point, and could make the theory more robust close to the glass transition point. Introducing ellipses instead of hard disks is also related with some complications.

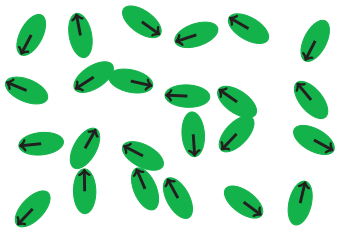

Figure 7.1: Schematic representation of active Brownian hard ellipses.

- The statical structure factor matrix does not take a simple diagonal structure that was exploited during evaluation of the MCT vertices frequently.

- The hard ellipse potential does also depend at the orientational angle, making the evaluation of the vertices even more cumbersome.

In chapter 5 we introduced a single active tracer particle in an active environment. That model can be extended by applying an external force $\vec{F}_{\text{ex}}$ (not necessarily small) to the tracer particle. The nonlinear response of the system to the external force is studied by active microrheology. The application of active microrheology to the passive Brownian disks is presented in great detail by Gazuz and Fuchs in [37]. By pulling the tracer particle with a constant force, it is possible to determine the friction coefficient by using the ITT-MCT formalism similar to the average swim speed from the chapter 6. By solving the

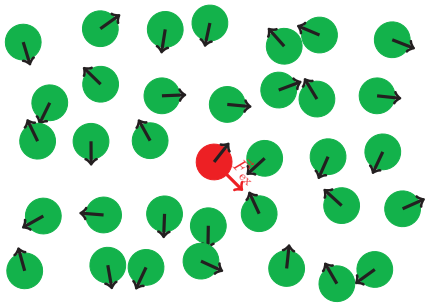

Figure 7.2: ABD system with an external force.

EOM of the correlator for ABD systems we used the transformation properties to simplify the wave vector dependence of the EOM to a wavenumber dependence. By introducing an external force the direction of the wave vector becomes important and the EOM has to be solved for a 2D wave vector. That is the major difficulty by introducing an external force, making the numerical algorithm much slower and not feasible. One has to rely on approximations e.g. assuming that the external force is always pointing parallel or perpendicular to all wave vectors.

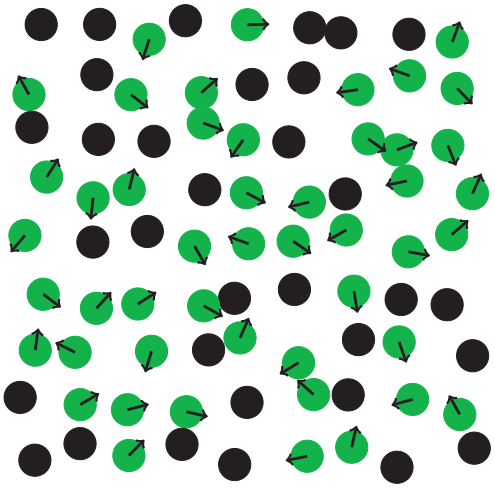

Figure 7.3: ABD system in a porous media. Black circles correspond to the static obstacles.

The mode coupling theory was applied to porous media by Krakoviack [54–56] for passive Brownian particles, that model can be expanded to a system of active Brownian disks with static obstacles. The obstacles are modeled by hard circles with infinite mass (denoted by black circles in Figure 7.3). Having additional obstacles makes the evaluation of the MCT vertices more complicated since additional structure factors will enter the equations.

Appendix A

Detailed Calculations of the MCT Vertices

A.1 Bulk Vertices

In this part of the appendix we present detailed calculations for the vertices entering the irreducible memory kernel after the MCT approximations. To get an expression for the vertices it is necessary to evaluate the equilibrium average of the three point function.

$$\begin{aligned}\left\langle \rho_1^* \rho_2^* \boldsymbol{Q} \Omega^\dagger \rho_3 \right\rangle &= \left\langle \rho_1^* \rho_2^* \Omega^\dagger \rho_3 \right\rangle - \frac{1}{N} \sum_{1',2',\vec{q}} \left\langle \rho_1^* \rho_2^* \rho_{1'}\left(\vec{q}\right) \right\rangle \boldsymbol{S}^{-1}_{1',2'}\left(\vec{q}\right) \left\langle \rho^*_{2'}\left(\vec{q}\right) \Omega^\dagger \rho_3 \right\rangle \\ &= \left\langle \rho_1^* \rho_2^* \Omega^\dagger \rho_3 \right\rangle + \sum_{1',2',\vec{q}} \left\langle \rho_1^* \rho_2^* \rho_{1'}\left(\vec{q}\right) \right\rangle \boldsymbol{S}^{-1}_{1',2'}\left(\vec{q}\right) \boldsymbol{\omega}_{2',3}\left(\vec{q}\right) \delta_{\vec{q},\vec{q}_3}.\end{aligned} \tag{A.1}$$

The frequency function $\boldsymbol{\omega}$ is a two point function and can be calculated by evaluating the Smoluchowski operator acting on a single density function.

$$\boldsymbol{\omega}_{l_1,l_2}\left(\vec{q}\right) = \left(D_r l_2^2 + D_t q^2\right)\delta_{l_1,l_2} - \frac{i v_0 q}{2} \mathrm{e}^{i(l_2-l_1)\alpha_q} \boldsymbol{S}_{l_1,l_1}\left(\vec{q}\right) \delta_{|l_2-l_1|,1}. \tag{A.2}$$

To increase the readability by calculating equilibrium averages of three point functions it is handy to introduce an one particle density function $\rho_{1,j} := \mathrm{e}^{i\vec{q}_1\cdot\vec{x}_j}\mathrm{e}^{il_1\phi_j}$ with $\sum_j \rho_{1,j} = \rho_1$. The Smoluchowski operator for active Brownian disks contains an orientational vector $\vec{o}$, that is parametrized by $\cos(\varphi)$ and $\sin(\varphi)$. After using the orthonormality of e^{ix} and e^{-ix} with respect to the scalar product

$\langle A|B\rangle = \frac{1}{2\pi}\int_{-\pi}^{\pi} d\varphi AB$, the following identities can be used:

$$\begin{aligned}\int_{-\pi}^{\pi} dx \mathrm{e}^{-inx}\mathrm{e}^{imx}\cos(x) &= \pi\Big(\delta_{n,m+1}+\delta_{n,m-1}\Big) && n,m\in\mathbb{Z},\\ \int_{-\pi}^{\pi} dx \mathrm{e}^{-inx}\mathrm{e}^{imx}\sin(x) &= -i\pi\Big(\delta_{n,m+1}-\delta_{n,m-1}\Big) && n,m\in\mathbb{Z}.\end{aligned} \tag{A.3}$$

Now the equilibrium average of a three point function together with the orientational vector can be calculated.

$$\begin{aligned}&\int d\Gamma\mathcal{P}_{eq}\sum_{i,j,k}\rho^*_{1,i}\rho^*_{2,j}\rho_{3,k}\vec{o}_k = \int d\boldsymbol{X}d\boldsymbol{\Phi}\mathcal{P}_{eq}\sum_{i,j,k}\rho^*_{1,i}\rho^*_{2,j}\rho_{3,k}\vec{o}_k\\ =&\int d\boldsymbol{X}d\boldsymbol{\Phi}\mathcal{P}_{eq}\sum_{i,j,k}\mathrm{e}^{-i\vec{q}_1\cdot\vec{x}_i}\mathrm{e}^{-il_1\varphi_i}\mathrm{e}^{-i\vec{q}_2\cdot\vec{x}_j}\mathrm{e}^{-il_2\varphi_j}\mathrm{e}^{i\vec{q}_3\cdot\vec{x}_k}\mathrm{e}^{il_3\varphi_k}\big(\cos(\varphi_k),\sin(\varphi_k)\big)^\top\\ =&\int d\boldsymbol{X}\mathcal{P}_{eq}\sum_{i,j,k}\mathrm{e}^{-i(\vec{q}_1\cdot\vec{x}_i+\vec{q}_2\cdot\vec{x}_j-\vec{q}_3\cdot\vec{x}_k)}\int d\boldsymbol{\Phi}\mathrm{e}^{-i(l_1\varphi_i+l_2\varphi_j-l_3\varphi_k)}\big(\cos(\varphi_k),\sin(\varphi_k)\big)^\top.\end{aligned} \tag{A.4}$$

To perform the integration over the angular part different cases have to be considered.
Case $\varphi_i\neq\varphi_j\neq\varphi_k$:

$$\begin{aligned}&\int d\boldsymbol{\Phi}\mathrm{e}^{-i(l_1\varphi_i+l_2\varphi_j-l_3\varphi_k)}\big(\cos(\varphi_k),\sin(\varphi_k)\big)^\top\\ =&\int d\boldsymbol{\Phi}_{\setminus\{d\varphi_i d\varphi_j d\varphi_k\}}\int_{-\pi}^{\pi}d\varphi_i\mathrm{e}^{-il_1\varphi_i}\int_{-\pi}^{\pi}d\varphi_j\mathrm{e}^{-il_2\varphi_j}\int_{-\pi}^{\pi}d\varphi_k\mathrm{e}^{il_3\varphi_k}\big(\cos(\varphi_k),\sin(\varphi_k)\big)^\top\\ =&\frac{1}{2}(2\pi)^N\delta_{l_1,0}\delta_{l_2,0}\Big(\delta_{l_3,1}+\delta_{l_3,-1},i\delta_{l_3,1}-i\delta_{l_3,-1}\Big)^\top,\end{aligned} \tag{A.5}$$

Case $\varphi_i=\varphi_j\neq\varphi_k$:

$$\begin{aligned}&\int d\boldsymbol{\Phi}\mathrm{e}^{-i(l_1\varphi_i+l_2\varphi_j-l_3\varphi_k)}\big(\cos(\varphi_k),\sin(\varphi_k)\big)^\top\\ =&\int d\boldsymbol{\Phi}_{\setminus\{d\varphi_i d\varphi_k\}}\int_{-\pi}^{\pi}d\varphi_i\mathrm{e}^{-i(l_1+l_2)\varphi_i}\int_{-\pi}^{\pi}d\varphi_k\mathrm{e}^{il_3\varphi_k}\big(\cos(\varphi_k),\sin(\varphi_k)\big)^\top\\ =&\frac{1}{2}(2\pi)^N\delta_{l_1,-l_2}\Big(\delta_{l_3,1}+\delta_{l_3,-1},i\delta_{l_3,1}-i\delta_{l_3,-1}\Big)^\top,\end{aligned} \tag{A.6}$$

Case $\varphi_i = \varphi_k \neq \varphi_j$:

$$\begin{aligned}
&\int d\mathbf{\Phi} \mathrm{e}^{-i(l_1\varphi_i + l_2\varphi_j - l_3\varphi_k)} \big(\cos(\varphi_k), \sin(\varphi_k) \big)^\top \\
=&\int d\mathbf{\Phi}_{\setminus\{d\varphi_j d\varphi_k\}} \int_{-\pi}^{\pi} d\varphi_i \mathrm{e}^{-il_2\varphi_j} \int_{-\pi}^{\pi} d\varphi_k \mathrm{e}^{i(l_3-l_1)\varphi_k} \big(\cos(\varphi_k), \sin(\varphi_k) \big)^\top \\
=&\frac{1}{2} (2\pi)^N \delta_{l_2,0} \Big(\delta_{l_3-l_1,1} + \delta_{l_3-l_1,-1}, i\delta_{l_3-l_1,1} - i\delta_{l_3-l_1,-1} \Big)^\top,
\end{aligned} \tag{A.7}$$

Case $\varphi_j = \varphi_k \neq \varphi_i$:

$$\begin{aligned}
&\int d\mathbf{\Phi} \mathrm{e}^{-i(l_1\varphi_i + l_2\varphi_j - l_3\varphi_k)} \big(\cos(\varphi_k), \sin(\varphi_k) \big)^\top \\
=&\frac{1}{2} (2\pi)^N \delta_{l_1,0} \Big(\delta_{l_3-l_2,1} + \delta_{l_3-l_2,-1}, i\delta_{l_3-l_2,1} - i\delta_{l_3-l_2,-1} \Big)^\top,
\end{aligned} \tag{A.8}$$

Case $\varphi_i = \varphi_j = \varphi_k$:

$$\begin{aligned}
&\int d\mathbf{\Phi} \mathrm{e}^{-i(l_1\varphi_i + l_2\varphi_j - l_3\varphi_k)} \big(\cos(\varphi_k), \sin(\varphi_k) \big)^\top \\
=&\int d\mathbf{\Phi}_{\setminus\{d\varphi_k\}} \int_{-\pi}^{\pi} d\varphi_k \mathrm{e}^{-i(l_1+l_2-l_3)\varphi_k} \big(\cos(\varphi_k), \sin(\varphi_k) \big)^\top \\
=&\frac{1}{2} (2\pi)^N \Big(\delta_{l_1+l_2-l_3,1} + \delta_{l_1+l_2-l_3,-1}, i\delta_{l_1+l_2-l_3,-1} - i\delta_{l_1+l_2-l_3,1} \Big)^\top,
\end{aligned} \tag{A.9}$$

the sum can be splitted into sub sums:

$$\sum_{i,j,k} = \sum_{i\neq j\neq k} + \sum_{i=j\neq k} + \sum_{i=k\neq j} + \sum_{j=k\neq i} + \sum_{i=j=k}. \tag{A.10}$$

After inserting the above expressions into (A.4) the three point function can be expressed as:

$$\begin{aligned}
&\sum_k \Big\langle \rho_1^* \rho_2^* \rho_{3,k} \vec{o}_k \cdot \vec{q}_3 \Big\rangle \\
\approx&\frac{N}{2} \vec{q}_3 \cdot \Big(\delta_{l_1+l_2-l_3,1} + \delta_{l_1+l_2-l_3,-1}, i\delta_{l_1+l_2-l_3,-1} - i\delta_{l_1+l_2-l_3,1} \Big)^\top \delta_{\vec{q}_1+\vec{q}_2,\vec{q}_3} \\
\times&\Bigg[\tilde{S}(\vec{q}_1) \tilde{S}(\vec{q}_2) \tilde{S}(\vec{q}_3) \delta_{l_1,0}\delta_{l_2,0} + \Big(1-\delta_{l_1,0}\Big)\Big(\tilde{S}(\vec{q}_3)-1\Big)\delta_{l_1,-l_2} \\
&+ \Big(1-\delta_{l_1,0}\Big)\Big(\tilde{S}(\vec{q}_2)-1\Big)\delta_{l_2,0} + \Big(1-\delta_{l_2,0}\Big)\Big(\tilde{S}(\vec{q}_1)-1\Big)\delta_{l_1,0} \\
&+ \Big(1-\delta_{l_1,0}\delta_{l_2,0}\Big) \Bigg],
\end{aligned} \tag{A.11}$$

where the approximation $\langle \rho_1^* \rho_3^* \rho_3 \rangle \approx N \boldsymbol{S}_1 \boldsymbol{S}_2 \boldsymbol{S}_3 \delta_{1+2,3}$ was used. Evaluating the Smoluchowski operator acting on the density function and making use of equation (A.1) allows us to write down the final form of the three point function.

$$\frac{1}{N} \left\langle \rho_1^* \rho_2^* \boldsymbol{Q} \Omega^\dagger \rho_3 \right\rangle = -D_t \vec{q}_3 \cdot \left[\vec{q}_1 \boldsymbol{S}_{2,2} + \vec{q}_2 \boldsymbol{S}_{1,1} - \vec{q}_3 \boldsymbol{S}_{1,1} \boldsymbol{S}_{2,2} \right] \delta_{1+2,3}. \tag{A.12}$$

After analogous calculation we also get the second vertex function which takes a more complicated form because of the Smoluchowski operator acting on a product of two density functions (for the derivatives the product rule has to be applied, which generates more terms).

$$\begin{aligned}
\frac{1}{N} \left\langle \rho_1^* \Omega^\dagger \boldsymbol{Q} \rho_2 \rho_3 \right\rangle =& -D_t \vec{q}_1 \cdot \left[\vec{q}_2 \boldsymbol{S}_{1-2,3} + \vec{q}_3 \boldsymbol{S}_{1-3,2} \right] - D_r \left(l_2 + l_3 \right)^2 \boldsymbol{S}_{1,1} \boldsymbol{S}_{2,2} \boldsymbol{S}_{3,3} \delta_{1,2+3} \\
&+ \frac{i v_0}{2} \boldsymbol{S}_{1,1} \begin{pmatrix} 1 \\ \pm_1^{3,2} i \end{pmatrix} \cdot \left[\vec{q}_2 \boldsymbol{S}_{1-3,1-3} \boldsymbol{S}_{3,3} + \vec{q}_3 \boldsymbol{S}_{2,2} \boldsymbol{S}_{1-2,1-2} \right] \delta_{\vec{q}_1, \vec{q}_2 + \vec{q}_3} \delta_{|l_1 - l_2 - l_3|,1} \\
&+ \left[\left(D_r l_1^2 + D_t q_1^2 \right) \delta_{l_1, l_2 + l_3} - \frac{i v_0}{2} \vec{q}_1 \begin{pmatrix} 1 \\ \pm_1^{3,2} i \end{pmatrix} \boldsymbol{S}_{1,1} \delta_{|l_2 + l_3 - l_1|,1} \right] \delta_{\vec{q}_1, \vec{q}_2 + \vec{q}_3} \boldsymbol{S}_{2,2} \boldsymbol{S}_{3,3}.
\end{aligned} \tag{A.13}$$

We use the definitions of the left $\mathrm{L} \equiv \left\langle \rho_l(\vec{q})^* \Omega^\dagger \boldsymbol{Q} \rho_1 \rho_2 \right\rangle \boldsymbol{g}_{1,2,3,4}$ and the right vertex $\mathrm{R} \equiv \boldsymbol{g}_{1',2',3',4'} \left\langle \rho_{3'}^* \rho_{4'}^* \boldsymbol{Q} \Omega^\dagger \rho_{l'}(\vec{q}) \right\rangle$ as introduced in the main theory chapter.

$$\begin{aligned}
\mathrm{L} =& -\frac{D_t}{2N} \vec{q} \cdot \left[\vec{q}_1 \boldsymbol{S}_{1,1}^{-1} + \vec{q}_2 \boldsymbol{S}_{2,2}^{-1} - \vec{q} \right] \overbrace{\delta_{\{l,\vec{q}\},1+2}}^{\equiv \delta_{l,l_1+l_2} \delta_{\vec{q},\vec{q}_1+\vec{q}_2}} \delta_{1,3} \delta_{2,4} \\
&+ \frac{i v_0}{4N} \boldsymbol{S}_{l,l}(\vec{q}) \begin{pmatrix} 1 \\ \pm_l^{1,2} i \end{pmatrix} \cdot \left[\vec{q}_1 \boldsymbol{S}_{l-l_2,l-l_2}(\vec{q}_1) \boldsymbol{S}_{1,1}^{-1} + \vec{q}_2 \boldsymbol{S}_{l-l_1,l-l_1}(\vec{q}_2) \boldsymbol{S}_{2,2}^{-1} - \vec{q} \right] \\
&\qquad \times \delta_{|l_1+l_2-l|,1} \delta_{\vec{q},\vec{q}_1+\vec{q}_2} \delta_{1,3} \delta_{2,4} \\
\equiv& \frac{1}{2N} \mathbf{L}^l_{l_1,l_2}(\vec{q}_1, \vec{q}_2, \vec{q}) \delta_{\vec{q},\vec{q}_1+\vec{q}_2} \delta_{1,3} \delta_{2,4}.
\end{aligned} \tag{A.14}$$

$$\begin{aligned}
\mathrm{R} &= \frac{-D_t}{2N} \boldsymbol{q} \cdot \left[\boldsymbol{q}_{1'} \boldsymbol{S}_{1',1'}^{-1} + \boldsymbol{q}_{2'} \boldsymbol{S}_{2',2'}^{-1} - \boldsymbol{q} \right] \delta_{1',3'} \delta_{2',4'} \delta_{3'+4',\{l',\boldsymbol{q}\}} \\
&\equiv \frac{1}{2N} \mathbf{R}_{l'}^{l_{3'},l_{4'}}(\vec{q}_{3'}, \vec{q}_{4'}, \vec{q}) \delta_{1',3'} \delta_{2',4'} \delta_{\vec{q}_{3'}+\vec{q}_{4'},\vec{q}}.
\end{aligned} \tag{A.15}$$

A.2 Tracer Vertices

Now we perform the MCT approximation of the tracer memory kernel, so we introduce a projector projecting in a space spanned by the product of tracer and

bulk density functions.

$$\boldsymbol{P}_2^s = \sum_{1,2,1',2'} \left|\rho_1^s \rho_2\right\rangle \boldsymbol{g}_{1,2,1',2'} \left\langle \rho_{1'}^{s*} \rho_{2'}^* \right|, \quad \boldsymbol{g}_{1,2,1',2'} = \frac{1}{N} \boldsymbol{S}_{1,1'}^{s^{-1}} \boldsymbol{S}_{2,2'}^{-1} = \frac{1}{N} \boldsymbol{S}_{2,2'}^{-1} \delta_{1,1'}. \quad \text{(A.16)}$$

The memory kernel gets projected into the product state.

$$\begin{aligned} \boldsymbol{m}_{\mathrm{T},l,l'}^s (\vec{q},t) &\approx \left\langle \rho_l^{s*} (\vec{q}) \, \Omega^\dagger \boldsymbol{Q}_s \boldsymbol{P}_2^s \mathrm{e}^{\Omega^{\dagger \mathrm{irr}} t} \boldsymbol{P}_2^s \boldsymbol{Q}_s \Omega^\dagger \rho_{l'}^s (\vec{q}) \right\rangle \\ &= \sum_{\substack{1,2,1',2' \\ 3,4,3',4'}} \left\langle \rho_l^{s*} (\vec{q}) \, \Omega^\dagger \boldsymbol{Q}_s \rho_1^s \rho_2 \right\rangle \boldsymbol{g}_{1,2,1',2'} \left\langle \rho_{1'}^{s*} \rho_{2'}^* \mathrm{e}^{\Omega^{\dagger \mathrm{irr}} t} \rho_3^s \rho_4 \right\rangle \\ &\qquad \times \boldsymbol{g}_{3,4,3',4'} \left\langle \rho_{3'}^{s*} \rho_{4'}^* \boldsymbol{Q}_s \Omega^\dagger \rho_{l'}^s (\vec{q}) \right\rangle. \end{aligned} \quad \text{(A.17)}$$

The four-point function will be approximated by a product of two two point functions similar to the bulk case.

$$\left\langle \rho_{1'}^{s*} \rho_{2'}^* \mathrm{e}^{\Omega^{\dagger irr} t} \rho_3^s \rho_4 \right\rangle \approx \left\langle \rho_{1'}^{s*} \mathrm{e}^{\Omega^\dagger t} \rho_3^s \right\rangle \left\langle \rho_{2'}^* \mathrm{e}^{\Omega^\dagger t} \rho_4 \right\rangle = N \boldsymbol{S}_{1',3}^s (t) \, \boldsymbol{S}_{2',4} (t) \,. \quad \text{(A.18)}$$

It is convenient to define the tracer-bulk static structure factor matrix, which represents the correlation between the bulk density and the tracer density at equilibrium.

$$\boldsymbol{S}_{l_1,l_2}^{\mathrm{tb}} (\boldsymbol{q}) \equiv \left\langle \rho_{l_1}^{s*} (\boldsymbol{q}) \, \rho_{l_2} (\boldsymbol{q}) \right\rangle = \left\langle \tilde{\rho}_{\boldsymbol{q}}^{s*} \tilde{\rho}_{\boldsymbol{q}} \right\rangle \delta_{l_1,0} \delta_{l_2,0} \equiv \tilde{S}_{\boldsymbol{q}}^{sb} \delta_{l_1,0} \delta_{l_2,0}. \quad \text{(A.19)}$$

In the next steps the three-point functions from the memory kernel will be approximated.

$$\begin{aligned} \left\langle \rho_{3'}^{s*} \rho_{4'}^* \boldsymbol{Q}_s \Omega^\dagger \rho_{l'}^s (\vec{q}) \right\rangle &= \left\langle \rho_{3'}^{s*} \rho_{4'}^* \Omega^\dagger \rho_{l'}^s (\vec{q}) \right\rangle - \left\langle \rho_{3'}^{s*} \rho_{4'}^* \boldsymbol{P}_s \Omega^\dagger \rho_{l'}^s (\vec{q}) \right\rangle \\ &= \left\langle \rho_{3'}^{s*} \rho_{4'}^* \Omega^\dagger \rho_{l'}^s (\vec{q}) \right\rangle + \sum_{l_1} \left\langle \rho_{3'}^{s*} \rho_{4'}^* \rho_{l_1}^s (\vec{q}) \right\rangle \boldsymbol{\omega}_{l_1,l'}^s (\vec{q}) \\ &= \left\langle \rho_{3'}^{s*} \rho_{4'}^* \Omega^\dagger \rho_{l'}^s (\vec{q}) \right\rangle + \sum_{l_1} \boldsymbol{S}_{l_1-l_{3'},l_{4'}}^{\mathrm{tb}} (\vec{q}_{4'}) \, \boldsymbol{\omega}_{l_1,l'}^s (\vec{q}) \, \delta_{\vec{q}-\vec{q}_{3'},\vec{q}_{4'}} \\ &= \left\langle \rho_{3'}^{s*} \rho_{4'}^* \Omega^\dagger \rho_{l'}^s (\vec{q}) \right\rangle + \tilde{S}_{\vec{q}_{4'}}^{\mathrm{tb}} \boldsymbol{\omega}_{l_{3'},l'}^s (\vec{q}) \, \delta_{\vec{q}-\vec{q}_{3'},\vec{q}_{4'}} \delta_{l_{4'},0}. \end{aligned} \quad \text{(A.20)}$$

The full adjoint Smoluchowski operator acts on a single tracer density function.

$$\Omega^\dagger \rho_{l'}^s (\vec{q}) = \left[D_t^s \left(-q^2 + i \vec{F}_s \cdot \vec{q} \right) + i v_0^s \vec{o}_s \cdot \vec{q} - D_r^s l'^2 \right] \rho_{l'}^s (\vec{q}) \,. \quad \text{(A.21)}$$

The first term in the equation A.20 can be evaluated.

$$\begin{aligned}\left\langle \rho^{s*}_{3'}\rho^{*}_{4'}\Omega^{\dagger}\rho^{s}_{l'}\left(\vec{q}\right)\right\rangle =& -\left[D^{s}_{t}q^{2}+D^{s}_{r}l'^{2}\right]\boldsymbol{S}^{\mathrm{tb}}_{l'-l_{3'},l_{4'}}\left(\vec{q}_{4'}\right)\delta_{\vec{q}-\vec{q}_{3'},\vec{q}_{4'}}\\ &+iD^{s}_{t}\vec{q}\cdot\left\langle \rho^{s*}_{3'}\rho^{*}_{4'}\rho^{s}_{l'}\left(\vec{q}\right)\vec{F}_{s}\right\rangle +iv^{s}_{0}\vec{q}\cdot\left\langle \rho^{s*}_{3'}\rho^{*}_{4'}\rho^{s}_{l'}\left(\vec{q}\right)\vec{o}_{s}\right\rangle\\ =& -\left[D^{s}_{t}\vec{q}\cdot\vec{q}_{3'}+D^{s}_{r}l'^{2}\right]\boldsymbol{S}^{\mathrm{tb}}_{l'-l_{3'},l_{4'}}\left(\vec{q}_{4'}\right)\delta_{\vec{q}-\vec{q}_{3'},\vec{q}_{4'}}\\ &+iv^{s}_{0}\vec{q}\cdot\left\langle \rho^{s*}_{3'}\rho^{*}_{4'}\rho^{s}_{l'}\left(\vec{q}\right)\vec{o}_{s}\right\rangle,\end{aligned} \tag{A.22}$$

with

$$\begin{aligned}\left\langle \rho^{s*}_{3'}\rho^{*}_{4'}\rho^{s}_{l'}\left(\vec{q}\right)\vec{o}_{s}\right\rangle =& \int d\Gamma\psi_{eq}\mathrm{e}^{i(\vec{q}-\vec{q}_{3'})\cdot\boldsymbol{x}_{s}}\mathrm{e}^{i(l'-l_{3'})\varphi_{s}}\vec{o}_{s}\rho^{*}_{4'}\\ =&\frac{1}{2}\int d\Gamma\psi_{eq}\tilde{\rho}^{s}\left(\vec{q}-\vec{q}_{3'}\right)\rho^{*}_{4'}\begin{pmatrix}\mathrm{e}^{i(l'-l_{3'}+1)\varphi_{s}}+\mathrm{e}^{i(l'-l_{3'}-1)\varphi_{s}}\\ -i\mathrm{e}^{i(l'-l_{3'}+1)\varphi_{s}}+i\mathrm{e}^{i(l'-l_{3'}-1)\varphi_{s}}\end{pmatrix}\\ =&\frac{1}{2}\left\langle \tilde{\rho}^{s}\left(\vec{q}_{4'}\right)\rho^{*}_{4'}\right\rangle \underbrace{\begin{pmatrix}\delta_{l'-l_{3'},1}+\delta_{l'-l_{3'},-1}\\ i\delta_{l'-l_{3'},1}-i\delta_{l'-l_{3'},-1}\end{pmatrix}}_{\vec{\delta}^{s}_{l',l_{3'}}}\delta_{\vec{q}-\vec{q}_{3'},\vec{q}_{4'}}\\ =&\frac{1}{2}\tilde{S}^{\mathrm{tb}}_{\vec{q}_{4'}}\delta_{l_{4'},0}\delta_{\vec{q}-\vec{q}_{3'},\vec{q}_{4'}}\vec{\delta}^{s}_{l',l_{3'}},\end{aligned} \tag{A.23}$$

where for simplicity reasons the delta function vector $\vec{\delta}$ was introduced.

$$\left\langle \rho^{s*}_{3'}\rho^{*}_{4'}\Omega^{\dagger}\rho^{s}_{l'}\left(\vec{q}\right)\right\rangle =-\left[\left[D^{s}_{t}\vec{q}\cdot\vec{q}_{3'}+D^{s}_{r}l'^{2}\right]\delta_{l',l_{3'}}-\frac{iv^{s}_{0}}{2}\vec{q}\cdot\vec{\delta}^{s}_{l',l_{3'}}\right]\tilde{S}^{\mathrm{tb}}_{\vec{q}_{4'}}\delta_{l_{4'},0}\delta_{\vec{q}-\vec{q}_{3'},\vec{q}_{4'}}. \tag{A.24}$$

Using the results for the full Smoluchowski operator acting on a single tracer density the frequency function will be determined.

$$\boldsymbol{\omega}^{s}_{l_{3'},l'}\left(\vec{q}\right)=-\left\langle \rho^{s*}_{l_{3'}}\left(\vec{q}\right)\Omega^{\dagger}\rho^{s}_{l'}\left(\vec{q}\right)\right\rangle =\left[D^{s}_{t}q^{2}+D^{s}_{r}l'^{2}\right]\delta_{l_{3'},l'}-\frac{iv^{s}_{0}}{2}\vec{q}\cdot\vec{\delta}^{s}_{l',l_{3'}}. \tag{A.25}$$

Using the above results the final form of the first full three point function can be calculated.

$$\left\langle \rho^{s*}_{3'}\rho^{*}_{4'}\boldsymbol{Q}_{s}\Omega^{\dagger}\rho^{s}_{l'}\left(\vec{q}\right)\right\rangle =D^{s}_{t}\vec{q}\cdot\vec{q}_{4'}\tilde{S}^{\mathrm{tb}}_{\vec{q}_{4'}}\delta_{l',l_{3'}}\delta_{l_{4'},0}\delta_{\vec{q}-\vec{q}_{3'},\vec{q}_{4'}}. \tag{A.26}$$

The second full three-point function contains a Smoluchowski operator acting on a product of the tracer and bulk density function and thus the product rule has

to be applied for the derivatives, therefore it contains more terms.

$$\begin{aligned}\left\langle \rho_l^{s*}\left(\vec{q}\right)\Omega^\dagger \boldsymbol{Q}_s\rho_1^s\rho_2\right\rangle =&\left\langle \rho_l^{s*}\left(\vec{q}\right)\Omega^\dagger\rho_1^s\rho_2\right\rangle + \sum_{l'}\boldsymbol{\omega}_{l,l'}^s\left(\vec{q}\right)\left\langle \rho_{l'}^{s*}\left(\vec{q}\right)\rho_1^s\rho_2\right\rangle \\ =&\left\langle \rho_l^{s*}\left(\vec{q}\right)\Omega^\dagger\rho_1^s\rho_2\right\rangle + \boldsymbol{\omega}_{l,l_1}^s\left(\vec{q}\right)\tilde{S}_{\vec{q}_2}^{\mathrm{tb}}\delta_{l_2,0}\delta_{\vec{q}-\vec{q}_1,\vec{q}_2},\end{aligned} \tag{A.27}$$

with

$$\begin{aligned}\Omega^\dagger\rho_1^s\rho_2 =&\Big[-\left(D_t^s q_1^2 + D_t q_2^2 + D_r^s l_1^2 + D_r l_2^2\right) + iD_t^s\vec{F}_s\cdot\vec{q}_1 + iv_0^s\vec{o}_s\cdot\vec{q}_1\Big]\rho_1^s\rho_2 \\ &+\sum_j\Big[iD_t\vec{F}_j\cdot\vec{q}_2 + iv_0\vec{o}_j\cdot\vec{q}_2\Big]\rho_{2,j}\rho_1^s,\end{aligned} \tag{A.28}$$

where $\rho_{2,j} = \mathrm{e}^{-i\vec{q}_2\cdot\vec{x}_j}\mathrm{e}^{il_2\varphi_j}$ is a single particle bulk density.

$$\begin{aligned}\left\langle \rho_l^{s*}\left(\vec{q}\right)\Omega^\dagger\rho_1^s\rho_2\right\rangle =& -\left[D_t^s q_1^2 + D_t q_2^2 + D_r^s l_1^2 + D_r l_2^2\right]\left\langle \rho_l^{s*}\left(\vec{q}\right)\rho_1^s\rho_2\right\rangle \\ &+ iD_t^s\vec{q}_1\cdot\left\langle \vec{F}_s\rho_l^{s*}\left(\vec{q}\right)\rho_1^s\rho_2\right\rangle + iv_0^s\vec{q}_1\cdot\left\langle \vec{o}_s\rho_l^{s*}\left(\vec{q}\right)\rho_1^s\rho_2\right\rangle \\ &+\sum_j iD_t\vec{q}_2\cdot\left\langle \vec{F}_j\rho_l^{s*}\left(\vec{q}\right)\rho_1^s\rho_{2,j}\right\rangle + iv_0\vec{q}_2\cdot\left\langle \vec{o}_j\rho_l^{s*}\left(\vec{q}\right)\rho_1^s\rho_{2,j}\right\rangle \\ =& -\left[D_t^s\vec{q}_1\cdot\vec{q} + D_r^s l^2\right]\tilde{S}_{\vec{q}_2}^{\mathrm{tb}}\delta_{l,l_1}\delta_{l_2,0}\delta_{\vec{q}-\vec{q}_1,\vec{q}_2} \\ &+\frac{i}{2}\left[v_0^s\vec{q}_1\vec{\delta}_{l_1,l}^s\delta_{l_2,0} + v_0\vec{q}_2\vec{\delta}_{l_2,0}^s\delta_{l,l_1}\right]\tilde{S}_{\vec{q}_2}^{\mathrm{tb}}\delta_{\vec{q}-\vec{q}_1,\vec{q}_2}.\end{aligned} \tag{A.29}$$

After using the intermediate results the second full three-point can be calculated.

$$\left\langle \rho_{l,\vec{q}}^{s*}\Omega^\dagger Q_s\rho_1^s\rho_2\right\rangle = \left[D_t^s\vec{q}\cdot\vec{q}_2\delta_{l,l_1}\delta_{l_2,0} + \frac{i\vec{q}_2}{2}\cdot\left[v_0\vec{\delta}_{l_2,0}^s\delta_{l,l_1} - v_0^s\vec{\delta}_{l_1,l}^s\delta_{l_2,0}\right]\right]\tilde{S}_{\vec{q}_2}^{\mathrm{tb}}\delta_{\vec{q}-\vec{q}_1,\vec{q}_2}. \tag{A.30}$$

In contradiction to the first vertex the second vertex does not only depend on the tracer parameters, in the latter case also the activity of the bulk particles enters the equation. Using the results of the two vertices the tracer memory kernel can be calculated. To shorten the notation it is useful to introduce $\vec{k} = \vec{q} - \vec{p}$.

$$\begin{aligned}\boldsymbol{m}_{\mathrm{T},l,l'}^s\left(\vec{q},t\right) \approx&\frac{D_t^s}{N}\sum_{l_1,l_2,\vec{p}}\left[D_t^s\delta_{l,l_1}\delta_{l_2,0}\left(\vec{q}\cdot\vec{k}\right)^2 + \frac{i\vec{q}\cdot\vec{k}}{2}\vec{k}\cdot\left[v_0\vec{\delta}_{l_2,0}^s\delta_{l,l_1} - v_0^s\vec{\delta}_{l_1,l}^s\delta_{l_2,0}\right]\right] \\ &\times\left[\delta_{l_2,0}\left(\tilde{S}_k^{-1}-1\right)+1\right]\tilde{S}_k^{\mathrm{tb}^2}\tilde{S}_k^{-1}\boldsymbol{S}_{l_1,l'}^s\left(\vec{p},t\right)\boldsymbol{S}_{l_2,0}\left(\vec{k},t\right) \\ \equiv&\frac{1}{N}\sum_{l_1,l_2,\vec{p}}\boldsymbol{\mathcal{V}}_{l,l_1,l_2}^s\left(\vec{k},\vec{p},\vec{q}\right)\boldsymbol{S}_{l_1,l'}^s\left(\vec{p},t\right)\boldsymbol{S}_{l_2,0}\left(\vec{k},t\right).\end{aligned} \tag{A.31}$$

Appendix B

Numerical Methods

In this chapter we develop the numerical algorithms that are used to solve the equation of motion of the dynamical density correlator in the time domain. One could assume that solving the equation in Laplace domain (that corresponds to an algebraic equation) is advantageous over the time domain equation that is an integro-differential equation for matrix like functions, but having the memory kernel only available in the time domain makes it not feasible to solve the equation in Laplace domain. To analyze the glassy behavior of the system the EOM has to be solved for many orders of magnitude in time ($t \sim 10^7$sec). Standard discretization methods of the differential equations like Runge-Kutta method or Predictor-Corrector methods can not be applied because of the time range we are interested in. To produce accurate results the standard numerical algorithms for PDE's rely on a small discretization step size. For a system with a time range of $t \sim 10^7$sec and a step size of h $\sim 10^{-2}$ the number of points needed to be evaluate would go beyond the capabilities of modern computers, even for these of Supercomputers. The numerical methods we develop, exploit the structure of the density correlator and the memory kernel, being smooth and slowly varying in time (the derivative for very long times vanishes). The algorithm used to avoid evaluating very large amount of numerical points is called the time decimation method, where the time interval gets splitted in blocks and in each block the time step size is kept constant. After changing from one block to the other the step size gets doubled. That way the problem that was linear in time can be reduced to a logarithmic problem. By doubling the step size after going from one block to the next allows us to explore a wide range in time without the problem of having too many numerical points that need to be saved. The Figure (B.1) illustrates a schematic representation of a decimation procedure with the initial block having 9 points. We point out that all the blocks contain the same amount of points, only the step size gets doubled. The first half of the block points get calculated from the previous block by dropping every second term. We obtain the second half of the block points by the numerical

algorithm (Backward Euler method) using the first half of the points as an input. The schematic representation of the algorithm is shown in Figure (B.2). To solve

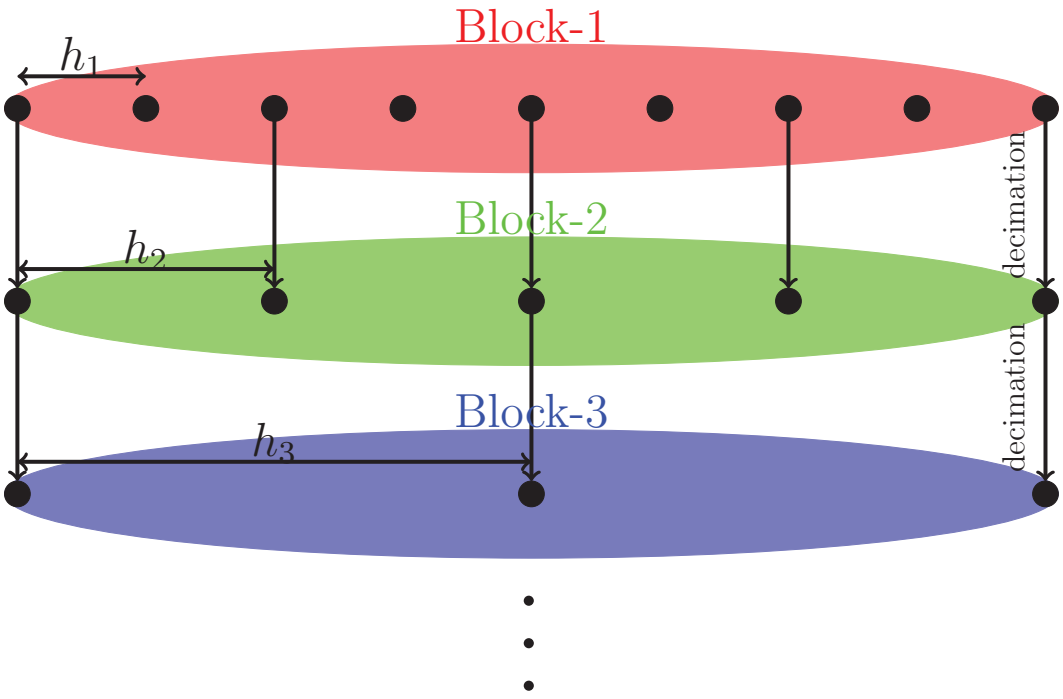

Figure B.1: Schematic representation of the decimation procedure.

the PDE in each block the Backward Euler method will be used. The Backward Euler method is the simplest iterative method for solving differential equations. The equation of motion we desire to solve can be written in the following general form (wavenumbers omitted).

$$\partial_t \boldsymbol{S}(t) = -\boldsymbol{A}\boldsymbol{S}(t) - \int_0^t dt' \boldsymbol{m}(t-t') \left[\partial_{t'} \boldsymbol{S}(t') + \boldsymbol{B}\boldsymbol{S}(t') \right]. \tag{B.1}$$

The bold letters denote matrix like functions and operators like differentiation and integration act component wise.
The initial time step size (Block-0) will be denoted by h_0. The discretized time can be expressed by the initial time and by the time step size. The step size will be equidistant in each block.

$$h_b = h_0 2^b, \quad t_i = t_0 + i h_b. \tag{B.2}$$

The goal is to discretize the equation B.1 in time. The partial time derivative will be evaluated by the backward finite difference method of the second order, taking

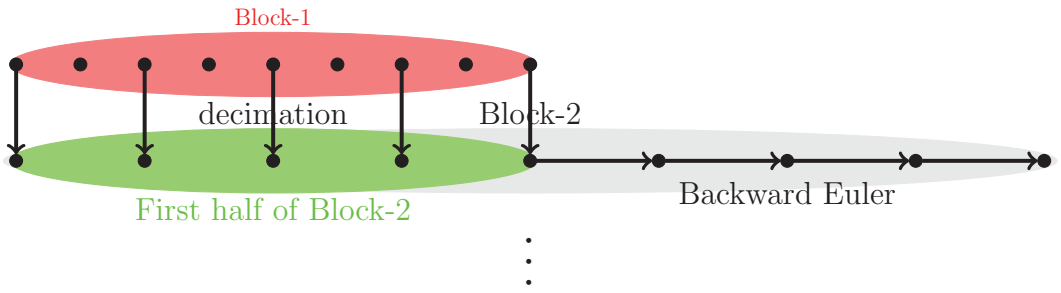

Figure B.2: Schematic representation of the numerical algorithm.

two previous points into account.

$$\partial_t \boldsymbol{S}_i \equiv \partial_t \boldsymbol{S}\left(t_i\right) = \frac{1}{h_b}\left[\frac{3}{2}\boldsymbol{S}_i - 2\boldsymbol{S}_{i-1} + \frac{1}{2}\boldsymbol{S}_{i-2}\right]. \tag{B.3}$$

One should notice that the discretization is only valid in a single block with equidistant steps. By dealing with the convolution integral it is useful to define the so-called moments as a time integral over two neighboring time steps.

$$d\boldsymbol{S}_i = \frac{1}{h_b}\int_{t_{i-1}}^{t_i} \boldsymbol{S}\left(t\right) dt, \qquad d\boldsymbol{m}_i = \frac{1}{h_b}\int_{t_{i-1}}^{t_i} \boldsymbol{m}\left(t\right) dt. \tag{B.4}$$

Using the moments for the correlator and the memory kernel, and the mean value theorem for integrals the convolution integral can be approximated.

$$\begin{aligned}
&\int_0^t dt' \boldsymbol{m}\left(t-t'\right)\partial_{t'}\boldsymbol{S}\left(t'\right) = \int_0^{\tilde{t}} dt' \boldsymbol{m}\left(t-t'\right)\partial_{t'}\boldsymbol{S}\left(t'\right) + \int_{\tilde{t}}^t dt' \boldsymbol{m}\left(t-t'\right)\partial_{t'}\boldsymbol{S}\left(t'\right) \\
&\overset{\text{PI}}{=} \boldsymbol{m}\left(t-t'\right)\boldsymbol{S}\left(t'\right)\Big|_{t'=0}^{t'=\tilde{t}} + \int_0^{\tilde{t}} dt' \partial_t \boldsymbol{m}\left(t-t'\right)\boldsymbol{S}\left(t'\right) + \int_0^{t-\tilde{t}} dt' \boldsymbol{m}\left(t'\right)\partial_t \boldsymbol{S}\left(t-t'\right) \\
&\approx \boldsymbol{m}\left(t_i-t'\right)\boldsymbol{S}\left(t'\right)\Big|_{t'=t_0}^{t'=t_{\tilde{i}}} + \sum_{k=1}^{\tilde{i}} \int_{t_{k-1}}^{t_k} dt' \partial_t \boldsymbol{m}\left(t_i-t'\right)\boldsymbol{S}\left(t'\right) \\
&\qquad\qquad + \sum_{k=1}^{i-\tilde{i}} \int_{t_{k-1}}^{t_k} dt' \boldsymbol{m}\left(t'\right)\partial_t \boldsymbol{S}\left(t_i-t'\right) \\
&\approx \boldsymbol{m}\left(t_i-t'\right)\boldsymbol{S}\left(t'\right)\Big|_{t'=t_0}^{t'=t_{\tilde{i}}} + \sum_{k=1}^{\tilde{i}} \Big[\boldsymbol{m}\left(t_{i-k+1}\right) - \boldsymbol{m}\left(t_{i-k}\right)\Big] d\boldsymbol{S}_k \\
&\qquad\qquad + \sum_{k=1}^{i-\tilde{i}} d\boldsymbol{m}_k \Big[\boldsymbol{S}\left(t_{i-k+1}\right) - \boldsymbol{S}\left(t_{i-k}\right)\Big],
\end{aligned} \tag{B.5}$$

and for the second term in the square bracket of B.1.

$$\begin{aligned}\int_0^t dt' \boldsymbol{m}\left(t-t'\right)\boldsymbol{B}\boldsymbol{S}\left(t'\right) \approx & \frac{h_b}{2}\sum_{k=1}^{\tilde{i}}\Big[\boldsymbol{m}\left(t_{i-k+1}\right)+\boldsymbol{m}\left(t_{i-k}\right)\Big]\boldsymbol{B}d\boldsymbol{S}_k \\ & +\frac{h_b}{2}\sum_{k=1}^{i-\tilde{i}} d\boldsymbol{m}_k\boldsymbol{B}\Big[\boldsymbol{S}\left(t_{i-k+1}\right)+\boldsymbol{S}\left(t_{i-k}\right)\Big]\end{aligned} \tag{B.6}$$

The index $\tilde{i}$ will be chosen such it lies in the middle of the interval $(0,t)$. To ensure that $\tilde{i}$ remains an integer the floor function will be used $\tilde{i}=\lfloor i/2\rfloor$.
Choosing the index $\tilde{i}$ that way guarantees a precise evaluation of $\partial_t\boldsymbol{m}$ and $\partial_t\boldsymbol{S}$ terms even for very high step sizes h, since for very long times the correlator and the memory kernel are expected to have an logarithmic change in time.
To get an recursive equation for the density correlator the terms will be separated in current times i and past times $j<i$.

$$\boldsymbol{\mathcal{S}}=\frac{3}{2h_b}\mathbb{I}+\boldsymbol{A}+d\boldsymbol{m}_1\left(\mathbb{I}+\frac{h_b}{2}\boldsymbol{B}\right),\quad \boldsymbol{\mathcal{M}}=\boldsymbol{S}_0-\left(\mathbb{I}+\frac{h_b}{2}\boldsymbol{B}\right)d\boldsymbol{S}_1 \tag{B.7}$$

$$\begin{aligned}\boldsymbol{\mathcal{I}}_i=&\sum_{k=2}^{\tilde{i}}\left[\boldsymbol{m}_{i-k+1}\left(\mathbb{I}+\frac{h_b}{2}\boldsymbol{B}\right)-\boldsymbol{m}_{i-k}\left(\mathbb{I}-\frac{h_b}{2}\boldsymbol{B}\right)\right]d\boldsymbol{S}_k,\\ &+\sum_{k=2}^{i-\tilde{i}} d\boldsymbol{m}_k\left[\left(\mathbb{I}+\frac{h_b}{2}\boldsymbol{B}\right)\boldsymbol{S}_{i-k+1}-\left(\mathbb{I}-\frac{h_b}{2}\boldsymbol{B}\right)\boldsymbol{S}_{i-k}\right]\\ &-\boldsymbol{m}_{i-1}\left(\mathbb{I}-\frac{h_b}{2}\boldsymbol{B}\right)d\boldsymbol{S}_1-d\boldsymbol{m}_1\left(\mathbb{I}-\frac{h_b}{2}\boldsymbol{B}\right)\boldsymbol{S}_{i-1}\\ &+\boldsymbol{m}_{i-\tilde{i}}\boldsymbol{S}_{\tilde{i}}-\frac{2}{h_b}\boldsymbol{S}_{i-1}+\frac{1}{2h_b}\boldsymbol{S}_{i-2}\end{aligned} \tag{B.8}$$

Using the prefactor matrices $\boldsymbol{\mathcal{S}}$, $\boldsymbol{\mathcal{M}}$ and $\boldsymbol{\mathcal{I}}$ a discretized EOM which corresponds to the equation (B.1) can be obtained.

$$\boldsymbol{\mathcal{S}}\boldsymbol{S}_i=\boldsymbol{m}_i\boldsymbol{\mathcal{M}}-\boldsymbol{\mathcal{I}}_i,\quad\Rightarrow\quad \boldsymbol{S}_i=\boldsymbol{\mathcal{S}}^{-1}\Big[\boldsymbol{m}_i\boldsymbol{\mathcal{M}}-\boldsymbol{\mathcal{I}}_i\Big]. \tag{B.9}$$

The later equation can not be solved directly for $\boldsymbol{S}_i$ as the memory kernel at current times depends itself on the correlator. The equation will be solved iteratively as illustrated in the figure B.3. The superscript in the parenthesis corresponds to the iteration number.
The following recipe describes how the iteration algorithm works.

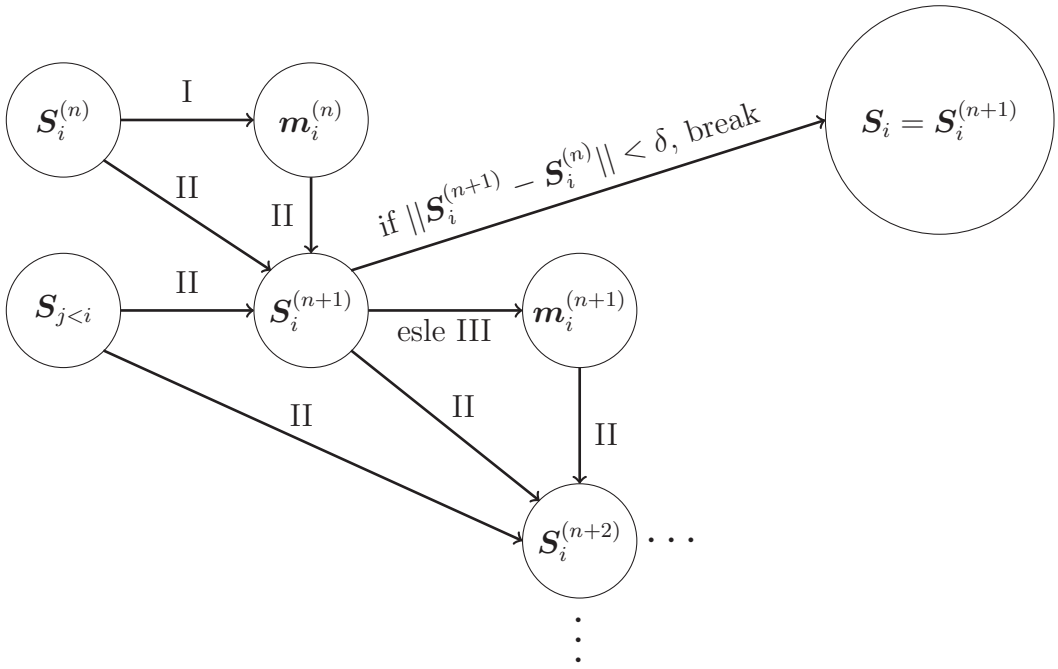

Figure B.3: Schematic representation of the numerical scheme for the iteration. Superscripts denote the iteration number.

- Step 0: Use as a starting value $\boldsymbol{S}_i^{(0)} = \boldsymbol{S}_{i-1}$.
- Step I: From the current value of the correlator at the iteration step (n) calculate the memory kernel $\boldsymbol{m}_i^{(n)}$.
- Step II: From the correlator at current time $\boldsymbol{S}_i^{(n)}$, the memory kernel $\boldsymbol{m}_i^{(n)}$ and the correlators from the past $\boldsymbol{S}_{j<i}$ calculate the new correlator $\boldsymbol{S}_i^{(n+1)}$ according to the rule (B.9).
- Check if the difference between the correlator after the iteration steps $(n+1)$ and (n) is smaller than the desired precision δ.

  $$\left|\left|\boldsymbol{S}_i^{(n+1)} - \boldsymbol{S}_i^{(n)}\right|\right| \stackrel{!}{<} \delta.$$

  As a norm $||\cdot||$ any matrix norm can be used (we used the L_1 norm). If the condition is fulfilled set the correlator at current times to $\boldsymbol{S}_i = \boldsymbol{S}_i^{(n+1)}$, and increase the time counter $i \to i+1$.

- Step III: If the desired precision is not achieved (we use machine precision for $\delta \sim 10^{-15}$) repeat the steps I and II.

- Repeat the steps I-III until the precision goal is reached or until the counter for the iterations will exceed some critical value. The critical value is normally set to 100 but close to the bifurcation point higher values are needed. At the bifurcation point not even an infinite number of iterations is enough to reach the precision goal.

The recursive algorithm is used to calculate the density correlator in each block. After all points in one block, denoted by Blocksize (normally Blocksize=128) are calculated the decimation procedure has to be applied. In the following the decimation rules for different quantities are shown.

- Double the step size: $h_{b+1} = 2h_b$.
- Drop every second term of the correlator and the memory kernel.

$$\boldsymbol{S}_i = \boldsymbol{S}_{2i}, \qquad \boldsymbol{m}_i = \boldsymbol{m}_{2i} \quad \forall i \leq \text{Blocksize}/2.$$

- The moments can be decimized exactly without dropping any terms ($i \leq$ Blocksize/2).

$$\begin{aligned} d\boldsymbol{S}_i^{(2h)} &= \frac{1}{2h}\int_{t_{i-1}}^{t_i} \boldsymbol{S}(t)dt = \frac{1}{2h}\int_{2h(i-1)}^{2hi} \boldsymbol{S}(t)dt \\ &= \frac{1}{2h}\left[\int_{h(2i-2)}^{h(2i-1)} \boldsymbol{S}(t)dt + \int_{h(2i-1)}^{h2i} \boldsymbol{S}(t)dt\right] = \frac{1}{2}\left[d\boldsymbol{S}_{2i-1}^{(h)} + d\boldsymbol{S}_{2i}^{(h)}\right], \\ d\boldsymbol{m}_i^{(2h)} &= \frac{1}{2}\left[d\boldsymbol{m}_{2i-1}^{(h)} + d\boldsymbol{m}_{2i}^{(h)}\right]. \end{aligned}$$

The memory kernel contains a double integral in the space of the wavenumbers. The integrand has a pole at the boundaries due to the Jacobian of the two dimensional transformation and to avoid divergent terms in the sum an open integration formula is used. To have the desired precision and performance a fifth order open extended formula is used (derived in [57]).

$$\int_{q_1}^{q_N} f(q)dq = h_q\left[\frac{55}{24}f_2 - \frac{1}{6}f_3 + \frac{11}{8}f_4 + \cdots + \frac{11}{8}f_{N-3} - \frac{1}{6}f_{N-2} + \frac{55}{24}f_{N-1}\right], \tag{B.10}$$

with $\cdots$ containing terms with unit coefficients only.

	N_{Blocks}	Blocksize	Step size	$N_{\text{Iteration}}$	δ	N_q	Λ_q	Λ_l
Values	60-70	128-256	10^{-12}	100|10000	10^{-15}	128|256	50	1|2

Table B.1: Typical values for the numerical parameters chosen in this work.

The wavenumber is in general in the set of real numbers, but we will introduce a cutoff $\Lambda_q = 50$ up to which point we integrate. We assume that for larger q values than the cutoff Λ_q the correlator is small enough that it will not change the results dramatically (see the wavenumber dependent correlator in the results chapter). N_q will be the number of q point we use to discretize the wavenumber. And the wavenumber step size $h_q = \Lambda_q/N_q$. In the Table (B.1) a typical choice of the numerical parameters are presented. Close to the bifurcation point a much higher number of iterations $N_{\text{Iteration}}$ is used.

B.1 Complexity and Memory Usage

In this section the complexity of the time domain algorithm and the usage of RAM-memory will be estimated. There are different settings that can be adjusted by numerical calculations. The first three parameters determine the precision of the time domain discretization. The number of blocks N_{Blocks}, the Blocksize and the initial time step-size h. The Blocksize is chosen between 128-256 time points, the number of blocks is in the range of 60-70 and the initial time step is chosen to be $h_0 \sim 10^{-12}$. That kind of adjustment allows us to reach times of the order $t_{\max} = h_0 2^{N_{\text{Blocks}}} \sim 10^6 - 10^9$, which is sufficient to study the glassy dynamics. The Blocksize only determines the resolution of each block and does not contribute to reach longer end times. Experience showed that choosing the precision between 128-256 time points is sufficient and does not produce discontinuous jumps by the time decimation procedure (that happens if the Blocksize is chosen to small). The number of points to be saved is given by: $N_{\text{Blocks}} * \text{Blocksize}/2$. The number of blocks changes the complexity linearly $\mathcal{O}(N_{\text{Blocks}})$, so doubling the number of blocks doubles the computational time. The remaining parameters N_q and Λ_l determine the number of wavenumber points and the size of the matrices (in the space of orientational indices) respectively. Typical values for N_q are between 128-256 points, that is a good compromise between calculation speed and precision. The double integral in the wavenumber space needs to be evaluated for all wavenumber components of the memory kernel, thus the complexity will be cubic in number of q points $\mathcal{O}(N_q^3)$. The size of the matrices is determined by the orientational cutoff Λ_l. The orientational indices run form $-\Lambda_l$ to Λ_l. Typically the cutoff is chosen to be 1 or 2. The first corresponds to a 3×3 dimensional and the latter to a 5×5 dimensional matrix. The memory kernel contains a sum over four orientational indices, so one could assume that the final complexity would depend on $(2\Lambda_l + 1)^4$, but it is not that simple to calculate the complexity since some orientational indices are delta correlated due to the structure of the vertices in the memory kernel and a clever optimization of the compiler reduces the number of evaluations significantly. The total complexity related to the orientational cutoff

can be estimated numerically by $\mathcal{O}\left((2\Lambda_l+1)^{2.9}\right)$. So going from $\Lambda_l = 0$ (only $S_{0,0}$, valid for passive particle) to a cutoff $\Lambda_l = 1$ (typical choice for our numerical algorithm) corresponds to a $3^{2.9} \sim 25$ times longer calculation time. By dealing with 5×5 ($\Lambda_l = 2$) dimensional matrices the algorithm in comparison to $\Lambda_l = 0$ is even by a factor of $5^{2.9} \sim 114$ slower. The major part of the numerical results are calculated by using $\Lambda_l = 1$. The total complexity of the time domain algorithm is estimated as $\mathcal{O}\left(N_{\text{Blocks}} * N_q^3 * (2\Lambda_l+1)^{2.9}\right)$.
Now we want to estimate the RAM-memory needed for the numerical algorithm. The main memory is used to save the values of the left and right vertex functions. The vertex functions do only depend on static (time independent) quantities and can be calculated and saved in RAM memory at the starting point of the algorithm. $L_{l,l_1,l_2}(k,p,q)$ and $R_{l',l_3,l_4}(k,p,q)$ contain three orientational indices and 3 wavenumbers running from 0 to q_{max}. The number of points needed to be evaluated are $N_p = (2\Lambda_l+1)^3 N_q^3$. Each value is a complex valued double precision number with 8Byte for each (16Byte for complex). So for a typical choice of the parameters the following memory usage can be estimated:

- $\Lambda_l = 1$ and $N_q = 128$, $\Rightarrow$ MEM = 2GiB
- $\Lambda_l = 2$ and $N_q = 256$, $\Rightarrow$ MEM = 68GiB

The memory needed for saving the dynamical values (time dependent correlator) in comparison to static values is negligible.

B.2 Computer Resources and Calculating Time

Finally we want to address the computer resources we had available and the calculation times for the typical settings. The calculations mainly were done on two different cluster systems.

- The supercomputer in Jülich "JURECA" : 1872 nodes with two Intel Xeon E5-2680 v3 Haswell CPUs on each (128 nodes could be used in parallel). Each node was equipped with 128GiB DDR4 RAM memory.
- Local cluster available in the institute: 16 nodes with two Intel Xeon E5-2650 v4 Broadwell CPUs on each. Each node equipped with 128GiB RAM memory.

The numerical algorithm was implemented in C/C++ language, by using OpenMP programming interface for parallelization on a single node. Matrix manipulations were done by highly optimized EIGEN library and for evaluating the Bessel functions related to a two dimensional Fourier-transform the BOOST library was used.

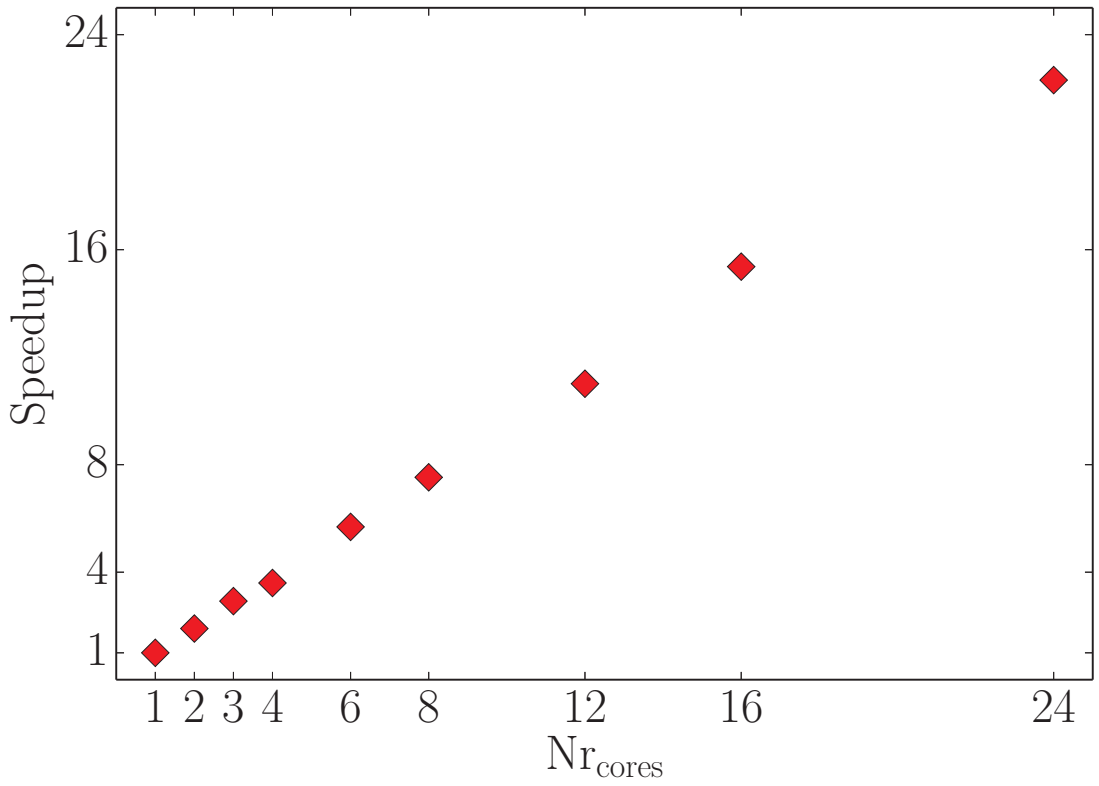

Figure B.4: Speedup of the time domain algorithm as a function of number of CPU cores on a single node. The algorithm was used for $N_q = 128$ wavenumber points.

The code can be parallelized very efficiently up to the number of discrete wavenumber points N_q. The Figure B.4 shows almost linear speedup of the algorithm by increase of the number of CPU cores on a single node. The speedup is up to 24 cores almost linear. The most time consuming part of the algorithm is to evaluate the memory kernel for all different wavenumbers. By parallelizing the algorithm the memory kernel for different wavenumbers (which do not depend on each other) can be performed in parallel. So for the choice of $N_q = 128$ up to 128 cores could be used without significant worsening of the speedup. Using more than 128 cores is useless since all the additional cores will be idle. The calculation time of the algorithm does not only depend on the numerical parameters for the precision e.g. (N_q, Blocksize, Λ_l) it also depends how close the system is to the glass transition. If the system is close to glass transition much more iterations are used in each time step which can drastically slow down the algorithm. In the following we want to show the calculation time of the algorithm for the following parameters:

Blocksize = 70, $\Lambda_l = 1$, $N_q = 128$.

- System far away from the glass transition point with $t_\alpha \sim 10^{-1}$.
  $t_{\text{calculation}} \approx 20\text{min}$.
- System closer to glass transition point with $t_\alpha \sim 10^2$.
  $t_{\text{calculation}} \approx 30\text{min}$.
- System very close to glass transition point $t_\alpha \sim 10^6$.
  $t_{\text{calculation}} \approx 109\text{min}$.
- System in the glassy state $t_\alpha \to \infty$.
  $t_{\text{calculation}} \approx 30\text{min}$.

Close to the glass transition point the calculation time is almost six times longer than for a system far away from the glass transition for the same numerical parameters.

Bibliography

[1] Thomas E. Angelini, Edouard Hannezo, Xavier Trepat, Jeffrey J. Fredberg, and David A. Weitz. Cell migration driven by cooperative substrate deformation patterns. *Phys. Rev. Lett.*, 104:168104, Apr 2010.

[2] Fernando Peruani, Jörn Starruß, Vladimir Jakovljevic, Lotte Søgaard-Andersen, Andreas Deutsch, and Markus Bär. Collective motion and nonequilibrium cluster formation in colonies of gliding bacteria. *Phys. Rev. Lett.*, 108:098102, Feb 2012.

[3] J Elgeti, R G Winkler, and G Gompper. Physics of microswimmers—single particle motion and collective behavior: a review. *Reports on Progress in Physics*, 78(5):056601, 2015.

[4] Ben Fabry, Geoffrey N. Maksym, James P. Butler, Michael Glogauer, Daniel Navajas, and Jeffrey J. Fredberg. Scaling the microrheology of living cells. *Phys. Rev. Lett.*, 87:148102, Sep 2001.

[5] Fernando Peruani, Jörn Starruß, Vladimir Jakovljevic, Lotte Søgaard-Andersen, Andreas Deutsch, and Markus Bär. Collective motion and nonequilibrium cluster formation in colonies of gliding bacteria. *Phys. Rev. Lett.*, 108:098102, Feb 2012.

[6] Tohru Minamino, Katsumi Imada, and Keiichi Namba. Molecular motors of the bacterial flagella. *Current Opinion in Structural Biology*, 18(6):693 – 701, 2008. Catalysis and regulation / Proteins.

[7] P. Romanczuk, M. Bär, W. Ebeling, B. Lindner, and L. Schimansky-Geier. Active brownian particles. *The European Physical Journal Special Topics*, 202(1):1–162, 2012.

[8] Debajyoti Debnath, Pulak K. Ghosh, Yunyun Li, Fabio Marchesoni, and Baowen Li. Communication: Cargo towing by artificial swimmers. *The Journal of Chemical Physics*, 145(19):191103, nov 2016.

[9] Jérémie Palacci, Cécile Cottin-Bizonne, Christophe Ybert, and Lydéric Bocquet. Sedimentation and effective temperature of active colloidal suspensions. *Phys. Rev. Lett.*, 105:088304, Aug 2010.

[10] Ivo Buttinoni, Julian Bialké, Felix Kümmel, Hartmut Löwen, Clemens Bechinger, and Thomas Speck. Dynamical clustering and phase separation in suspensions of self-propelled colloidal particles. *Phys. Rev. Lett.*, 110:238301, Jun 2013.

[11] Sela Samin and René van Roij. Self-propulsion mechanism of active janus particles in near-critical binary mixtures. *Phys. Rev. Lett.*, 115:188305, Oct 2015.

[12] A. Scala, Th. Voigtmann, and C. De Michele. Event-driven brownian dynamics for hard spheres. *The Journal of Chemical Physics*, 126(13):134109, 2007.

[13] R. Ni, M.A.C. Stuart, and M. Dijkstra. Pushing the glass transition towards random close packing using self-propelled hard spheres. *Nature Communications*, 4(2704), 2013.

[14] Ludovic Berthier. Nonequilibrium glassy dynamics of self-propelled hard disks. *Phys. Rev. Lett.*, 112:220602, Jun 2014.

[15] Yaouen Fily, Silke Henkes, and M. Cristina Marchetti. Freezing and phase separation of self-propelled disks. *Soft Matter*, 10:2132–2140, 2014.

[16] Ludovic Berthier and Jorge Kurchan. Non-equilibrium glass transitions in driven and active matter. *Nat Phys*, 9(5):310–314, May 2013. Article.

[17] Hui-Shun Kuan, Robert Blackwell, Loren E. Hough, Matthew A. Glaser, and M. D. Betterton. Hysteresis, reentrance, and glassy dynamics in systems of self-propelled rods. *Phys. Rev. E*, 92:060501, Dec 2015.

[18] M. Bayer, J. M. Brader, F. Ebert, M. Fuchs, E. Lange, G. Maret, R. Schilling, M. Sperl, and J. P. Wittmer. Dynamic glass transition in two dimensions. *Phys. Rev. E*, 76:011508, Jul 2007.

[19] W Gotze. The mode-coupling theory of liquid-to-glass transitions. *Journal of Physics: Condensed Matter*, 2(S):SA201, 1990.

[20] S. C. Takatori, W. Yan, and J. F. Brady. Swim pressure: Stress generation in active matter. *Physical Review Letters*, 113(2), jul 2014.

[21] Wen Yan and John F. Brady. The swim force as a body force. *Soft Matter*, 11(31):6235–6244, 2015.

[22] Christina Kurzthaler, Sebastian Leitmann, and Thomas Franosch. Intermediate scattering function of an anisotropic active brownian particle. *Scientific Reports*, 6(1), nov 2016.

[23] Wolfgang Götze. *Complex Dynamics of Glass-Forming Liquids*. Oxford University Press, dec 2008.

[24] Grzegorz Szamel and Hartmut Löwen. Mode-coupling theory of the glass transition in colloidal systems. *Physical Review A*, 44(12):8215–8219, dec 1991.

[25] M. Bayer, J. M. Brader, F. Ebert, M. Fuchs, E. Lange, G. Maret, R. Schilling, M. Sperl, and J. P. Wittmer. Dynamic glass transition in two dimensions. *Physical Review E*, 76(1), jul 2007.

[26] T. F. F. Farage and J. M. Brader. Dynamics and rheology of active glasses, 2014.

[27] Elijah Flenner, Grzegorz Szamel, and Ludovic Berthier. The nonequilibrium glassy dynamics of self-propelled particles. *Soft Matter*, 12:7136–7149, 2016.

[28] Matthias Fuchs and Michael E. Cates. Theory of nonlinear rheology and yielding of dense colloidal suspensions. *Phys. Rev. Lett.*, 89:248304, Nov 2002.

[29] J. M. Brader, T. Voigtmann, M. Fuchs, R. G. Larson, and M. E. Cates. Glass rheology: From mode-coupling theory to a dynamical yield criterion. *Proceedings of the National Academy of Sciences*, 106(36):15186–15191, aug 2009.

[30] L. Sjögren. Kinetic theory of current fluctuations in simple classical liquids. *Phys. Rev. A*, 22:2866–2882, Dec 1980.

[31] In N.G. VAN KAMPEN, editor, *Stochastic Processes in Physics and Chemistry (Third Edition)*, North-Holland Personal Library, pages iv –. Elsevier, Amsterdam, third edition edition, 2007.

[32] A. Einstein. Über die von der molekularkinetischen theorie der wärme geforderte bewegung von in ruhenden flüssigkeiten suspendierten teilchen. *Annalen der Physik*, 322(8):549–560, 1905.

[33] R Kubo. The fluctuation-dissipation theorem. *Reports on Progress in Physics*, 29(1):255, 1966.

[34] Denis J Evans and Gary P Morriss. *Statistical Mechanics of Nonequilibrium Liquids*. ANU E Press, 2010.

[35] Jean-Pierre Hansen and I. R. McDonald. *Theory of Simple Liquids*. Academic Press, 2006.

[36] Debajyoti Debnath, Pulak K. Ghosh, Yunyun Li, Fabio Marchesoni, and Baowen Li. Communication: Cargo towing by artificial swimmers. *The Journal of Chemical Physics*, 145(19):191103, nov 2016.

[37] I. Gazuz and M. Fuchs. Nonlinear microrheology of dense colloidal suspensions: A mode-coupling theory. *Physical Review E*, 87(3), mar 2013.

[38] Rolf Schilling. Reference-point-independent dynamics of molecular liquids and glasses in the tensorial formalism. *Physical Review E*, 65(5), may 2002.

[39] Rolf Schilling and Thomas Scheidsteger. Mode coupling approach to the ideal glass transition of molecular liquids: Linear molecules. *Phys. Rev. E*, 56:2932–2949, Sep 1997.

[40] T. Theenhaus, R. Schilling, A. Latz, and M. Letz. Microscopic dynamics of molecular liquids and glasses: Role of orientations and translation-rotation coupling. *Physical Review E*, 64(5), oct 2001.

[41] J. M. Brader. Solution of the ornstein–zernike equation in the critical region. *International Journal of Thermophysics*, 27(2):394–412, 2006.

[42] J. L. Lebowitz and J. K. Percus. Mean spherical model for lattice gases with extended hard cores and continuum fluids. *Physical Review*, 144(1):251–258, apr 1966.

[43] Jerome K. Percus and George J. Yevick. Analysis of classical statistical mechanics by means of collective coordinates. *Physical Review*, 110(1):1–13, apr 1958.

[44] M Baus and J L Colot. Theoretical structure factors for hard-core fluids. *Journal of Physics C: Solid State Physics*, 19(28):L643, 1986.

[45] Kyozi Kawasaki. Correlation-function approach to the transport coefficients near the critical point. i. *Phys. Rev.*, 150:291–306, Oct 1966.

[46] Wolfgang Götze. Recent tests of the mode-coupling theory for glassy dynamics. *Journal of Physics: Condensed Matter*, 11(10A):A1, 1999.

[47] G. Brambilla, D. El Masri, M. Pierno, L. Berthier, L. Cipelletti, G. Petekidis, and A. B. Schofield. Probing the equilibrium dynamics of colloidal hard spheres above the mode-coupling glass transition. *Phys. Rev. Lett.*, 102:085703, Feb 2009.

[48] Dapeng Bi, Xingbo Yang, M. Cristina Marchetti, and M. Lisa Manning. Motility-driven glass and jamming transitions in biological tissues. *Physical Review X*, 6(2), apr 2016.

[49] A. Sharma and J. M. Brader. Communication: Green-kubo approach to the average swim speed in active brownian systems. *The Journal of Chemical Physics*, 145(16):161101, oct 2016.

[50] Michael E. Cates and Julien Tailleur. Motility-induced phase separation. *Annual Review of Condensed Matter Physics*, 6(1):219–244, mar 2015.

[51] Gabriel S. Redner, Michael F. Hagan, and Aparna Baskaran. Structure and dynamics of a phase-separating active colloidal fluid. *Physical Review Letters*, 110(5), jan 2013.

[52] Joakim Stenhammar, Davide Marenduzzo, Rosalind J. Allen, and Michael E. Cates. Phase behaviour of active brownian particles: the role of dimensionality. *Soft Matter*, 10(10):1489–1499, 2014.

[53] Julian Bialké, Hartmut Löwen, and Thomas Speck. Microscopic theory for the phase separation of self-propelled repulsive disks. *EPL (Europhysics Letters)*, 103(3):30008, aug 2013.

[54] V. Krakoviack. Mode-coupling theory for the slow collective dynamics of fluids adsorbed in disordered porous media. *Physical Review E*, 75(3), mar 2007.

[55] V. Krakoviack. Liquid-glass transition of a fluid confined in a disordered porous matrix: A mode-coupling theory. *Physical Review Letters*, 94(6), feb 2005.

[56] V Krakoviack. Liquid–glass transition of confined fluids: insights from a mode-coupling theory. *Journal of Physics: Condensed Matter*, 17(45):S3565–S3570, oct 2005.

[57] William H. Press, Brian P. Flannery, Saul A. Teukolsky, and William T. Vetterling. *Numerical Recipes in C: The Art of Scientific Computing, Second Edition*. Cambridge University Press, 1992.